Université d'Ottawa · University of Ottawa

EXPERIMENTAL STUDY AND DISCRETE ELEMENT SIMULATION OF SAND-STEEL INTERFACE BEHAVIOUR

by

Tieming FU

A Thesis
submitted to the School of Graduate Studies and Research
under the supervision of

Dr. Erman Evgin

in partial fulfillment of the requirements for the degree of
Master in Applied Sciences in Civil Engineering

Department of Civil Engineering
University of Ottawa
Ottawa, Ontario
Canada

May 1998

The Master in Applied Sciences in Civil Engineering is a joint program between Carleton University and the University of Ottawa, which is administered by the Ottawa-Carleton Institute for Civil Engineering

0-612-36693-6

ACKNOWLEDGMENTS

I would like to express my sincere thanks to my supervisor, Dr. Erman Evgin, for his generous advice, continuous encouragement and financial support through this research.

The financial support from NSERC, NEB, the Ontario Graduate Scholarship (OGS) and University of Ottawa Excellence Scholarship are gratefully acknowledged.

I also wish to thank Mr. R.J. Moore, Ms. B. Mavrantzas and Y. Hogan for their assistance during this research.

DEDICATION

This thesis is dedicated to my wife Rong for her continuous encouragement, patience and support.

ABSTRACT

The response of soil-structure systems subjected to static or dynamic loading is influenced significantly by the nature of mechanical behaviour of interfaces. An experimental and numerical study of sand-steel interface behaviour is the subject of the research described in this thesis. The main objectives of this study are to explore the possibility of simulating sand-steel interface behaviour using the Discrete Element Method, to investigate numerically the movements of particles in sand-steel interface tests, and to simulate experimentally the liquefaction phenomenon. The thesis is divided into two parts.

In the first part, sand-steel interface tests were conducted using an automated 3-D apparatus C3DSSI (Cyclic 3-Dimensional Simple Shear Testing of Interfaces). A dense sand-rough steel plate interface test was carried out under constant normal stress conditions and the results were used in the discrete element simulations. The tests on the loose sand-smooth steel plate interface samples were carried out to investigate the effects of the initial state of the sample (i.e., relative density and normal stress) and the boundary conditions on the sand-steel interface behaviour. Under monotonic and cyclic loading conditions, the liquefaction phenomenon was successfully simulated in the loose sand-smooth steel plate interface tests with constant volume.

In the second part, an attempt was made to explore the advantages and limitations of using the discrete element method to simulate the behaviour of an interface between a granular soil and a steel plate. A two-dimensional discrete element program PFC^{2D} was used in the simulations. The particle shape plays an important role in the DEM simulations. The simulations using the "peanut" shape particle units produced better results than using round particles for both strength and deformation behaviour of a sand-steel interface. The movements of particles in sand-steel interface tests were observed numerically. The effects of side walls on the movements of sand particles in a direct shear box and the interface thickness were also determined. These simulation results agree well with the experimental results provided by other investigators.

TABLE OF CONTENTS

LIST OF FIGURES

LIST OF TABLES

CHAPTER 1
INTRODUCTION

1.1 Statement of Problem

In geotechnical engineering practice, there are many situations where soils interact with structural materials. The contact zone between the soil and a structural material is normally referred to as "interface". According to theoretical investigations and experimental observations, the interface is a thin layer of material through which stress is transferred from one medium to the other. It exhibits localized strains which are also called "shear bands". This behaviour is mainly due to the contrast in mechanical properties of the soil and the structural material. The response of soil-structure systems subjected to static or dynamic loading is influenced significantly by the nature of mechanical behaviour of interfaces.

There are many examples of soil-structure interaction problems. One obvious example is a pile foundation. The ultimate load capacity and the behaviour at working load of a pile are largely a function of the load transfer capability of the pile shaft-soil interface. During the installation of piles, hammer or vibratory pile-driving causes impact-type or cyclic vertical loading which results in relative displacement of the pile shaft and the surrounding soil. Under the action of earthquakes, wind and waves, the loading on the interface becomes cyclic. In such case, the pile and the surrounding soil will loose contact and a gap may develop between them. Similar to piles, the capacity of anchors is also determined by the properties of the interface between the anchor and the surrounding soil.

Another example is the buried underground structures. Buried structures are often used in lifeline systems such as gas and oil pipelines, water mains, highway culverts and electrical conduits. The behaviour of the interface between soil and structure has drawn considerable attention in several decades for engineering problems involving underground structures subjected to dynamic loading like blast, ground shock, or earthquake. Experimental results indicate that failures at the interface between soil and structure could occur at relatively low stress levels. Historically, severe damage to such structural systems has been reported in several earthquakes.

In addition, there are other soil-structure interaction problems such as retaining walls, shallow foundations, reinforced earth and so on, where the parameters related to the interface become important in the design of these structures.

Often, the numerical analysis of soil-structure systems is performed by assuming complete bonding at the interface. Although this assumption simplifies the calculation, it can cause errors in the prediction of the stresses and deformations. The description of the mechanical behaviour of interfaces requires information on the strength characteristics and load-displacement relation. The behaviour of interfaces is very complex. This is mainly due to the fact that relative motions such as sliding, separation or debonding and rebonding may take place during the loading which in turn influence the stress-deformation response of the interface. Inclusion of the relative motions and resulting mechanisms of load transfer at the interface introduce strong nonlinearities. The advancement of our current knowledge on interface behaviour requires additional experimental and numerical investigations.

The mutual effect of soils and pile shaft materials in the transmission of forces from one to the other through the contact surface is called skin friction. Before 1960's, the values of skin friction were obtained from pile load tests, or they were calculated from the resistance of soil to pile driving. These investigations provided only average values of skin friction along the pile shaft. It was difficult to relate them to the behaviour of interfaces at different depth along the pile shaft which might be going through different soil layers. Furthermore, no consideration was given to the surface roughness of different construction materials. Subsequently, engineers started to conduct laboratory investigations on the behaviour of soil-structural material interfaces as the need for reliable estimates of soil-structure interface behaviour has increased.

Since Potyondy (1961) first performed a comprehensive series of direct shear type interface tests to determine the skin friction between different types of soils and construction materials, more and more investigations regarding soil-structure interface behaviour have been done using various interface testing devices. However, there are still some uncertainties about the influence of relative density of sand and normal stress level on the interface behaviour.

Also some other tests need to be conducted in order to provide insight into some other engineering phenomena. The interface stress-displacement relation depends on the normal condition, i.e., the boundary condition in the direction normal to the interface surface. Most of the existing test results are obtained under the condition of constant normal stress. Under different normal conditions, the sample with different relative density will have different tendency of deformation, such as dilation and contraction, which influences the volume change and normal stress. A limited amount of work has been done in the investigation of the soil-structure interface behaviour under the condition of constant volume. Boulon and Nova (1990) reported the direct shear type interface tests using dense coarse Hostun sand and a rough metal plate under constant volume conditions. There is a clear difference between the results of constant normal stress and constant volume tests. In engineering practice, the constant volume condition applies to the undrained cases where both soil mass and interface material have no volume change. More specifically, the interface behaviour under constant volume conditions should be tested on saturated samples under undrained conditions. During undrained loading, a significant amount of excess pore water pressure may develop in the interface zone and a reduction in the normal effective stress may lead to liquefaction. The load transfer at interfaces in undrained loading conditions may have significant practical importance and needs to be studied. However, there is no experimental and theoretical investigations reported in the literature in relation to liquefaction studies at soil-structure interfaces.

In engineering applications, laboratory experiments are carried out to determine the shear strength parameters and stress-displacement relations of interfaces. Only in a limited number of research work on sand, observations on particle movements were made to gain a deeper understanding of the pattern of particle movements and the shear band formation. It is very difficult, however, to observe both the translations and rotations of the sand particles accurately.

On the numerical analysis side of investigations of soil-structure interface behaviour, several interface models and constitutive relations have been developed. Up to now, almost all models are derived from interface test results and use conventional continuum mechanics concepts. More recently, a number of constitutive models for interfaces used the Cosserat continuum concepts. These models account for grain rotations and use the mean grain diameter as the characteristic length. There is no model that can take into consideration particle size distribution, soil fabric and particle movements. There is no model at present which can simulate the formation of shear bands.

Before conducting this research, there were three questions raised regarding the sand-steel interface behaviour:

(1) Is it possible to simulate sand-steel interface behaviour using some numerical method which takes into consideration the particle size distribution, soil fabric and particle movements?

(2) Are the numerical observations of particle movements at the interface reasonable?

(3) Is it possible to create experimentally the conditions required for liquefaction at the sand-steel interface based on the existing interface testing device?

1.2 Research Objectives

The main objectives of this research are as follows:

1. To determine the advantages and limitations of using the Discrete Element Method, DEM, in the simulations of soil-structure interface behaviour.
2. To investigate numerically the movements of particles in sand-steel interface tests and to determine the effects of the side walls on the movements of soil particles in a direct shear box using DEM simulations.
3. To determine numerically the interface thickness.
4. To investigate experimentally the effects of the initial state of a sample and the boundary conditions on the sand-steel interface behaviour.
5. To simulate experimentally the liquefaction phenomenon.

1.3 Scope of Research

In order to achieve the above objectives, the following studies were conducted in this research:

1. A series of sand-steel interface tests were carried out on samples with various initial states under various normal boundary conditions. First the constant normal stress tests were conducted to provide a basis for comparison with the constant volume test results and to provide input information for conducting DEM simulation. Then the constant volume tests were conducted to simulate undrained conditions under monotonic and cyclic loading conditions.
2. Numerical simulations of sand-steel interface tests were performed using the discrete element method. The effects of particle shape and sample fabric were evaluated for a dense sand–rough steel plate interface test under constant normal stress conditions. Then, the behaviour of a loose sand–smooth steel plate interface test under constant volume condition is examined.
3. Particle movements in the numerical simulation of a sand–steel interface were determined. Using DEM simulations, the interface thickness and the effects of the side walls of the soil container were evaluated.

1.4 Outline of Thesis

The thesis is organized in the following way.

Chapter 2 presents a literature review on the experimental investigations of soil-structure interface behaviour. Presently available interface testing apparatuses, their characteristics, boundary conditions, stress paths, and observed interface behaviour are discussed.

Chapter 3 presents the results of two-dimensional monotonic and cyclic tests under constant normal stress and constant volume conditions. In this chapter, the behaviour of interface between sand and steel were experimentally investigated. First, the effects of initial relative density and normal stress on interface behaviour were examined in dense sand-rough steel plate interface tests under constant normal stress condition. Then, constant volume tests were conducted on an interface between loose sand and a smooth steel plate, while measurements were taken under monotonic as well as cyclic loading conditions.

Chapter 4 describes the main developments in numerical simulation of soil-structure interface behaviour, including the advantages and disadvantages of various existing interface models and constitutive relations.

Chapter 5 presents an introduction to the discrete element methods. A two-dimensional discrete element method program PFC^{2D} employed in this research is also described including its mechanics and formulations to some detail.

Chapter 6 presents the results of the discrete element simulation of sand–steel interface behaviour under constant normal stress and constant volume conditions. PFC^{2D} is used in the simulations. Circular particles, as well as units of two circular particles bonded together, i.e., peanuts, are used in various calculations to investigate the effect of particle shape. The advantages and limitations of using the discrete element method to simulate the behaviour of an interface between a granular soil and a steel plate, are evaluated.

Chapter 7 describes the numerical "observations" of particle movements at sand-steel interface using the discrete element method. First, existing experimental investigations, reported in the literature, of sand particle movements at the interface are summarized. Then, the discrete element method is used to investigate the interface mechanism, side wall effects of direct shear box and velocity field at a sand-steel interface test.

Chapter 8 presents the conclusions of the present research and the suggestions for further studies.

In Appendix A, the procedures for conducting interface tests with C3DSSI under various boundary conditions are described.

PART 1 EXPERIMENTAL STUDY ON SAND-STEEL INTERFACE BEHAVIOUR

CHAPTER 2

EXPERIMENTAL INVESTIGATION OF SOIL-STRUCTURE INTERFACE BEHAVIOUR — LITERATURE REVIEW

2.1 Development of Interface Test Apparatuses

Most soil-structure interface testing devices are designed to measure relative displacement between the soil and the structural materials under applied loads. For research purposes, it is also necessary to measure separately the slip at the interface and the shear deformation of the soil mass. Ideally, an interface testing device should be capable of imposing all possible boundary conditions and any desired stress path.

2.1.1 Boundary conditions of interfaces

The boundary condition in the direction normal to the soil-structure interface surface is an important factor affecting the interface behaviour. In engineering practice, these boundary conditions may take multiple forms ranging from free to full constraint. The constraint provided by the surrounding material gives rise to a change in the normal stress across the interface. The significance of proper modelling of the in-situ normal stress in the interface test has been pointed out among others by Goodman et al. (1968) for jointed rocks.

There are certain types of engineering problems, for example, in studies of slope stability, which hold the boundary condition of constant normal stress. However, there exists a class of practical problems where the normal stress acting on the interface may not remain constant as sliding occurs. If dilation or contraction were to accompany the shear motion and if soil, rock, or structure on both sides of the interface were constrained in any way, then the normal stress could change during the shearing process. In such cases, it could be unrealistic to model the interface behaviour in the laboratory by maintaining a constant normal stress during shearing. More representative behaviour would be observed if the laboratory tests were carried out under conditions of constant normal stiffness. A particular example in practice where conditions of constant normal stiffness are likely to prevail is at the interface between a pile socketed into rock or a pile section grouted into a soil or rock foundation.

The aforementioned normal stiffness in the direction normal to the interface plane, is usually denoted by K defined as the ratio of the variation of normal stress to the variation of normal displacement, i.e., $K = d\sigma_n / dv$. This normal stiffness may vary between zero for an interface under constant normal stress (Fig.2.1a) and infinity if no change in interface normal deformation is allowed (i.e., dilation and contraction are completely prohibited) (Fig.2.1b). The latter refers to as the normal boundary condition of constant volume. The normal stiffness is constant if the change in normal stress remains proportional to the change in normal displacement of the interface (Fig.2.1c). This normal stiffness may also vary with the load history of the surrounding soil or rock mass. Note that above defined normal stiffness K is a property of the surrounding soil or rock mass or any applied reinforcement system and should not be confused with the interface normal stiffness in numerical modelling.

In engineering practice, constant volume condition only applies to the undrained cases where both soil mass and interface material have no volume change and the rock with very high stiffness. Theoretically speaking, the interface behaviour with constant volume condition should be tested on the saturated sample under the undrained condition. For the dry soils, the high deformability makes constant normal stress and stiffness tests more applicable.

Generally speaking, a constant or variable normal stiffness condition is more likely to exist in situ rather than a constant normal stress or volume. In the case of a variable normal stiffness, K may be either increasing or decreasing from an initial value as the shear stress increases.

2.1.2 Stress paths of interfaces

In the interfaces, stress path can be divided into two components, i.e., shear and normal stress paths. Due to the evident coupling effect of shear and normal components, the shear behaviour of the interface can be adequately modelled only if the normal stress path is properly considered.

Under the condition of constant normal stress, the normal stress path is very simple. In other cases, however, loading, unloading and reloading may occur in shear direction as well as in the normal direction. This makes stress path of the interface complicated. The stress path is also influenced by the load form, which includes monotonic, cyclic and dynamic. In some cases, the cyclic loading can be used to represent dynamic environment.

Besides two-dimensional consideration of the interface, three-dimensional simulation is also necessary due to the fact that most of practical problems are three-dimensional. In three-dimensional cases, shear forces, act not only in one direction but also in other direction such as orthogonal direction within the interface plane. The resultant shear force direction may remain unchanged or rotate. An evident example is the pile in soil under the action of axial load and torsion which may be monotonic or cyclic. The resulted displacement path within the interface plane may be a circle, an ellipse, or in any form. As a second example, the soil-structure systems subjected to cyclic rotational loading paths have also been pointed out (Fakharian, 1996). Some approaches for anti-seismic design allow the sliding of structures or the relative displacements between soil and structure during earthquakes. The displacement of a sliding structure depends on the coefficient of friction at its base. Since the direction of cyclic loads resulted from earthquakes usually change during the response of the soil-structure systems, the interfaces may be subjected to rotational loads or rotational displacement paths.

2.1.3 Apparatuses and characteristics

(1) Direct shear type

The direct shear testing of interfaces is similar to the direct shear testing of soils. A hollow square box, containing the soil sample, rests on a construction material such as steel, concrete or wood. A normal load is applied by a loading platen to the top of the soil sample, and then a horizontal load is applied to shear the interface between the soil and the construction material.

Potyondy (1961) was the first to perform a comprehensive series of direct shear tests to determine the skin friction between different type of soils and construction materials, both by strain controlled and stress controlled methods. For the strain controlled tests, the box had an area of 3600 mm^2. A box with an area of 8000 mm^2 was used for the stress controlled tests. The samples of construction materials were placed in the lower half of the box, and the soil such as sand and clay was placed in the upper half. Constant normal load was applied throughout the tests.

Since the mid of 1970, Desai et al. started to develop a cyclic multi-degree-of-freedom interface shear device to study the friction between sand and steel/concrete under cyclic loading conditions. By this apparatus, both cyclic shear tests under constant normal stress and cyclic combined normal and shear tests can be conducted (Desai et al., 1985).

Leichnitz (1985) developed a computer-controlled direct shear device to study the behaviour of rock discontinuities, where a servo-valve and a hydraulic jack were used for providing constant normal stiffness condition. Ooi and Carter (1987) described another constant normal stiffness direct shear device capable of applying static and cyclic shear loading to a specimen containing one of a variety of possible interfaces.

Boulon and Plytas (1986) developed a direct shear type apparatus capable of testing soil-construction material interfaces under constant normal stress, constant volume and constant normal stiffness conditions. For achieving constant normal stiffness, the direct shear box was modified, where the weight which generates constant normal stress was replaced by a spring of an adequate stiffness.

The direct shear type apparatus is the simplest system in sample preparation and test procedure. The direct shear device for soil testing is available in most of geotechnical laboratories, which may easily be employed for interface testing with some modifications. However, the major shortcomings of this apparatus are the development of heterogeneity in the sample along the direction of shear as the test progresses, the stress concentration at the ends, a loss of material between the half boxes or the half box and the plate, a tilting of the half box inducing additional friction, and also the difficulty of separating the interface sliding displacement and the displacement due to soil deformation. Comparing with other apparatuses, this type of device can be operated in three-dimensional space.

(2) Annular shear type

The annular shear type apparatus has been used by Brummund and Leonards (1973) for experimental study of static and dynamic friction between sand and typical construction materials. It consists of a cylinder of sand encased in a rubber membrane with a 28.6 mm diameter, 356 mm long rod located along its axis. By evacuating air from within the membrane, a normal stress is applied to the sand-rod interface that ranges from 8.6 to 86 kPa. The rod is then caused to slip relative to the sand by gradually applying static forces to the rod in the axial direction. The dynamic force is applied using a shock tube. The coefficient of friction between sand and different materials such as steel, Teflon, cement mortar, and graphite was measured using this apparatus.

Annular shear apparatus, actually, is the axisymmetric direct shear type device, and is geometrically identical to shaft resistance of pile shafts and also frictional resistance of steel reinforcement elements. The stress field in this test proves to be very inhomogeneous both radially and axially and only average values can be obtained. Moreover, with this system there are unknown normal stresses on the interface and stress concentration occurs at all ends.

Annular shear type apparatus may simulate three-dimensional stress conditions by applying a torque, in addition to the axial load, to the rod surrounded by soil. However, distinguishing between shear deformation of soil and slip at the interface is not possible along the circumferential direction. So, there is no practical way to extend this type device to operate in three-dimensional mode.

(3) Ring torsion type

Huck et al. (1973) and Huck and Saxena (1981) conducted valuable experimental investigation on soil-concrete interface phenomena under static and dynamic shear loading conditions. In their works, a ring simple shear apparatus was used, where the soil sample confined inside and outside by standard triaxial membranes was in contact with the lower and upper concrete rings which were held by steel holders.

A ring torsion apparatus (simple shear) was used by Yoshimi and Kishida (1981a,b). Dry sand was rained into an annular container lined with 0.3 mm thick rubber membrane, and the top surface of the sand was levelled with a suction device. Then a ring shaped metal sample was place on the sand as the construction material. A static torque was applied to shear the interface under either constant normal stress or constant volume conditions. In addition to measurements of circumferential and vertical displacements of the metal ring, the deformation of the sand and slippage at the soil-metal contact were measured in some tests using x-ray radiography.

The geometry of the device allows unlimited circumferential displacement, and reduces somewhat the non-uniformities, due to edge effect, of normal and shear stresses at the contact surface and within the soil sample. The constitution of the sample makes it difficult to differentiate between simple and direct shear phenomena, although the sliding displacement and the displacement due to shear deformation can be distinguished by using x-ray photography. The ring torsion type apparatus is a complicated system in terms of sample preparation and measurement of shear displacements. Besides, a systematic error arises due to a radial gradient of tangential relative displacement. The ring torsion type apparatus cannot be modified to operate in three-dimensional mode.

(4) Simple shear type

Uesugi and Kishida (1986a) developed a simple shear type device which was capable of measuring both sliding displacement between steel and soil as well as shear deformation of soil mass. The contact surface between steel and sand was originally 400 mm in length and 100 mm in breadth. The area of friction surface remained constant during a test even if sliding occurred, since the steel plate was longer than the friction surface. Normal and tangential loads were applied by the vertical and horizontal hydraulic actuators. The container of sand specimen was a stack of rectangular 2 mm thick aluminium plates with 400 mm $\times$ 100 mm space in the middle. The surface of each plate was lubricated to allow the container to follow the shearing deformation of sand with minimum friction resistance.

Uesugi and Kishida (1986b) also used another simple shear type apparatus in which the sample had a smaller contact surface of 100 mm $\times$ 40 mm. This apparatus was used for one-way and two-way repeated loading of interfaces between sand-steel and sand-concrete (Uesugi et al. 1989, 1990). In these two apparatuses, normal load was measured by a strain gage type transducer and kept constant by a servomechanism. Tangential load was measured by the same type of transducer, and applied by another servomechanism to keep the tangential displacement in control.

Besides having the advantages of the direct shear type apparatus, the simple shear type apparatus has solved the problem of separation between sliding displacement and shear deformation of soil sample. But it still has the disadvantage of stress concentration at the ends. This type of device can be extended to operate in three-dimensional space.

(5) Plane strain apparatus

A modified plane strain apparatus was used by Tejchman and Wu (1995) for measurement of friction between a sand specimen and a steel plate. The cross section of the sand specimen was chosen to be 4 cm × 8 cm. A wooden wedge with an angle of 67.5° against the horizontal was covered with a steel plate. The angle of the wooden wedge was chosen to be the inclination of the mobilised plane according to the Coulomb failure criterion. The wooden wedge was placed at the bottom of the sand mould. The wedge and the sand specimen were enclosed by a rubber membrane, and confined between two rigid platens. The whole set-up was placed into a chamber with pressure supplied by pressurised air and kept constant throughout the test. The vertical driving force was applied by moving the loading piston downwards. In comparison with other shear devices, the plane strain apparatus has the advantage that all stress components in the plane of shearing can be determined. The disadvantages are: (1) stress concentration at the end of the specimen; (2) decreasing shear surface during the deformation and (3) validity of results only in the range of high cell pressures. After the experiments were terminated, the volume change along the steel plate observed by means of X-rays. On the radiographs the dilated zone was marked by a dark region because dense sand absorbed more X-rays than loose sand.

(6) 3-D apparatus

Experimental studies of soil-structure interfaces have been carried out using different techniques. They generally measure two-dimensional interface behaviour. This kind of testing is appropriate for interfaces in two-dimensional soil-structure systems such as axially loaded piles. Many other practical systems, however, are subjected to three-dimensional loading. For example, the wind, waves, ice, and ocean currents result in combined repeated axial and lateral loads on offshore gravity structures; power transmission lines are subjected to loads caused by wind and earthquakes, resulting in repeated loads on their foundations; and highway bridges are subjected to a combination of a large dead load, repeated axial and lateral loads from traffic, and repeated lateral loads from wind. The solution of these problems require that the interface tests be conducted in three-dimensional mode.

For this purpose, a computer-automated apparatus for monotonic and cyclic testing of interfaces between soil and structural materials under three-dimensional stress conditions was developed by Fakharian and Evgin (1993, 1996). The soil is placed in the shear box on the underlying steel plate. Either displacement-controlled or load-controlled test can be conducted simultaneously in all three directions. Direct shear type and simple shear type soil container can be used with an inside area of 100 mm × 100 mm. The simple shear box consists of a stack of 2 mm thick anodised, Teflon coated, square aluminium plates. The sliding displacement can be distinguished from the shear deformation of the soil mass. Two identical ball screw stepper motors are used to directly apply the tangential forces to the contact surface in two orthogonal directions, a motorised air regulator, which is operated by a built-in stepper motor, adjusts the pressure for the E / P actuator to apply load in normal direction. The control and data-acquisition are performed by a closed-loop computer controlled system. Therefore, various interface shearing paths can be easily realised. Besides constant normal stress and constant volume conditions, constant normal stiffness condition can also be applied in the direction normal to the interface.

2.2 Test Results

2.2.1 Summary of tests

With the publication of the results of experimental studies on soil-structure interfaces, some factors have been recognised to have effects on shear strength and stress-displacement relation of the interfaces. Table 2.1 shows a summary of some existing soil-structure interface tests, where Apparatus includes type of apparatus used, type of control on tangential displacement or load, two- or three-dimensional testing conditions; Loading conditions include type of loading, rate of loading (R_l) or frequency (f or ω), and normal condition; Sample dimensions include area of contact surface (A), sample height (h), length (L), diameter (d), inside diameter (d_{in}), outside diameter (d_{out}); Soil properties include soil composition, initial relative density (D_r) and moisture content (ϖ); and Structural material includes material type and roughness (R). According to the tests listed in this table, typical testing results and effects of some influencing factors are summarised in the following subsections.

2.2.2 Test results

Coulomb's law of friction is widely used in engineering practice. It means that if a material, such as soil is in contact with another material like a steel plate, the frictional force can be obtained by $T = \mu N$ where T is the frictional or tangential force required to induce relative displacement at the contact surface, μ is the coefficient of friction, and N is the normal load between the two materials. Here, the adhesion between two materials is neglected. If dividing the normal load and shear force by the contact surface area to convert them to normal stress and shear stress and considering the adhesion c between the two materials, then the Mohr-Coulomb failure criterion is obtained as follows

$$\tau_f = c + \sigma_n \tan\delta \tag{2-1}$$

where τ_f and σ_n are the shear stress and normal stress at failure along the contact surface,

Table 2.1 Description of some existing soil-structural materials interface tests

Conducted by	Apparatus	Loading conditions	Sample dimensions	Soil properties	Structural material
Potyondy (1961)	Direct shear type, strain- and stress-controlled, 2-D	Monotonic, constant normal stress	A = 6×6 cm^2 and 9×9 cm^2	(1) Sand, low and high D_r, dry and saturated (2) Clay, medium PI (3) Mixture of 50% sand and 50% clay	(1) Mild steel, smooth and rough (2) Wood, shaped by planning (3) Concrete, smooth and rough
Brumund and Leonards (1973)	Annular shear type, stress-controlled, 2-D	Static and dynamic (step-type force), constant normal stress	d = 1 1/8 in or 2 in, L = 10 in, h = 3 - 3 7/8 in	(1) Uniformly graded sand, $D_r \approx$ 90%, Dry (2) Crushed sand, $D_r \approx$ 90%, Dry	(1) Plain steel (2) Teflon coated steel (3) Graphite coated steel (4) Plain smooth mortar (5) Teflon coated smooth mortar (6) Graphite coated smooth mortar (7) Plain rough mortar
Huck et al. (1973) Huck and Saxena (1981)	Ring simple shear torsion type, 2-D	Static and dynamic, constant normal stress	d_{in} = 12.7 cm, d_{out} = 17.7 cm, h_{max} = 2.5 cm	(1) Ottawa sand, $D_r \approx$ 80% (2) Edgar plastic Kaolin clay, ϖ = 5.5%	Concrete, rough and smooth
Yoshimi and Kishida (1981a,b)	Ring simple shear torsion type, displacement-controlled, 2-D	Static, R_l = 0.6 mm/min, constant normal stress or constant volume	d_{in} = 24 cm, d_{out} = 28.8 cm, h = 0.9 - 4.2 cm	Sands, 3 kinds, D_r = 40% - 90%, Dry	Steel, brass, and aluminium, smooth to rough
Acar et al. (1982)	Direct shear type, deformation-controlled, 2-D	Static, constant normal stress		Quartz sand	(1) Steel, smooth (2) White pine without irregularities (3) Concrete
Boulon and Plytas (1986) Boulon and Nova (1990)	Direct shear type (circular shaped shear box), 2-D	Monotonic, constant normal stress, constant volume, and constant normal stiffness	d = 10 cm and 6 cm	Hostun sand, dense, coarse - medium, dry	Metal plate, rough
Uesugi and Kishida (1986a) Kishida and Uesugi (1987)	Direct and simple shear type, displacement-controlled, 2-D	Static, constant normal stress	A = 400×100 mm^2, h = 10 - 29 mm	Sands 3 kinds, D_{50} = 0.15 - 0.62 mm, $D_r \approx$ 90%, Dry	Low-carbon steel, smooth to rough
Uesugi and Kishida (1986b)	Direct and simple shear type, displacement-controlled, 2-D	Static, constant normal stress	A=100×40 mm^2 h = 24 mm (17 mm for direct hear box)	Sands 3 kinds, D_{50} = 0.16 - 1.82 mm,	Low-carbon steel, smooth to rough
Uesugi et al (1988)	Simple shear type, stress- and displacement-controlled, 2-D	Static, constant normal stress	A = 400×100 mm^2, h = 30 mm	Seto sand, $D_r \approx$ 90%, Dry	Low-carbon steel, smooth to rough
Uesugi et al (1989)	Simple shear type, displacement-controlled, 2-D	Monotonic, R_l = 1 mm/min, repeated, constant normal stress	A = 100×40 mm^2, h = 24 mm	Sands, 3 kinds, $D_r \approx$ 90%, almost dry	Low-carbon steel, smooth to rough
Uesugi et al (1990)	Simple shear type, displacement-controlled, 2-D	Monotonic, R_l = 1 mm/min, repeated, two-way (sinusoidal), constant normal stress	A = 100×40 mm^2, h = 24 mm	Toyoura sand, Seto sand, Air-dried	Concrete, two kinds of cement mortars, R_{max} = 6 - 50 µm (L = 0.2 mm)
Tejchman and Wu (1995)	(a) Direct shear type, displacement-controlled, 2-D (b) Modified plane strain type, displacement-controlled, 2-D	(a) Static, constant normal stress (b) Static, varying normal stress	(b) Width = 4 cm, height = 8 cm	Karlsruhe sand, D_{50} = 0.45 - 0.50 mm, Dry	Steel, smooth to rough
Paikowsky et al. (1995)	Direct and simple shear type, displacement-controlled, 2-D	Static, R_l = 1.3 mm/min, constant normal stress and constant volume	A = 40×12.5 cm^2	Ottawa sand, Dry	Steel, smooth to rough

respectively; δ is the angle of interface friction. The above equation defines a failure envelope for the friction between the two materials shown in Fig.2.2, where δ is the slope of the failure envelope and c is its intercept with the τ_f axis, τ_f and σ_n are obtained from interface stress-displacement relation curves.

Potyondy (1961) proposed to express the skin friction resistance in a similar form to Eq.(2-1) as a sum of the adhesion and the normal stress dependent component. Previously, the mutual effect of soils and structures in the transmission of forces from one to the other through the contact surface was called "skin friction". Other terms such as skin resistance and frictional resistance were also used. They are often expressed as the coefficient of friction at yield $\mu_y = T / N$ or $\mu_y = \tau_f / \sigma_n$, which is indicated in Fig.2.3. It should be noted that the relation $\mu_y = \tan\delta$ exists only for the case where the adhesion is not considered. The residual coefficient of friction, μ_r, is defined as shown in Fig.2.3.

The interface shear strength parameters are normally required for instability investigation of practical engineering problems such as retaining walls, foundations and piles. However, because skin friction is usually not statically determinate, for rigorous and realistic analysis of soil-structure systems, e.g., for establishing the constitutive model of soil-structure interface in order to conduct the finite element analysis of the whole failure process, not only the maximum interface frictional resistance but also the stress-displacement relations at the interface are essentially required.

Based on reviewing the results of the tests listed above, soil-structure interface behaviour is generally summarised in the following.

Observations of the soil-structure interface friction test results indicate that such interface behaves nonlinearly from the viewpoint of stress development accompanying relative sliding displacement. Before shear stress ratio reaches the maximum coefficient of friction, the shear deformation of sand is the major factor of tangential displacement. After the yielding of the interface, the sliding displacement becomes the major factor of tangential displacement while the shear deformation of sand remains almost constant.

Both the surface roughness and the soil density are found to have a considerable effect on the interface behaviour. The stress-displacement curves for dense sand along a rough surface show a clear peak with a pronounced strain softening. After an initial contraction stage, the volume change is strongly dilatant and finally stagnates at a certain stage of displacement. Both the stress ratio and the volume change increase with increasing roughness. But the shear deformation of sand mass is not affected by the surface roughness. It should be noted that in the case with a very high normal stress, after a reduction in shear stress ratio just after the peak, the shear stress ratio increases again gradually with the increase of total displacement rather than remains constant as usual. For loose sand the stress-displacement curves reach asymptotically a plateau. The corresponding volume change is contractant throughout.

Under one-way repeated loading, the frictional resistance is close to that under monotonic loading. During the unloading and re-loading stages, there is little sliding at the interface. Under two-way repeated loading, the interface sliding is much smaller than the total displacement and the maximum shear stress ratio decreases gradually in the early numbers of loading cycles. After several cycles, the amplitude of sliding becomes close to the total displacement, and the maximum shear stress ratio becomes constant. Under two-way repeated loading, the interface sliding is not negligibly small in the reloading stage. This sliding displacement can be attributed to the inelastic deformation of shear zone under stress reversal. The shear deformation of sand mass does not return to zero and remains positive even the tangential load is applied in the reverse direction.

The static coefficient of friction is affected by sand type (i.e., soil composition considering the size distribution, angularity, and surface texture of the sand grains), regardless of the nature of the surface against which slip is occurring. When the sliding surface is rough in comparison to the grain size of the sand, the angle of interface friction exceeds the angle of shearing resistance of the sand and sand / sand slip occurs. In static tests, shearing rate has no effect on coefficient of friction for dry sand. However, the dynamic coefficient of friction is about 20% greater than the static coefficient of friction, unless the conditions for sand / sand slip are approached. It has been observed that the apparatus type and the sample dimension have minor effects on the maximum coefficient of friction in some tests.

The roughness of contact surface is determined in a certain gauge length for which the particle size (i.e., D_{50}) must be taken into account. It is found that the maximum coefficient of friction is mainly dependent on the surface roughness of solid material and mean particle diameter. The effects of these two factors can be combined into the influence of so-called normalised roughness. The upper limit to the maximum coefficient of friction is the maximum shear stress ratio of sand dependent on the relative density.

There are some conflicts on the effects of normal stress and relative density of sand (i.e., minor or apparent), type of interface failure envelope (i.e., linear or nonlinear, with or without adhesion) for the sand-solid interface. In some tests, relative density of sand and normal stress are found to play a negligible role. However, other tests confirmed that the maximum coefficient of friction decreases with increasing normal stress and decreasing relative density of sand. This variation has the order of about 0.1 to 0.2. In the tests with loose sand, shear failure takes place within the sand mass rather than the sand-solid interface. For the loose sand cases, the maximum coefficient of friction is almost constant irrespective of contact surface roughness.

Residual coefficient of friction under two-way repeated loading remains constant irrespective of the interface roughness and the type of sand. This value is close to the residual coefficient of friction under monotonic loading and the residual shear stress ratio of sand. However, some type of sand has a lower residual coefficient of friction at lower roughness because of the fact that the normal stress makes difference in residual coefficient of friction for this type of sand.

The interface is a thin shear zone along the contact surface between soil and construction material. The interface soil undergoes very large structural changes and grains crushing during the localised shear. The interface thickness is usually within the range of 2 to 8 times the mean grain size. The relative density of sand in shear zone is lower than that of the sand before the interface failure. The lower density of sand in the shear zone results in the lower maximum shear stress ratio. Therefore the upper limit to the coefficient of friction decreases because of the shear zone formation.

2.3 Recommendation

Due to the elaborate works done by Uesugi and others, it seems that only the normalised roughness of contact surface influences the interface behaviour. It might be true in the maximum coefficient of friction on the interface. But there are many other factors influencing the shape of the shear stress - tangential displacement curves and the volume change characteristics, and even the maximum coefficient of friction to some extent. For establishing interface failure criteria and constitutive models in order to represent reasonably the real life in engineering analysis, the following aspects need to be further considered.

(1) The sand may have certain moisture content, or may be fully saturated. Two kinds of drainage conditions, i.e., consolidated - drained condition and consolidated - undrained condition, may exist at the interface.

(2) The interface behaviour under earthquakes may be evaluated with the test results under cyclic loading. However, other dynamic loading conditions such as impact may make interface behaviour totally different from the behaviour in static and cyclic loading.

(3) Normal boundary condition influences the interface behaviour. The type of normal boundary condition is different in different situations, and also the value of normal boundary condition may actually change during shearing (e.g., normal stress or stiffness change due to the volume change of interface zone). Also the various normal stresses related to certain initial relative density of the sample result in some change in the interface behaviour curves (Fakharian, 1996). Most existing test results are for constant normal stress condition. Although constant or variable normal stiffness conditions are more likely to exist across the interface in situ rather than constant normal stress or displacement, the interface response under constant or variable normal stiffness has not received much attention in the literature.

(4) The initial relative density of sand is determined by the sample preparation method, then is changed by the application of normal load. Overconsolidation or prestress (stress history) might make difference in interface behaviour and failure envelope. Sample preparation method, application of normal load and overconsolidation change sample

fabric and relative density. The relative density is the only thing which can be measured on the sample. So, test results might be summarised with respect to the relative density of the sample just before shearing.

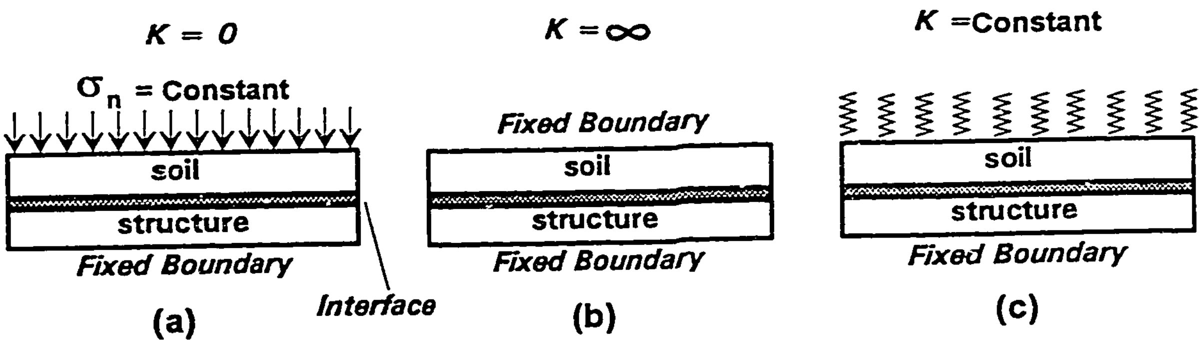

Fig.2.1 Boundary conditions in the normal direction: (a) constant normal stress, (b) constant volume, (c) constant normal stiffness (after Fakharian, 1996)

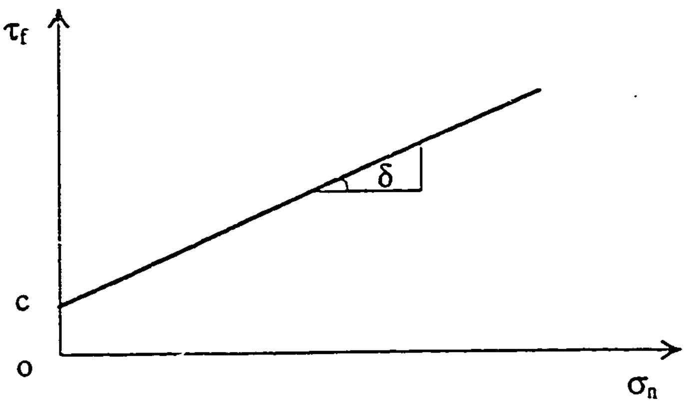

Fig.2.2 Mohr-Coulomb failure criterion

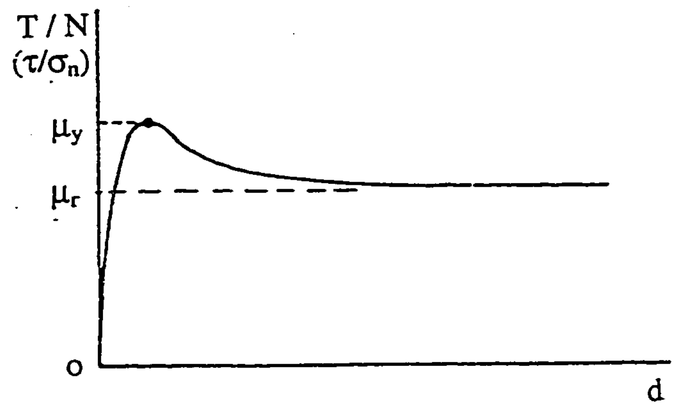

Fig.2.3 Shear stress ratio curve

CHAPTER 3

EXPERIMENTAL OBSERVATIONS OF SAND-STEEL INTERFACE BEHAVIOUR

3.1 Introduction

Yoshimi and Kishida (1981a,b) have reached the conclusion that the coefficient of friction is essentially governed by the surface roughness of the structural material. The relative density of the sand and the type of structural material play a negligible role on the value of coefficient of friction. The type of sand also has little influence on the coefficient of friction if the surface roughness R_{max} (L = 2.5 mm) exceeds about 20 μm. By using the experimental results, Uesugi and Kishida (1986a) concluded that the influence of sand type and the surface roughness of steel on coefficient of friction is significant, while the effects of normal stress and mean grain size are of poor significance. Only little influence of normal stress up to 3.9 MPa was observed on frictional coefficient. Later, they (1986b) concluded that the relative density of the sand only makes the upper-bound of the coefficient of friction different, and that the mean grain size (D_{50}) also has a significant influence on the coefficient of friction at yield. In contrast, Acar et al. (1982) conducted direct shear testing on interfaces between sand and structural materials such as steel, wood and concrete, and concluded that relative density of sand and normal stress obviously influenced the angle of friction. This evidence showed that the influence of relative density of sand and normal stress level on the interface behaviour were also given by others, such as Desai et al. (1984) and Fakharian and Evgin (1996). This literature review indicates that there exists an unclear understanding of the influence of relative density of sand and normal stress level on the interface behaviour due to the limitations of test data and the differences in testing methods.

The interface stress-displacement relation depends on normal boundary conditions. Most of the existing test results were obtained under the condition of constant normal stress. Initial normal stress level influences the relative density of sand. Under different normal boundary conditions, samples with different relative densities will have different tendency of deformation, such as dilation and contraction, which influences the variation of volume and changes of normal stress. Limited work has been done in the investigation of the soil-structure interface behaviour under the condition of constant volume and constant normal stiffness. Boulon and Nova (1990) reported the results of direct shear tests on an interface of dense coarse Hostun sand and a rough metal plate under constant volume condition. A clear difference exists between the results of constant normal stress and constant volume tests. Actually, this study has been done in the midth of 1980 (Boulon and Plytas, 1986). Evgin and Fakharian (1996) conducted series of tests on interfaces between sand and steel under conditions of constant normal stress and constant normal stiffness considering 2-D and 3-D monotonic loading by using a 3-D cyclic interface testing device. They concluded that the peak stress ratio is dependent on the magnitude of the normal stress measured at the time when the stress ratio is at its peak, and shear stress behaviour is largely affected by the magnitude of the normal stiffness in 2-D tests under constant normal stiffness condition.

Liquefaction is an important phenomenon in engineering practice. During undrained loading, a significant amount of excess pore water pressure would develop in the interface zone and a reduction in the normal effective stress would lead to liquefaction. Liquefaction in the interface zone would damage the load transfer capability of an interface. The load transfer at interfaces in undrained loading conditions has significant practical importance and needs to be studied. However, there is no experimental and theoretical investigations reported in the literature in relation to liquefaction at soil-structure interfaces. And also there is a need for further research to develop and to validate mathematical models which can account for both drained and undrained behaviour of interfaces.

Constant volume interface tests (Evgin et al., 1996) showed that the magnitude of the normal stress would reduce to zero during shearing. This presents a strong physical analogy relation between the constant volume test of interface and the liquefaction at interface where pore water pressure increases and both effective normal stress and shear stress would reduce to zero during the process of shearing. On the other hand, Negussey et al. (1988) have concluded that the presence of pore water had no noticeable effect on the observed value of constant-volume friction angle of Ottawa sand. All these studies justify that it is reasonable to qualitatively investigate the liquefaction at interfaces by using constant volume interface tests.

In this chapter, the behaviour of an interface of sand and steel was experimentally investigated. First, the effects of initial state of the sample such as initial relative density and normal stress were examined in dense sand - rough steel plate interface tests under constant normal stress condition. Then, constant volume tests were conducted on the interface of loose sand and a smooth steel plate, while measurements were taken under monotonic as well as cyclic loading conditions. The influence of the initial state of sand samples were also examined in constant volume tests.

3.2 C3DSSI Apparatus

An automated 3-D apparatus C3DSSI (i.e., Cyclic 3-Dimensional Simple Shear testing of Interfaces) was used in this study. The schematic view of this apparatus is shown in Fig.3.1. The operation of the interface apparatus and the data acquisition are automated by a computer controlled system. The apparatus consists of three major parts:

(1) Loading System

- Reaction frame
- Vertical loading unit (pneumatic actuator)
- Horizontal loading unit (stepper motors)

(2) Soil Containers

- Direct shear type container
- Simple shear type container

(3) Data Acquisition and Computer Control System

- Load cells
- Displacement transducers
- Interface unit

- Computer
- Menu-form software

The apparatus was described in detail by Evgin and Fakharian (1996). A pneumatic actuator is used to apply the normal load on the interface. The operation of this actuator is controlled by a computer to impose a constant normal stress, a constant volume or a constant normal stiffness condition. It is also possible to conduct variable normal stress and variable normal stiffness tests. The constant normal stiffness can be realized by specifying a set point for the stiffness K, while the variable normal stiffness can be simulated by expressing the set point of the stiffness K as a function of the normal stress applied to the interface. The tangential forces are applied to the interface plane through an X-Y loading table by using two ball screw stepper motors, which are capable of applying displacement- or load-controlled shear in both x- and y-directions independently. In this study, displacement-controlled tests were used with a velocity of 1mm/min at which the loading table moved horizontally in x-direction.

This apparatus has both direct shear type and simple shear type soil containers. In this study, a direct shear type soil container was used which is shown in Fig.3.2. The soil container is a 25 mm thick, square aluminum box with an inside area of 100 mm × 100 mm. The bottom of the aluminum container is sealed to a foam to minimize the leakage of sand during shearing. In addition, a 1 mm thick sheet of Teflon is glued to the bottom of the foam layer to minimize the friction between the steel surface and the aluminum box. The box was placed on a 300 mm × 300 mm low carbon steel plate. Since the steel plate is longer than the sand surface, the area of the contact surface remains constant during shearing.

The C3DSSI apparatus was equipped with two transducers measuring the tangential loads (in the x and y directions) and five LVDTs monitoring the displacements (tangential and normal). In this study, only one transducer and two LVDTs were in operation. The transducer was used to measure the tangential load in the x direction. One of the LVDTs was used to measure the tangential displacement in the x direction (i.e., the sliding displacement along the contact surface) (accuracy: 0.002 mm) and the other measured the change of sand height (accuracy: 0.004 mm).

3.3 Testing Materials

(1) Sand

Air-dry-quartz (Silica) sand was used in this study. This medium crushed quartz sand has a D_{50} of 0.6 mm, γ_{max} of 16.05 kN/m^3 and γ_{min} of 12.88 kN/m^3. Its grain size distribution is illustrated in Fig.3.3.

(2) Steel plates

In this investigation, 300×300 mm low carbon steel plates were used as the structural material. Two types of surfaces were investigated in the tests. The smooth plate is well polished and has a roughness R_{max} of 4 μm for a sampling length of L = 0.8 mm. The rough plate was obtained after uniformly sand-blasting the smooth plate and had a roughness R_{max} of 25 μm for a sampling length of L = 0.8 mm.

3.4 Sample Preparation

To prepare the specimen for each test, the hollow aluminum box (direct shear type soil container) is positioned at the center of the steel plate. The sand is rained into the container at the desired density by one of the methods described below. The top surface of the sand is leveled by a suction device. Then the plate is fixed to the top of the loading table of the interface testing device, and the loading platen is moved downward to touch the sand surface.

There are three methods to prepare sand with the desired density:

(1) Scooping method: Loose to medium dense sand samples can be prepared by means of this method. The sand is taken gently by using a scoop and then rained into the container smoothly and uniformly. By using this method, a sand sample with a relative density of about 60% can be obtained.

(2)Multiple sieving pluviation method: Medium to dense sand samples can be prepared by means of this method. The multiple-sieve-pluviation method was described earlier by

Miura and Toki (1982) and then modified by Fakharian and Evgin (1996). It has a funnel at the top for storing the sand. The funnel is supported by a perspex cylinder. Six No.4 sieves (opening 4.75 mm) are placed under the funnel. Below these sieves at an adjustable distance is the soil container. The reason for stacking six sieves is to ensure uniform deposition of sand, and therefore produce a homogeneous sample. The rate of sand discharge is controlled by changing the diameter of the nozzle attached to the bottom of the funnel. A knife edge collar is placed on top of the soil container during sand pluviation to prevent sand particles from falling back into the container.

(3) Low-falling height single-sieving pluviation method: For obtaining a stable and uniform loose state of sand samples, a small raining device was designed, which is a square area funnel with outside dimensions of 100 mm × 100 mm. It has a bottom on which many holes are driven uniformly. During the preparation of samples, the raining device was first placed onto the soil container and in touch with steel plate, second the sand was spooned into the device, then the raining device was smoothly lifted up so that the sand was rained down into the shear box, finally the sand was leveled by suction. After applying an initial normal stress of 5 kPa for reducing seating area and considering the weight of the loading platen, an initial relative density of 15% was achieved.

3.5 Test Plan

A two-dimensional monotonic interface test was first conducted on a dense sand sample with a measured relative density of 81% after the application of a constant normal stress of 100 kPa, which was placed on a rough steel plate with a roughness of 25 μm. The results of this test were used to evaluate the simulation of soil-structure interface behaviour using the discrete element method which will be reported in Chapter 6.

In this chapter, only those tests conducted on the loose sand - smooth steel plate specimens are reported.

In these tests, the effect of relative densities of sand samples was examined. After applying a normal stress of 100 kPa, the sample had a relative density of 24%. If applying a normal stress of 500 kPa, the sample became denser and had a relative density of 34%. After this stage, even if the normal stress was reduced from 500 kPa to 100 kPa, the sample expanded very little. Therefore, it was assumed that the relative density remained at about 34%.

The test plan is shown in Table 3.1. The monotonic and cyclic tests under the conditions of constant normal stress and constant volume were conducted. In the constant normal stress tests, the intensities of the normal stress were 100 kPa and 500 kPa. The constant normal stress tests were conducted to provide a basis for comparison with the constant volume test results and to provide some basic information for conducting DEM simulation. The constant volume tests were conducted to simulate undrained conditions. The intensities of the initial normal stress in the constant volume tests were also 100 kPa and 500 kPa as in the case of constant normal stress tests.

Table 3.1 Test plan

Test No.	$\sigma_{n\ ini}$ (kPa)	Normal condition	Type of shearing	Initial relative density (%)
MS1	100	constant normal stress	monotonic	24
MS2	500	constant normal stress	monotonic	34
MS3	500 → 100	constant normal stress	monotonic	34
MV1	100	constant volume	monotonic	24
MV2	500	constant volume	monotonic	34
MV3	500 → 100	constant volume	monotonic	34
CV1	500	constant volume	cyclic	34
CV2	500 → 100	constant volume	cyclic	34

3.6 Test Results

3.6.1 Constant normal stress tests

The results of the monotonic tests under constant normal stress condition are presented in Fig.3.4. The stress ratio (i.e., shear stress to normal stress) versus tangential displacement curves (Fig.3.4a) show that the values of the maximum stress ratio and the post-peak behaviour of the interface are influenced by the magnitude of the normal stress. For the same initial relative density, lower normal stress (MS3) gives a higher maximum stress ratio at a smaller tangential displacement and a higher residual stress ratio. On the same normal stress level, lower initial relative density (MS1) gives a lower maximum stress ratio at a larger tangential displacement but gives the same post-peak behaviour as in the case with a higher initial relative density. In all three constant normal stress tests, the samples were compressed (Fig.3.4b). Higher normal stress makes the sample compress more during shearing. It can be observed that the sample with a higher initial relative density under lower normal stress (MS3) dilated a little bit initially and then was compressed.

3.6.2 Monotonic constant volume tests

The results of monotonic constant volume tests are shown in Fig.3.5. The shear stress versus tangential displacement curves (Fig.3.5a) show that the shear stress first increases to a peak value while was much lower than that in the corresponding constant normal stress tests and then reduces steadily as the normal stress decreases from its initial value (Fig.3.5b). Since the sample decreased in volume during shearing in constant normal stress tests, the tendency of the sample would also be to decrease in volume in the constant volume tests. Therefore, the normal stress must be reduced in order to prevent any volume change. During the test with 100 kPa initial normal stress (MV1), the reduction in the normal stress is rapid and it becomes "zero" indicating liquefaction. It should be noted that there was heavy fluctuation in the curves when normal stress became lower than certain value , so a dotted line is used to indicate the average tendency of MV1 curves. Due to the fact that the loading platen has a weight of 50 N, a normal stress of 5 kPa was always present on the sample during the tests. So, a normal stress of 5 kPa was adopted in the tests as a "zero" standard for indicating liquefaction. Comparatively, Test MV3 with higher relative density had an initial increase in normal stress, so the peak value of stress ratio was not that much lower than the corresponding value in the constant normal stress test. In the tests MV2 and MV3, the reduction in the value of normal stress during shearing is substantial, yet, the remaining normal stress is still large. That is why cyclic constant volume tests were conducted on these two samples to see whether the normal stress would reduce to zero during shearing cycles.

3.6.3 Cyclic constant volume tests

The last part in this experimental program was cyclic constant volume tests. With an initial normal stress of 500 kPa, the tangential displacement was cycled with an amplitude of one quarter of the tangential displacement at failure in the corresponding constant normal stress test, i.e., between +0.15 mm and -0.15 mm around the original position of the sample as shown in Fig.3.6a and 3.6b. With an initial normal stress of 100 kPa, the tangential displacement was cycled with an amplitude of one quarter of the tangential displacement at failure in the corresponding constant normal stress test, i.e., between +0.04 mm and -0.04 mm around the original position of the sample as shown in Fig.3.6c and 3.6d. In these tests, the normal stress decreased as the number of cycles increased and eventually became "zero" indicating the occurrence of liquefaction.

In Test CV1, normal stress reduced very fast, it was about one quarter of the initial value just after the first cycle. Accordingly, the maximum shear stress in each cycle was quickly reduced by more than 50% after one complete cycle. This is due to the fact that 500 kPa normal stress produced larger compression in the constant normal stress test. Corresponding to the normal deformation characteristic in the constant normal stress test with a normal stress of 100 kPa, normal stress first increased a little bit then reduced gradually with the cycles in Test CV2, the maximum shear stress value in each cycle reduced slowly. These are two different patterns of stress variation during cyclic constant volume tests determined by the initial value of normal stress.

3.7 Summary

In this study, the effects of initial state of sand samples (i.e., relative density and initial normal stress) was examined and the liquefaction at soil-structure interfaces was simulated experimentally. Although there was no water involved in the samples, the constant volume condition was maintained, and the gradual reduction of normal stress to zero was observed as in the case of undrained loading resulting in liquefaction. From the test results of the interface on loose sand - smooth steel plate, the following observations were made which provides insight into the influencing factors of interface behaviour and the liquefaction mechanism at soil-structure interfaces:

(1) The initial state of sample effects the sand-steel interface behaviour. If only the stress ratio is considered, the effect may look small. However, when the development of peak stress, the whole process of load-deformation relation and the development of normal deformation are considered, the effect of the initial state is obvious.

(2) Under the monotonic constant volume loading condition, the shear stress can reach a peak value which is much lower than that in the corresponding constant normal stress test, and then reduces steadily as the normal stress decreases from its initial value. With a relatively loose sand under a low initial normal stress level, the reduction in both normal and shear stresses is rapid and these stresses become "zero" indicating liquefaction.

(3) The cyclic constant volume loading condition can also cause liquefaction at the interface with a relatively dense sand sample indicated by "zero" normal stress. Liquefaction is possible even at small amplitude of displacement cycles such as one quarter of the tangential displacement at failure under the constant normal stress condition. The initial normal stress obviously influences the pattern of stress variation in the cyclic constant volume loading condition. With a high initial normal stress, both the normal stress and the maximum shear stress in each cycle reduce very fast almost suddenly. In contrast, both the normal stress and the maximum shear stress reduce slowly when the initial normal stress is low.

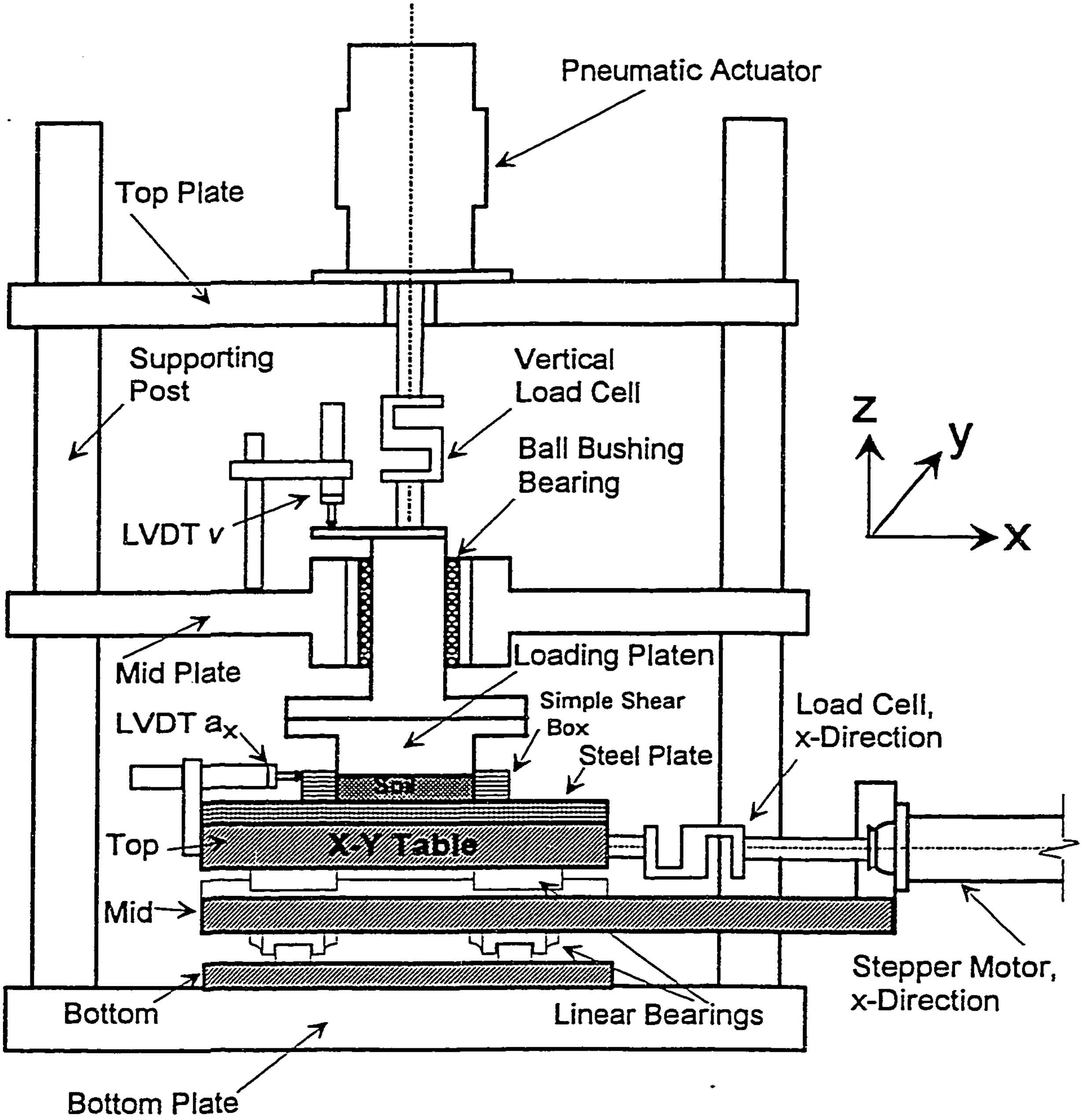

Fig.3.1 Schematic view of C3DSSI (after Fakharian, 1996)

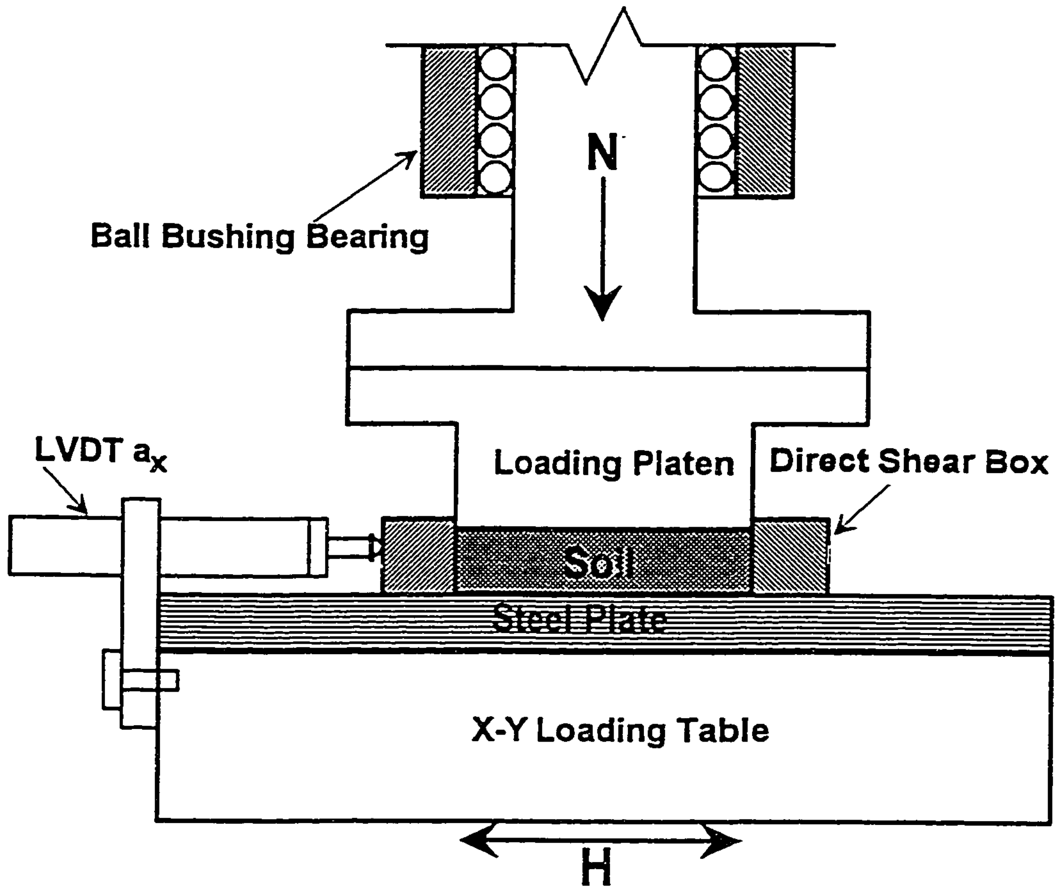

Fig.3.2 Schematic of the direct shear box assembly (C3DI)
(after Fakharian, 1996)

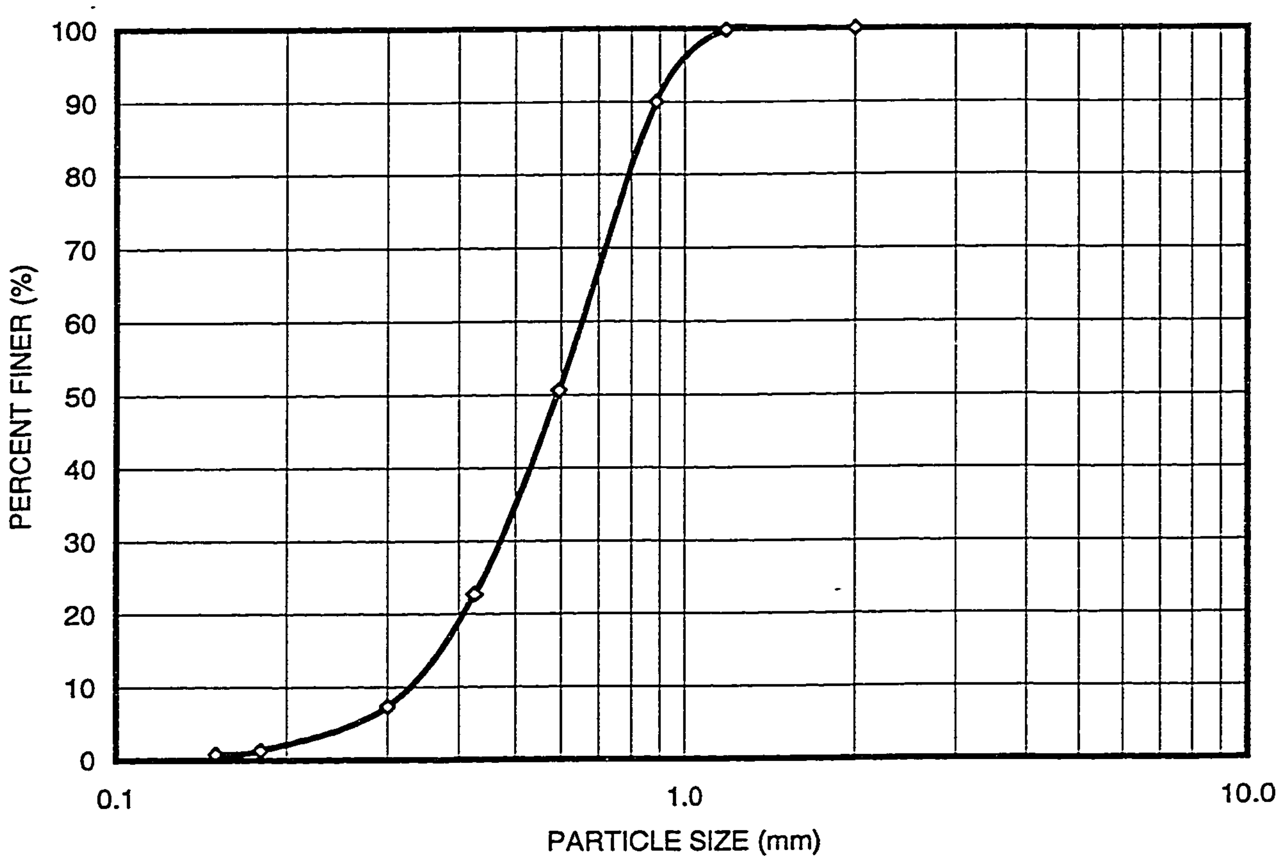

Fig.3.3 Particle size distribution of the sand

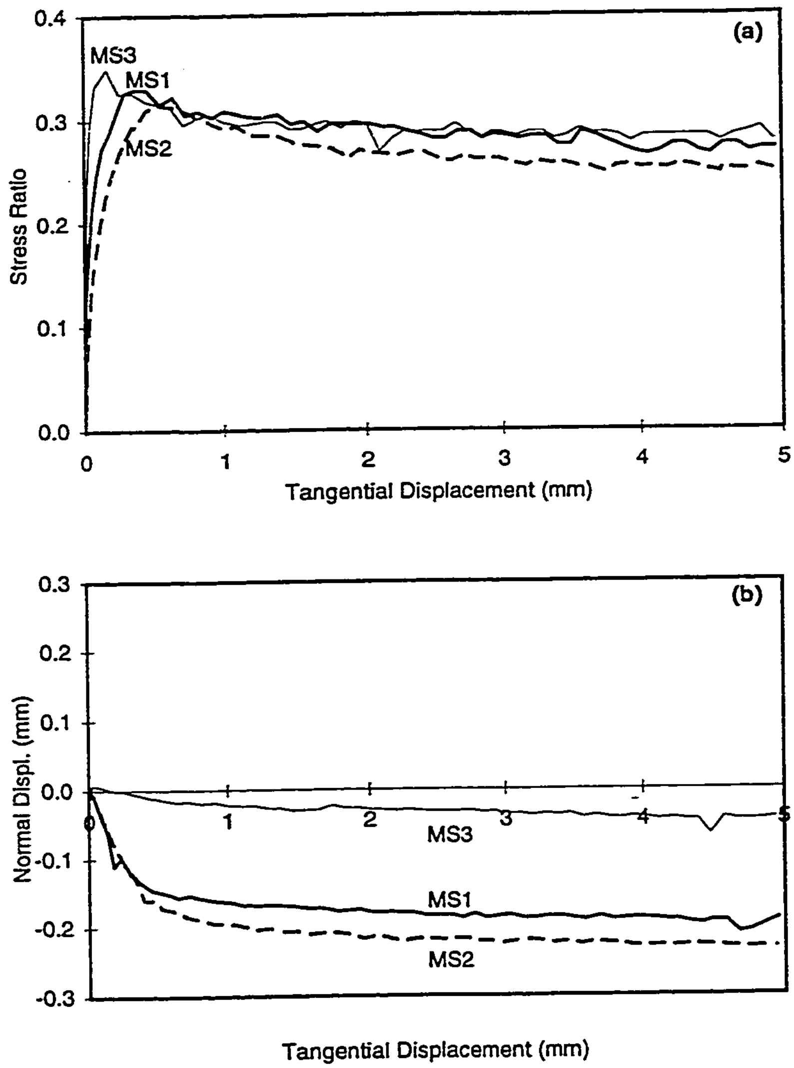

Fig.3.4 Results of monotonic tests under constant normal stress condition

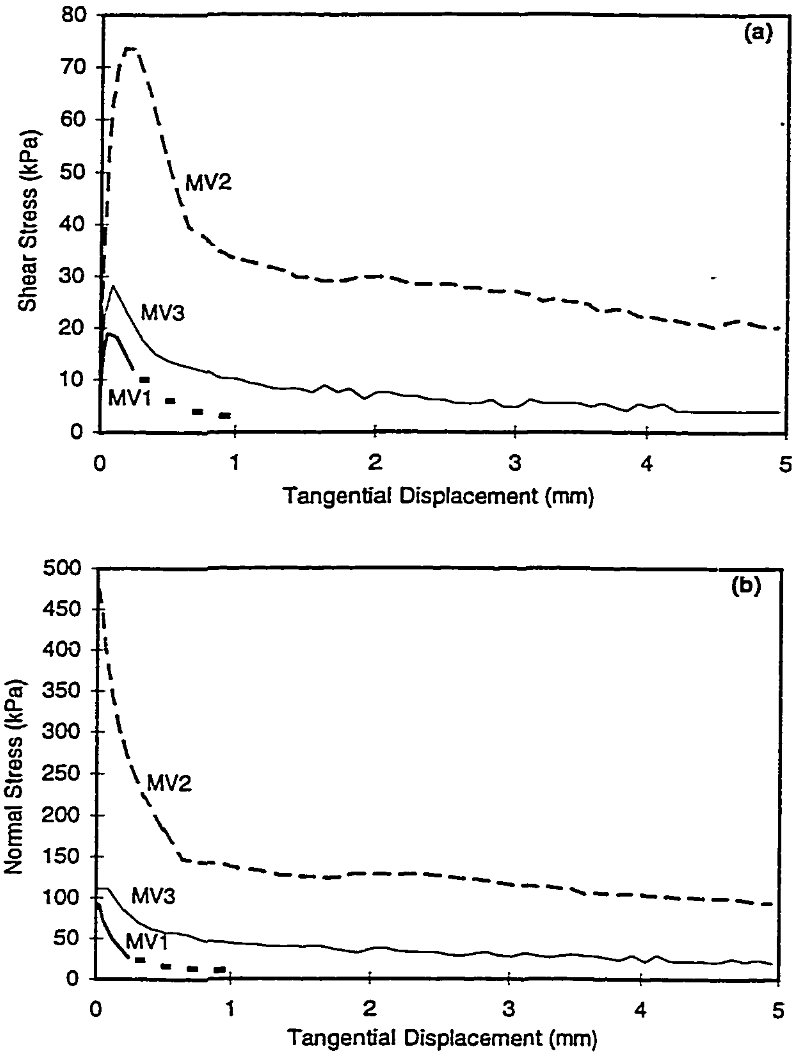

Fig.3.5 Results of monotonic tests under constant volume condition

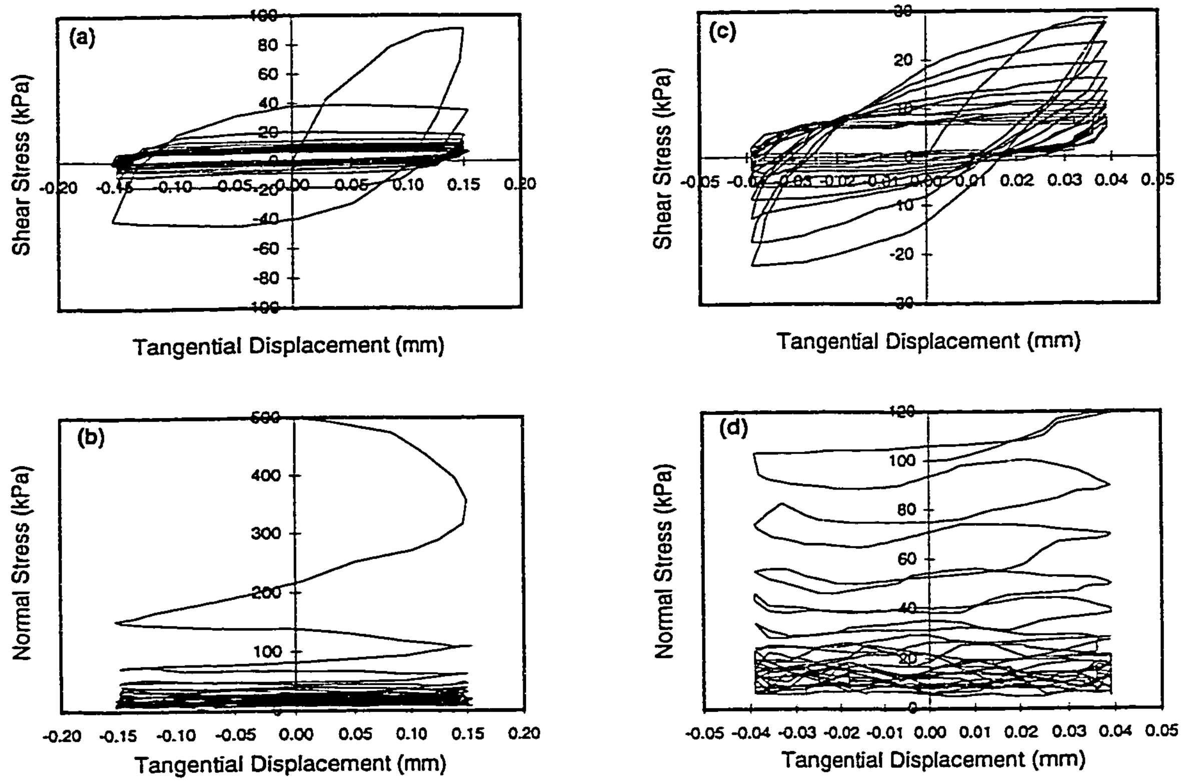

Fig.3.6 Results of cyclic tests under constant volume condition

PART 2 DISCRETE ELEMENT SIMULATION OF SAND-STEEL INTERFACE BEHAVIOUR

CHAPTER 4

NUMERICAL SIMULATION METHODS OF SOIL-STRUCTURE INTERFACE BEHAVIOUR — LITERATURE REVIEW

In this chapter, major developments in numerical simulation of soil-structure interface behaviour are reviewed, and then some recommendations are made for further studies in this field.

4.1 Joint/Interface Elements

4.1.1 Zero-thickness joint/interface elements

Due to the obvious influence of interfaces on the behaviour of jointed rocks, most of pioneering works were done first for simulating rock joints. Based on the analysis of actual prototype joints, Goodman et al.(1968) developed a two-dimensional linear joint element for the stability analysis of jointed rock. This element has zero width as the corresponding nodal point pairs initially have identical co-ordinates. Like for usual continuum element stiffness, the joint element stiffness is derived based on an energy equation and minimising with respect to nodal point displacements. This makes the joint element compatible with continuum elements, and so that the joint element stiffness (determined by unit joint stiffness) can be directly added into the structural stiffness matrix as the direct stiffness method.

The unit joint stiffness, k_n and k_s, representing the relationship between the relative displacements of the joint and resistance in the normal and tangential directions, can be determined by direct shear test. It is assumed that no tension can exist in joint elements. During solving a problem, the joint stresses are calculated from the known nodal displacement. If the joint normal stress is tensile in any element, both k_n and k_s are set equal to zero for the element and the problem is repeated to redistribute the unbalanced loads. Also, the joint cohesion, joint friction, and residual tangential stiffness are read in as data and the shear strength is calculated for the indicated normal pressure on each joint. If the joint shear stress exceeds the shear strength, then k_s is set equal to $k_{sresidual}$ and the problem is repeated. Any problem can be restarted where it was left off previously so that the number of cycles can be increased gradually till a stable state is found.

This work has been extended by Mahtab and Goodman (1970), who developed plane joint elements of triangular and quadrilateral shapes in the same way for three-dimensional finite element analysis of jointed rock slopes.

The above-stated analysis technique proposes a nondilatant model, more specifically, one in which shear and normal deformations could be coupled only indirectly through the coupling of shear and normal stresses imposed by superposition of a Coulomb type strength criterion. Later on, Goodman and DuBois (1972) proposed a method of representing dilatancy by defining nondilatant properties of the joint in terms of a p-q co-ordinate system. The angle, γ, is assumed to depend on the physical angle of asperities to the plane of the joint (s-axis) and on the normal stress, σ_n. By a transformation of co-ordinates, the constitutive properties may then be expressed in terms of the n-s system. The amount of dilatancy, according to this method, thus depends on intrinsic properties (i.e., the normal and shear stiffness of the local joint plane), or the geometry of asperities in the joint, and on the normal stress.

With applying this model to simulate soil-structure interface behaviour, a new term "interface" was used first by Clough and Duncan (1971). In their work, the joint element is employed to represent the interface between a retaining wall and the adjacent backfill. In evaluating the stiffness of these elements, it is assumed that both normal and shear displacements vary linearly along the length of the element, which is compatible with the external boundary displacements of the two-dimensional elements.

Goodman's joint element model was also adopted by Desai with assuming zero-thickness for the interface element. Desai and co-workers formalised the use of this model including extension for axisymmetric problems (Desai and Holloway, 1972; Desai, 1974). Desai and Appel (1976), Desai et al.(1982) further developed this model for three-dimensional nonlinear soil-structure interaction problems.

Toki et al. (1981) have successfully simulated the separation and sliding at the interface between the soil and structure using the joint element proposed by Goodman et al.(1968) during analysing dynamic response of structures under seismic excitation. In their model, an idealised Mohr-Coulomb failure law and elasto-perfectly plastic shearing model are also applied. Due to the consideration of numerical instability, the values of k_n and k_s are determined to be nearly equal to the stiffness of the elements of the foundation structure. The equation of motion is solved by the step-by-step integration method in the time domain with a time interval of 0.002 s. The load transfer method of iterative computation is found to be most effective in this analysis, in which the stiffness matrix is kept constant during the computation and only the external force is modified so as to satisfy the equilibrium condition. By using this method, systems with non-linear constitutive relations can be treated as linear systems with constant stiffness excited by quasi-external forces. The computation of the inverse stiffness matrix is required only at the first step of the response analysis and therefore the computation time is greatly reduced.

4.1.2 Isoparametric joint element

Zienkiewicz et al. (1970) advocate the use of continuous isoparametric elements to represent the joints with a simple nonlinear material property for shear and normal stresses. The pairs of nodes on either side of such joint element are geometrically so close that they are specified by the same co-ordinates providing the thickness t is used when computing the joint element properties (so, the thicknesses are given as separate information). The simple joint element is adequate if the main analysis is based on the simplest triangular elements. That such elements are not ideal for all occasions has been demonstrated and more complex, curved isoparametric elements give even in two-dimensional situations a generally improved accuracy. So, compatible, higher-order joint elements will be correspondingly used.

It should be mentioned that numerical difficulties may arise from ill-conditioning of the stiffness matrix due to very large off-diagonal terms or very small diagonal terms which are generated by these joints elements in certain cases. So, it is important to note that the elastic stiffness characteristics of joint elements should not differ from those of adjacent, solid elements by large amounts or else risk of ill-conditioning of the assembled equations will exist. While the exact limits of possible stiffness ratios depend on the precision of the computer word length and on the total number of elements it is a safe rule that ratios of 1:1000 should not be exceeded. Another point need to be mentioned is that the stiffness of the joint element in directions associated with the important shear and normal deformations is proportional to E/t (if E is the elastic modulus at t the thickness dimension). Thus if the joint is made very thin as compared with the adjacent ones its original E values should be appropriately reduced.

4.1.3 Using relative displacements as unknowns

For avoiding theoretical difficulties of other joint elements (e.g., with Goodman's joint elements, adjacent blocks of continuous elements can penetrate into each other; with the isoparametric joint elements proposed by Zienkiewicz et al. (1970), numerical difficulties may arise from ill-conditioning of the stiffness matrix), Ghaboussi et al. (1973) proposed a new joint element which uses relative displacements as the independent degree-of-freedom. The displacement degree-of-freedom of one side of the slip surface are transformed into the relative displacements between the two sides of the slip surface. The joint element is assumed to have only two strain components: normal strain (ε_n)and shear strain (ε_s) which are respectively equal to the relative normal and tangential displacements divided by the assumed thickness t of the element. Then the stiffness matrix relating the relative displacements and internal resisting forces of the joint element can be established

Nondilatant joints are the simplest to model mathematically since there is no volume change due to shearing strains. Dilatancy of joints can be represented by the same method proposed by Goodman and DuBois (1972) through defining nondilatant properties of the joint in terms of a p-q co-ordinate system. Ghaboussi et al. (1973) also developed a direct method for representing dilatancy by adapting the strain hardening theory of plasticity. The basic idea is contained in the capped model, which uses a perfectly plastic yield surface to limit shear stresses and a strain hardening cap to control dilatancy.

By using a simple one-dimensional problem, Wilson (1977) further examined the numerical problem created by very stiff elements, and pointed out that this problem could be avoided by transforming the equilibrium equations in terms of both absolute and relative displacements rather than in terms of absolute displacements only. He also further presented the formulations for two- and three-dimensional cases in great detail.

Based on similar assumptions, a joint/interface element has been presented by Beer (1985), which performs well in three-dimensional stress analysis involving nonlinear slip and separation. The formulation of the element is quite general and mutations of the generic element can be used for shell-to-shell, shell-to-solid and solid-to-solid interfaces in either two or three dimensions. Because of the assumption that it has zero thickness, the element is particularly suited for modelling rock joints and fractures.

4.2 Thin Interface Element / Thin-Layer Element

The above-stated interface models consider relative motions between structure and soil, but still the displacements of two initially adjacent points after loading follow the requirement of continuity. That is, these models, in reality, do not allow for discontinuities caused by very large relative slip and debonding. Such fact makes it possible to consider the interface as a "thin" solid element and simulate the same effect due to the relative motion.

Pande and Sharma (1979) investigated the idea of using an 8-node isoparametric element as a thin interface element. Earlier Zienkiewicz et al (1970) adopted a 6-node para-linear joint element (no mid-side nodes in the thickness direction). Although the thickness of the joint element may be very small, sharp variations in the strains of adjacent continuum elements can take place and a linear interpolation of strains is required. Thus, the mid-side nodes in the formulation of Pande and Sharma (1979) were retained. The ability of this element using both absolute and relative displacements as independent unknowns is also compared by analysing a specific plane-strain slippage problem consisting of two continuum elements connected by an interface element and loaded vertically. It was found that the conventional 8-node isoparametric element approach could give satisfactory results up to very high aspect ratios of the interface.

Griffiths (1985) further looked into the use of the above-proposed 8-node quadratic isoparametric interface element with elasto-plastic behaviour to model slippage with performing parametric studies of aspect ratio, relative stiffness and plasticity convergence criterion on the same problem. It was found firstly that the interface with an aspect ratio of 10 reproduced sliding behaviour quite well although increasingly conservatively as the interface inclination was decreased. Secondly, for higher aspect ratios of 100 and especially 1000, over-stiff behaviour was obtained with less convincing modelling of sliding. In these cases, reducing Young's modulus in the interface made little difference.

The concept of thin interface element was also incorporated in dynamic analysis. Isenberg and Vaughan (1981) and Vaughan and Isenberg (1983) gave a detailed consideration to interface behaviour under dynamic loading. A continuum (soil) element was used as an interface element by assigning special properties to it. Sliding, separation or debonding and rebonding aspects were simulated by imposing constraints upon their allowable stress states in addition to those imposed by the constitutive relations for soil. These additional constraints restrict the normal and shear forces transferred between soil and structure. The model was used to obtained solutions for a number of interaction problems including nuclear containment structures and buried cylinders subjected to shock loading from a travelling air blast.

In 1981, Desai also proposed the idea of using the thin solid element to represent interfaces. As a result of the works of Desai and his co-workers, a new term "thin-layer element" was finally used (Desai et al., 1984).

The basic stipulation in the thin-layer element concept is that the contact or interface can be replaced by an equivalent solid or continuum element with a (small) finite thickness. Among various possibilities, the following represent three practical situations. First, a different material with (small) thickness occurs between two solid bodies (or elements) as in the case of a rock joint with inclusion of a thin soil layer. Second, interface occurs between two bodies with different properties such as soil and concrete (or steel). Then the interface element represents a thin zone in the (softer) material, in which the action is mainly concentrated. For example, it is found from field and laboratory tests that a thin layer of clay participates in the interface action and stress transfer between a cohesive soil and a steel (or concrete) pipe. Third, contact occurs directly between two bodies, in which case the thin element represents a "smeared" zone that has properties different from those of the two bodies. The main appeal of the thin-layer element lies in its ability to simulate contacts when the interface action does not occur exactly at the junction but involves a finite zone of action as in soil-structure interfaces, joints filled with different materials, and smeared zones in other contacts. In these cases, the thin-layer element provides a direct formulation in which its behaviour, nonlinear elastic or elastoplastic with nonassociativeness, damage and softening, can be formulated in the same manner as the surrounding solid element.

The distinguishing features of the thin-layer element lie in the special treatment of the constitutive laws, choice of its thickness, incorporation of various models of deformation and implementation for a number of problems with displacement, mixed and hybrid finite element procedures.

The quality of simulation of the interface behaviour will depend on a number of factors such as physical and geometrical properties of the surrounding media, non-linear material behaviour and the thickness of the thin-layer element. If the thickness is too large in comparison with the dimension B of the surrounding elements, the thin-layer element will behave essentially as a solid element. If it is too small, computational difficulties may arise. The choice of thickness can, therefore, be an important question, and can be resolved by performing parametric studies. The choice of thickness can become particularly important for dynamic analysis where the mass and damping properties need to be considered. By performing a two-dimensional plane-strain finite element analysis on direct shear tests of sand-concrete interface, it was concluded that satisfactory simulation of interface behaviour could be obtained for t/B ratios in the range from 0.01 to 0.1 according to the comparison of both displacements and uniformity of computed stresses.

4.3 Elastoplastic Cosserat Model

The above-mentioned joint/interface elements only provide some possible ways to represent the interface effects on the behaviour of the whole system when performing numerical analysis. However, more important thing is what really occurs within the interface. As it is well known, the interface involves a thin layer of material with a defined thickness adjacent to the contact surface. Within the interface, pronounced grain rotations and large strain gradients are observed. The determination of the thickness of the shear zone along the interface is important for the estimation of forces transferred from the surrounding material to the structure. Extensive studies on interfaces have been done by Desai et al. (1985), Uesugi and Kishida (1986a,b), Boulon (1988), Boulon and Nova (1990), and others. However, most of the proposed interface models have been developed within a conventional continuum. As a consequence, they are unable to account for the thickness of the shear zone along the interface and to properly predict the wall friction angle; nor can the scale effect due to grain size and dilatancy constraint of the material in the interface be described.

Another important aspect which fails to be accounted for by most of the existing interface models is the effect of boundary conditions of the whole system on the wall friction angle and the thickness of the shear zone along the contact structure. In engineering practice, these boundary conditions may take multiple forms ranging from free constraint to full constraint. The constraint of the surrounding material gives rise to a change in the normal stress across the interface. It is clear that the wall friction angle and the thickness of the shear zone determined from the shear tests, where the material dilatancy can freely develop, cannot simply be transferred to other boundary value problems where the dilatancy is partially hindered.

If the material behaviour involves strain softening, the governing differential equations will change and give rise to ill-posed boundary value problems (Schaeffer, 1990; Benallal et al., 1991). The results also show spurious dependence on the mesh size (Bazant and Lin, 1988). The problem of ill-posedness can hardly be solved in the conventional continuum. A reasonable way to get around this problem is to include factors, such as grain rotation, higher-order strain gradient, non-locality and viscoplastic terms, which become significant as soon as localised deformation occurs, but remain otherwise negligible.

As early as 1909, Cosserat studied the influence of grain size within the medium and established a basic theory of couple stress. Different from the classical continuum theory which only considers translational degree of freedom and describes the macroscopic behaviour of materials, Cosserat theory takes full account of the presence of the couple stress and the influence of the strain gradient and the "grain" size. The theory holds that the stress gradient approaches a certain characteristic length, which is derived from some material constants, and there exist strain gradients in the body. If the "grain" size is considerable, in general the continuum elements cannot be regarded as infinitesimal. Therefore, the stress distribution in the elements is not uniform and stress tensor is not symmetric. Mühlhaus et al. (1987, 1989) further extended this theory to include plasticity terms referred to as an elastoplastic Cosserat model, which takes grain rotations and couple stresses into consideration using the mean grain diameter as the characteristic length, for the modelling of shear banding of granular materials. Such a model can be used for the prediction of the shaft resistance along a pile embedded in sand or for the description of soil-structure interfaces in general.

Tejchman and Wu (1994, 1995) carried out a finite element analysis on a sand-steel plate interface using an elastoplastic Cosserat model. Calculations of a planar simple shear test were carried out. An updated Lagrange formulation enabled the large deformation to be considered. Due to the assumption of the smooth vertical sides the displacements along them deviated slightly from the initial configuration. With rough and very rough surfaces, localised zones with a definite thickness could be observed. The localised zone was manifested by a concentration of plastic deformation and a presence of Cosserat rotations. Rotation seems to be the optimal criterion for detecting localised zones. The thickness of the calculated localised zone in dense sand was found to depend largely on the surface roughness: 7.5 mm (i.e., $15d_{50}$) for a very rough surface and 1.5 mm (i.e. $3d_{50}$) for a rough surface. The sand particles for a very rough surface were fixed according to the imposed boundary condition along the bottom. For a rough surface the particles experienced both sliding and rotation. In the case of a smooth interface, the shear zone did not appear. The sand mass simply slid along the surface (the calculated rotations for smooth surfaces were about 200 times smaller than for the very rough interface). This was found to be consistent with the previous experimental results. The calculated maximum vertical displacements of the free top were : 0.60 mm (very rough), 0.53 mm (rough) and 0.29 mm (smooth), respectively.

The difference between results obtained in a polar and a non-polar continuum was evident. The thickness of the shear zone in the non-polar continuum was smaller than in the polar continuum. It was approximately 3 mm with a fine mesh and 4 mm with a coarse mesh. The transitions between horizontal displacements in the shear zone between the elements were not as smooth as in polar continuum. The loss of ellipticity in the conventional constitutive relations with softening was responsible for the mesh size dependence and for the abrupt development of displacements. Due to the smaller effect of the dilatancy constraint in the shear zone, the maximum and the residual wall friction angles obtained with a non-polar approach were smaller than the values calculated in a polar continuum.

For loose sand, the calculated thickness of the shear zone was about 9 mm and it was slightly larger than that for dense sand. The calculated maximum and residual wall friction angles were 33° and 32°, respectively. They agreed fairly with the experimental data.

The numerical results show that the formation of shear zones along the wall can be described with an elastoplastic Cosserat model. The thickness and the kinematics of the shear zones are described realistically. The Cosserat rotations are noticeable in the shear zones. The thickness of the wall shear zone is independent of the mesh size, so a coarser mesh is sufficient.

4.4 Summary and Recommendations

4.4.1 Summary

Instead of using simple representations of interfaces in analysing soil-structure interaction problems, the recognition of the complicated interface behaviour resulted from laboratory tests and field observations, makes it necessary to develop more realistic models for simulating various modes of interface deformation.

As stated in the previous sections, there are several kinds of joint/interface elements developed to simulate rock joints and soil-structure interfaces. All elements with a zero-thickness have certain amount of penetration between adjacent continuum elements at joint/interface. For avoiding this unrealistic penetration, a high value of the order of 10^8 - 10^{12} units is arbitrarily assigned for the normal stiffness. There is no logical basis for adaptation of such values. This will introduce high normal stress and unreliable normal response at the interface. This type of elements generally can provide satisfactory solutions for the stick (or no slip or bonded) and slip modes for which the normal stress remains compressive. For other modes such as separation and rebonding, the results are often unreliable.

As further development, thin interface element/thin-layer element has been proposed, which uses an isoparametric element to represent interface material. This type of elements includes the zero-thickness as a special case, and is physically more consistent and provides application potential for a wider range of problems. It is capable of predicting all interface deformation modes correctly to some extent. The assumed thickness of the interface element is the result of parametric studies on discretized finite element model, but not based on the real behaviour of the interface under consideration.

In most of the previous works, essentially only the shear response is considered, while for the normal response at the interface, arbitrary values of the normal stiffnesses are often adopted. This means no coupling of normal and shear responses. The shear stiffness is evaluated as a tangent modulus from laboratory stress-strain behaviour in direct shear tests, for which a linear relation is usually assumed. The yield criteria are usually based on classical Coulomb's theory. For soil-structure interfaces, this method cannot provide the simulation of dilatancy.

All previously developed interface elements are applicable conditionally. As the first approximation or starting point for further analysis, they still have certain distance from more realistically simulating complicated soil-structure interface behaviour.

Due to the limitations of experimental techniques and the assumption that Coulomb's friction principle holds for interfaces of deformable bodies, there have been a limited number of investigations of interface phenomena. Huck et al. (1973) and Huck and Saxena (1981) earlier conducted valuable experimental investigation on soil-concrete interface behaviour. The results from their interface tests under static and dynamic shear loading indicated that localisation of large deformations resulting from material softening seemed to occur adjacent to the interface, in a region characterised as a shear band. Drum and Desai (1983) worked on soil-structure interface tests under static and cyclic loading. It was found from their test results that the interface strength was less than that of soil, and gradual separation might occur at or near the interface. Vermeer (1983) investigated interface behaviour between granular materials and metals during powder compaction in a die. From tests, it was pointed out that the powder-wall slip plane was in fact a thin shear band. By analysing these experimental results, shear slip appears to be initiated somewhere in the post-peak or softening regime, and the relative slip is believed to be the most likely failure mechanism of a soil-concrete interface that occurs after the formation of the shear band (Chen and Schreyer, 1986). It is clear that the shear response coupled with normal response at the interface (shear band) cannot be simply expressed as a linear model. And the change in the state of the material is larger in the shear band than in the surrounding soil. So, the concept of strain, associated with the continuum scheme is not suitable for these phenomena to be considered at the grain scale, and the notion of relative displacements is much more adapted. Coulomb's law can perfectly work with the contact problem of similar materials like rock-rock. However, as mentioned above, instead of a slip, a band with large shear deformation is observed at the soil-structure interface. So, Coulomb's law may not be still applicable for such cases.

In general, the soil-structure interface is much more complex and involves the influence of various factors such as concentration of stresses and deformation in zones in the vicinity of the junction including compression and dilation in these zones, roughness and asperities of contact surface, cyclic loading and unloading, and separation and rebonding. To consider these vital factors it is important to develop appropriate interface constitutive models to account for normal and shear responses and their coupling based on careful laboratory testing. It is believed, therefore, that significant attention and efforts are needed toward development of constitutive models and yield criteria. Although some complicated constitutive models have already been developed and have the potential for being applied to interface elements, there are many problems arising in performing the more rigorous response analysis.

Mohr-Coulomb type models were the earliest models used. The rigid-plastic model does not account for shear and normal displacements before failure or slip occurs. The elastic-perfectly plastic models consider the shear displacement, but lack the possibility of considering the non-recoverable (plastic) deformations before failure. Although such models has the advantage of simplicity, they are poor in terms of modelling the normal displacements and post-peak behaviour of interfaces. In 1985, Desai et al. introduced a piecewise non-linear elastic model based on Ramberg-Osgood model to account for non-linearity involved in interface behaviour. Although unloading and reloading are included, inelastic deformations are not included in the sense of the theory of plasticity. The model also lacks the ability of considering the normal displacements at the contact surface.

For considering the coupling between normal and shear behaviour, a two-dimensional direction-dependent constitutive relation was proposed by Boulon and Plytes (1986) in which a path dependent interpolation function was applied. Meanwhile, an elasto-plastic constitutive model was developed by Fishman and Desai (1987) and Desai and Fishman (1991) for hardening behaviour of rock joints with associative and non-associative flow rules. The same model was modified by Navayogarajah (1990) and Navayogarajah et al. (1992) for monotonic and cyclic behaviour of interfaces between sand-steel and sand-concrete. In 1996, Fakharian expanded this model to three-dimensional case.

The thickness of the shear zones depends on the wall roughness, the grain diameter, the specimen size and the boundary value problem considered. The results of wall friction angles from simple shear tests cannot be thus transferred to other boundary value problems, because the wall friction angle does not only depend on wall roughness and the properties of the granular material but also on the boundary conditions of the whole system.

A general model for interface behaviour should include both translational and rotational relative displacement modes. Each mode should include provision for relative slip, debonding and rebonding. Consideration of all deformation modes makes the model complicated especially in dynamics. For this reason, previously developed interface models for some specific modes may not still work.

Although the material behaviour of previously developed interface elements may be considered to be nonlinear to arbitrarily complicated degree, the node numbers of an interface element are initially fixed corresponding to adjacent two solid elements. So, these two solid elements cannot relatively move too far along the tangential direction. This means that these interface elements can only simulate small relative displacement but not very large relative displacement such as the displacements which take place in continuous pile-driving process.

By using Cosserat model which considers both translational and rotational movement components of grains, some interface behaviour such as thickness can be analysed. However, a complicated elastoplastic constitutive model is also involved, which is the function of testing boundary conditions and needs to be assumed prior to calculation.

4.4.2 Recommendations

In contrast to continuum models, the discrete element method has the potential to simulate all aspects of soil-structure interface behaviour due to its distinguishing characteristics which will be introduced in the next chapter. It can consider both very large relative displacements and complicated interface movement modes and material constitutive model. In the discrete element method, both relative rotation and translation components of individual grains are involved. This movement mechanism also provides the basis of simulating complicated constitutive behaviour and formation mechanism of shear band at interfaces by using only a few particle-particle and particle-wall mechanical parameters which can be determined in some basic experiments. In general, the discrete element method has apparent advantages in analysing and simulating soil-structure interface behaviour, its application may provide further improvement in more precisely understanding and simulating the soil-structure interaction mechanism.

CHAPTER 5
DISCRETE ELEMENT METHOD

5.1 Development of Discrete Element Method

Among numerous physical and industrial problems, only limited number of them can be analytically solved with continuum solution, meanwhile others can only be solved approximately by means of numerical methods which may approach, as closely as desired, the true continuum solution as the number of discrete variables increases. These numerical approaches were more rapidly developed with the advent of digital computers, which mainly include finite difference method (FDM), finite element method (FEM), boundary element method (BEM). In the finite element method, the solution region is considered as built up of many small, interconnected subregions called "finite elements". In the boundary element method, the fundamental solution is derived within the entire space, and the boundary of the region being studied is divided in "boundary elements" in order to obtain a solution of the problem. These methods can be considered as the region-type solutions which are suitable to solve continuum problems.

In contrast, the discrete element method (DEM) is a numerical technique which solves engineering problems that are modeled as a large system of distinct interacting general shaped rigid or deformable bodies or particles that are subject to gross motion. The behavior of such systems depends on the geometry and packing of individual particles. Engineering problems that exhibit such large scale discontinuous behavior cannot be solved with a conventional continuum based procedure such as the finite element method, boundary element method and so on as the basic assumption of continuity is inappropriate or has to be relaxed due to the physics of these problems. The methodology behind the discrete element method is relatively simple. Basically, the discrete element method uses the Newton's second law as the fundamental premise to calculate the movements of an individual particle considering its interaction with surrounding particles (Cundall and Strack, 1979). By using this method, discontinuous bodies are represented as a collection of rigid or deformable bodies, and the dynamic contact topology of the bodies is determined. It accounts for complex non-linear interaction phenomena between bodies and numerically solves the equations of motion. One of the primary issues involved in discrete element modeling is the geometric representation of the objects. The ability of the method to handle arbitrary shaped objects, and the speed of the contact checking between objects, depends on this representation.

The origins of the discrete element method can be traced to the late sixties. A model by Goodman et al (1968), for example, was aimed at the simulation of jointed rock and was accomplished by introducing discontinuities into an existing continuum. In the early seventies, the discrete element method was originally conceived as a means to model the progressive failure of rock slopes (Cundall, 1971), with later application being made to industrial processes such as granular media (Cundall and Strack, 1979) and shear flow (Walton, 1982), structural engineering (Kawai, 1977, 1979; Kawai et al, 1978), ice mechanics (Watanabe and Kawai, 1980; Williams et al, 1986; Hocking et al, 1985, 1987), and so on. Further developments took place in the eighties with the incorporation of deformable behaviour for the more precise modeling of individual elements and the term discrete element methods became widely accepted. The continuum representation of individual elements was dealt with through polynomial approximation of the strain field (Williams and Mustoe, 1987; Shi and Goodman, 1988) or by incorporation of central difference procedures (Lemos et al, 1985). Fracture models were either based on rigid fracture energy release rate concepts or on the breakage of cohesive links between discrete elements.

Many variations of the discrete element method exist, especially within the area of rock mechanics, including rigid block method, distinct element method, rigid block spring method and discontinuous deformation analysis. In general, the formulations of the discrete element method started with the engineering empiricism of Burman (1971), Cundall (1971), and Maini et al (1978), and proceeded to the more rigorous derivations of Kawai (1977), Belytschko et al (1984), Williams et al (1985) and Mustoe (1989). The discrete elements have evolved from the early rigid and simply deformable elements to the present state of complex elements.

Recent developments (Mustoe et al, 1989; Williams and Mustoe, 1993) have centered on improved physical models and associated computational algorithms. Notable advances include improved contact detection and interaction algorithms and the introduction of advanced computational concepts (parallel and distributed computing, object oriented programming and in core data bases). As an efficient numerical technique, the discrete element method has been applied in a wide variety of areas including constitutive behavior of granular material, transport phenomena in granular media, failure analysis of brittle material, analysis of rock-support interaction and stability analysis of blocked media.

5.2 Background and Overview of PFC^{2D} Program

PFC^{2D} (Itasca, 1994d) models the movement and interaction of circular particles by the discrete element method. The original application of this method was as a tool to perform research into the behaviour of granular materials. Representative elements containing several hundred particles were tested numerically. It was anticipated that the results from such tests could be used to develop constitutive models for continuum calculations of boundary-value problems. With the spectacular increase in power of small computers, it is now possible to model entire problems with particles, and therefore the constitutive behaviour is built into the model automatically. PFC^{2D} is designed to be an efficient tool to model complicated problems in solid mechanics and granular flow.

A physical problem that is concerned with the movement and interaction of circular particles may be modeled directly by PFC^{2D}. It is also possible to create particles of arbitrary shape by bonding two or more particles together. These groups of particles act as autonomous objects, provided that their bond strength is high. As a limiting case, every particle may be bonded to its neighbor. The resulting assembly can be regarded as "solid" that has elastic properties and is capable of "fracturing" when bonds break in a progressive manner.

Comparing with other distinct element programs UDEC (Itasca, 1994a) and 3DEC (Itasca, 1994b) which deal with angular blocks, PFC^{2D} has three advantages. First, it is potentially more efficient, since contact detection between circular objects is much simpler than contact detection between angular objects; second, there is essentially no limit to the magnitude of displacement that can be modeled; and third, it is possible for the blocks to break (since they are composed of bonded particles), unlike blocks modeled with UDEC or 3DEC which cannot break. The drawback to modeling a blocky system with PFC^{2D} is that block boundaries are not planar.

The specification of the geometry, properties and solution conditions is not so straightforward in PFC^{2D} as in programs such as FLAC (Itasca, 1994c) and UDEC. For example, with a continuum program, a grid is created, initial stresses installed, and boundaries set as fixed or free. In a particle code such as PFC^{2D}, a compacted state cannot be pre-specified in general, since there is no unique way to pack a number of particles within a given volume. A process analogous to physical compaction must be followed until the required porosity is obtained. For obtaining the required porosity and initial stress state, a trial-and error process is required, because there is no complete theory that can predict macroscopic behaviour from microscopic properties and geometry.

The calculation method is a timestepping, explicit scheme. There are several advantages of such a scheme. Systems that exhibit physical instability may be modeled without numerical difficulty. Large populations of particles require only modest size of computer memory, since matrices are never stored. PFC^{2D} may be used to model static or dynamic problems, but the full dynamic equations of motion are solved even when static solutions are required.

A PFC^{2D} model is constructed of circular particles (or balls). The smallest possible model that can be analyzed with PFC^{2D} consists of only one particle. If two balls are moved together so that they touch, then a point contact will be formed. Each ball in a PFC^{2D} model can touch several other balls, and the number of contacts that form can change dynamically during a model calculation as the balls move.

Model generation with PFC^{2D} involves the creation of assemblies of particles and the compaction of these assemblies to a desired compacted state. Walls are used in PFC^{2D}

both to define boundaries of a model and assist with the generation and compaction of balls. Walls can be positioned to generate clusters of balls in different regions of the model and then deleted after the generation phase is complete.

The general DEM can handle deformable polygonal-shaped particles. PFC^{2D} can be viewed as a simplified implementation of the DEM because of the restriction to rigid circular particles. However, it has been seen that it has many advantages over other DEM programs especially the suitability of simulating sand-type granular materials. Therefore, PFC^{2D} is chosen in this investigation.

5.3 Mechanics of Using PFC^{2D}

In order to set up a model and run a simulation with PFC^{2D}, three fundamental components of a problem must be specified: (1) an assembly of particles, (2) contact behaviour and material properties, and (3) boundary and initial conditions. The particle assembly consists of the locations and size distribution of particles. The contact behaviour and associated material properties dictate the type of response the model will display upon disturbance (e.g., deformational response due to excavation). Boundary and initial conditions define the in-situ state (i.e., the condition before a change or disturbance in problem state is introduced).

After these conditions are defined in PFC^{2D}, the initial equilibrium state is calculated for the model. An alteration is then made (e.g., excavate material or change boundary conditions), and the resulting response of the model is calculated. PFC^{2D} uses an explicit time-marching method to solve the algebraic equations. The solution is reached after a series of computational steps.

5.3.1 Simple model generation

5.3.1.1 Particle generation

There are two ways to create particles. One way is to create one particle at a time with a specified radius and location. Each particle has an ID number. When a new particle is created, a new number is chosen for it that is one greater than the current maximum ID number. The single particle can overlap existing particles. Overlapping particles will cause large repulsive forces to be produced. The two overlapping particles will then be propelled away from each other at high speed unless they have been declared fixed.

The second way is frequently used since it generates many particles at the same time. It chooses a random radius and location within the specified ranges. If the particle does not fit (i.e., it would overlap an existing particle), the radius is retained, but another location is chosen at random. It is possible to use walls to modify the region in which particles are created. Once particles are created, the initial wall can be deleted.

5.3.1.2 Compaction of the generated assembly

The starting point for most PFC^{2D} simulations is an assembly of particles that are contained within a given region of space and are in equilibrium. However, the above-stated two procedures usually create a loose assembly of particles; and at this stage, particles are not necessarily touching each other. Before we can make a simulation with PFC^{2D}, we need to bring the particles into contact and perhaps specify an initial stress state. The simplest and most robust way is to produce a compacted assembly is to expand the radii of all particles and allow them to move freely until they reach a state of equilibrium within a set of confining walls. Since all particles are expanded by the same factor, conditions throughout the assembly may be expected to be similar, resulting in isotropic, uniform conditions. To a first approximation, the adjustments that individual particles must make are local, since all parts of the assembly are affected equally. Therefore, the time necessary to reach equilibrium is much less than that for a scheme in which the compaction is achieved by moving walls inward (which requires information to propagate from the boundary toward the center). Furthermore, the final geometry in the wall-moving scheme is uncertain, in contrast to the radius-expansion scheme which preserves the boundary geometry. The only drawback to the radius-expansion scheme is that the final particle radii are different from those specified initially. However, this can be anticipated.

In general, the initial porosity and the initial mean stress are not independent quantities. It may not be possible to achieve desired values for both quantities simultaneously if the material properties are fixed. However, there is some scope for varying stress independently of porosity if the conditions during initial cycling are varied. For example, if friction is present, then the particles will tend to "lock up" earlier and thereby reach equilibrium at a higher stress level.

5.3.2 Contact model

The material behaviour of an assembly of particles is described in PFC^{2D} by contact models that represent the deformation and strength behaviour at ball-ball or ball-wall contacts. The selection of an appropriate contact model and properties for a real problem requires "fitting" the contact parameters to produce a response of the particle assemblage that resembles the expected material behaviour for the real problem. Contact models and properties are associated with individual particles and contacts. The contact models in PFC^{2D} may consist of up to three parts: (1) a stiffness model, (2) a slip model, and (3) a bonding model.

The default stiffness model is the linear-spring model. This model is invoked automatically when two stiffness properties, contact normal (spring) stiffness and contact shear (spring) stiffness, are specified for balls and walls.

Slip between two balls or between a ball and a wall is prescribed in terms of a friction coefficient that limits the shear force at a contact. If two balls (or a ball and a wall) with different friction coefficients are in contact, the coefficient used for the slip calculation is the minimum of the two values.

Particles may also be bonded together at a contact. Only particles may be bonded together; a particle may not be bonded to a wall. PFC^{2D} supports two types of bonds: contact bonds, which reproduce the effect of an adhesion acting over the vanishingly small area of the contact point, thus the name contact-point bond, or simply contact bond; and parallel bonds, which reproduce the effect of additional material (e.g., cementation) deposited after the balls are in contact. The effective stiffness of this additional material acts in parallel with the contact point stiffness, thus the name parallel bond is used.

Contact bonds are only installed at existing contacts of balls that are physically touching. The tensile normal and shear contact strengths are specified for a contact bond. If the magnitude of the tensile normal or shear contact force exceeds the respective strength, the bond breaks.

A parallel bond provides a connection between two particles that resists both forces and moments applied to the particles after the bond has been installed. Parallel bonds acting like a cylinder of elastic glue are installed at existing contacts and between all proximate balls (those that are within a distance d of one another, where d is equal to 10-6 times the mean radius of the two balls). The forces and moments applied to the particles after the bond has been installed produce normal and shear stresses within the elastic cylinder. If the magnitude of these stresses exceeds the respective strength, the bond breaks.

5.3.3 Applying boundary and initial conditions

After the particle assembly is generated and compacted, boundary and initial conditions are applied to achieve the desired initial equilibrium state. The boundary conditions in PFC^{2D} consist of the values of field variables that are prescribed at the boundary of the model. Boundaries can be real or artificial – real boundaries exist in the physical object being modeled, while artificial boundaries are introduced to enclose the chosen number of particles.

Artificial boundaries fall into two categories: lines of symmetry, and lines of truncation. A symmetry line takes advantage of the fact that the geometry and loading in a system are symmetrical about one or more lines. A truncation line is a boundary sufficiently far from the area of interest that the behaviour in that area is not greatly affected.

Boundary conditions can be applied to walls or to balls. Walls can be fixed in space or moved translationally and/or rotationally. Balls can also be moved by applying translational and angular velocities. Forces can also be applied to balls but not to walls. Displacements cannot be controlled directly in PFC^{2D}; in fact, they play no part in the calculation process. In order to apply a given displacement to a boundary, it is necessary to prescribe the wall or ball velocity for a given number of steps.

Unlike the boundary condition, the initial condition assigns initial values to selected variables; these can change while the computation proceeds. By setting the initial conditions in a PFC^{2D} model, an attempt is made to reproduce the state like in-situ state because it will influence the subsequent behaviour of the model. Initial stresses, however, are not prescribed directly in PFC^{2D}. The desired stress state must be derived from initial conditions specified for the compaction of the ball assembly.

5.3.4 Stepping to initial equilibrium

The PFC^{2D} model must be at an initial force-equilibrium state before alterations are performed. It is necessary to cycle the model to both an initial compaction and an initial equilibrium state under the given boundary and initial conditions. The model is in perfect equilibrium when the net force vector at each particle centroid is zero. The maximum force vector is called the maximum "out-of-balance" or "unbalanced" force. For a numerical analysis, the out-of-balance force will never reach exactly zero. It is sufficient, though, to say the model is in equilibrium when the maximum (or average) unbalanced force is small compared to the maximum (or average) contact force in the model for a packed assembly of particles.

If the assembly of particles is not tightly packed, then the contact forces in the model may be zero or negligible. In this case, the unbalanced force should not be compared to the contact force to test for equilibrium. It is better to monitor the movement of particles to assess if equilibrium is reached.

It is very important in an analysis that the model be at equilibrium before alterations are made. Several histories should be recorded throughout a model to ensure that a large force imbalance does not exist. It does not affect the analysis adversely if more steps are taken than are needed to reach equilibrium. However, it will affect the analysis if an insufficient number of steps is taken.

5.3.5 Performing alterations

PFC^{2D} allows model conditions to be changed at any point in the solution process. These changes may be of the following forms: (1) add or delete walls, (2) fix or free velocities for any wall, (3) change material properties for any wall, (4) add balls and ball loads, (5) delete balls, (6) fix or free velocities for any ball , and (7) change contact or ball material model or properties.

5.4 DEM Formulations

In this section, only those important formulae related to PFC^{2D} code are introduced.

5.4.1 Force-displacement law

The force-displacement law relates the relative displacement between two entities at a contact to contact force acting on the entities. For both ball-ball and ball-wall contact, this contact force arises from contact occurring at a point. For ball-ball contact, an additional force and moment arising from contact occurring over the finite-sized disk represented by a parallel bond can also act on each particle.

The force-displacement law operates at a contact and can be described in terms of a contact point, $x_i^{[C]}$, lying on a contact plane that is defined by a unit normal vector n_i . (n_i lies in the plane of the model.) The contact point is within the interpenetration volume of the two entities. For ball-ball contact, the normal vector is directed along the line between ball centers; for ball-wall contact, the normal vector is directed along the line defining the shortest distance between the ball center and the wall. The contact force is decomposed into a normal component acting in the direction of the normal vector and a shear component acting in the contact plane. The force-displacement law relates these two components of force to the corresponding components of the relative displacement via the normal and shear stiffness at the contact.

For ball-ball contact, the relevant equations are presented for the case of two spherical particles, labeled A and B in Fig.5.1; for ball-wall contact, the relevant equations are presented for the case of a spherical particle and a wall, labeled b and w, respectively, in Fig.5.2. In both cases, U^n denotes overlap.

For ball-ball contact, the unit normal n_i is given by

$$n_i = \frac{x_i^{[B]} - x_i^{[A]}}{d} \qquad \text{(ball-ball)} \qquad (5\text{-}1)$$

where $x_i^{[A]}$ and $x_i^{[B]}$ are the position vectors of the centers of balls A and B, and d is the distance between the ball centers.

For ball-wall contact, n_i is directed along the line defining the shortest distance d between the ball center and the wall. This direction is found by mapping the ball center into a relevant portion of space defined by the wall. The idea is illustrated in Fig.5.3 for a two-dimensional wall composed of two line segments $\overline{AB}$ and $\overline{BC}$. All space on the active side of this wall can be decomposed into five regions by extending a line normal to each wall segment at its endpoints. If the ball center lies in regions 2 or 4, it will contact the wall along its length, and n_i will be normal to the corresponding wall segment; however, if the ball center lies in regions 1, 3 or 5, it will contact the wall at one of its endpoints, and n_i will lie along the line joining the endpoint and the ball center.

The overlap U^n, defined to be the relative contact displacement in the normal direction, is given by

$$U^n = \begin{cases} R^{[A]} + R^{[B]} - d & (ball - ball) \\ R^{[b]} - d & (ball - wall) \end{cases} \qquad (5\text{-}2)$$

where $R^{[\Phi]}$ is the radius of ball Φ.

The location of the contact point is given by

$$x_i^{[C]} = \begin{cases} x_i^{[A]} + (R^{[A]} - \frac{1}{2}U^n)n_i & (ball - ball) \\ x_i^{[b]} + (R^{[b]} - \frac{1}{2}U^n)n_i & (ball - wall) \end{cases} \tag{5-3}$$

The contact force vector F_i (which represents the action of ball A on ball B for ball-ball contact and represents the action of the ball on the wall for ball-wall contact) can be resolved into normal and shear components with respect to the contact plane as

$$F_i = F_i^n + F_i^s \tag{5-4}$$

where F_i^n and F_i^s denote the normal and shear component vectors, respectively.

The normal contact force vector is calculated by

$$F_i^n = K^n U^n n_i \tag{5-5}$$

where K^n is the normal stiffness [force/displacement] at the contact.

The shear contact force is computed in an incremental fashion. When the contact is formed, the total shear contact force is initialized to zero. Each subsequent relative shear-displacement increment results in an increment of shear force that is added to the current value. The motion of the contact is considered during this procedure by updating n_i and $x_i^{[C]}$ every timestep.

The relative motion at the contact, or the contact velocity V_i (which is defined as the velocity of ball B relative to ball A at the contact point for ball-ball contact, and is defined as the velocity of the wall relative to the ball at the contact point for ball-wall contact), is given by

$$\begin{aligned} V_i &= \left(\dot{x}_i^{[C]}\right)_{\Phi^2} - \left(\dot{x}_i^{[C]}\right)_{\Phi^1} \\ &= \left(\dot{x}_i^{[\Phi^2]} + e_{i3k}\omega_3^{[\Phi^2]}\left(x_k^{[C]} - x_k^{[\Phi^2]}\right)\right) - \left(\dot{x}_i^{[\Phi^1]} + e_{i3k}\omega_3^{[\Phi^1]}\left(x_k^{[C]} - x_k^{[\Phi^1]}\right)\right) \end{aligned} \tag{5-6}$$

where $\dot{x}_i^{[\Phi^j]}$ and $\omega_3^{[\Phi^j]}$ are the translational and rotational velocity, respectively, of entity Φ^j given by

$$\{\Phi^1, \Phi^2\} = \begin{cases} \{A, B\} & (ball - ball) \\ \{b, w\} & (ball - wall) \end{cases} \tag{5-7}$$

(note that $\omega_3^{[W]}$ is the rotational velocity of the wall with respect to $x_i^{[W]}$, the center of the wall.)

The contact velocity can be resolved into normal and shear components with respect to the contact plane. Denoting these components by V_i^n and V_i^s for the normal and shear components, respectively, the shear component of the contact velocity can be written as

$$V_i^s = V_i - V_i^n = V_i - V_j n_j n_i \tag{5-8}$$

The shear component of the contact displacement-increment vector occurring over a timestep of Δt is calculated by

$$\Delta U_i^s = V_i^s \Delta t \tag{5-9}$$

and is used to calculate the shear force-increment vector

$$\Delta F_i^s = -k^s \Delta U_i^s \tag{5-10}$$

where k^s is the shear stiffness [force/displacement] at the contact.

The new shear contact force is found by summing the old shear force vector existing at the start of the timestep with the shear force-increment vector

$$F_i^s \leftarrow F_i^s + \Delta F_i^s \tag{5-11}$$

The values of normal and shear contact force determined by Eq.(5-5) and Eq.(5-11) are adjusted to satisfy the contact constitutive relations. After this adjustment, the contribution of the final contact force to the resultant force and moment on the two entities in contact is given by

$$
\begin{aligned}
&F_i^{[\Phi^1]} \leftarrow F_i^{[\Phi^1]} - F_i \\
&F_i^{[\Phi^2]} \leftarrow F_i^{[\Phi^2]} + F_i \\
&M_3^{[\Phi^1]} \leftarrow M_3^{[\Phi^1]} - e_{3jk}\left(x_j^{[C]} - x_j^{[\Phi^1]}\right)F_k \\
&M_3^{[\Phi^2]} \leftarrow M_3^{[\Phi^2]} + e_{3jk}\left(x_j^{[C]} - x_j^{[\Phi^2]}\right)F_k
\end{aligned}
\qquad (5\text{-}12)
$$

where $F_i^{[\Phi^j]}$ and $M_3^{[\Phi^j]}$ are the force and moment sums for entity Φ^j.

5.4.2 Law of motion

The motion of a single rigid particle is determined by the resultant force and moment vectors acting upon it and can be described in terms of the translational motion of a point in the particle and the rotational motion of the particle. The translational motion of the center of mass is described in terms of its position x_i, velocity $\dot{x}_i$, and acceleration $\ddot{x}_i$; the rotational motion of the particle is described in terms of its angular velocity ω_i and angular acceleration $\dot{\omega}_i$.

The equation of motion can be expressed as two vector equations, one of which relates the resultant force to the translational motion and the other of which relates the resultant moment to the rotational motion. The equation for translational motion can be written in the vector form

$$F_i = m(\ddot{x}_i - g_i) \qquad \text{(translational motion)} \qquad (5\text{-}13)$$

where F_i is the resultant force, the sum of all externally applied forces acting on the particle; m is the total mass of the particle; and g_i is the body force acceleration vector (e.g., gravity loading).

The equation for rotational motion can be written in vector form

$$M_i = \dot{H}_i \tag{5-14}$$

where M_i is the resultant moment acting on the particle; $\dot{H}_i$ is the angular momentum of the particle. This relation is referred to a local coordinate system that is attached to the particle at its center of mass. If this local system is oriented such that it lies along the principal axes of inertia of the particle, the Eq.(5-14) reduces to Euler's equation of motion:

$$\begin{aligned} M_1 &= I_1\dot{\omega}_1 + (I_3 - I_2)\omega_3\omega_2 \\ M_2 &= I_{21}\dot{\omega}_{21} + (I_1 - I_3)\omega_1\omega_3 \\ M_3 &= I_3\dot{\omega}_3 + (I_2 - I_1)\omega_2\omega_1 \end{aligned} \tag{5-15}$$

where I_1, I_2 and I_3 are the principal moments of inertia of the particle; $\dot{\omega}_1$, $\dot{\omega}_2$ and $\dot{\omega}_3$ are the angular accelerations about the principal axes; and M_1, M_2 and M_3 are the components of the resultant moment referred to the principal axes.

For either a spherical or a disk-shaped particle, whose mass is distributed uniformly throughout its volume, the center of mass coincides with the geometric center. For a spherical particle, any local-axis system attached to the center of mass is a principal-axis system, and the three principal moments of inertia are equal to one another. For a disk-shaped particle whose axis remains in the out-of-plane direction, $\omega_1 = \omega_2 \equiv 0$. Thus, Eq.(5-15) can be simplified and referred to the global-axis system as

$$M_3 = I_3\dot{\omega}_3 = (\beta m R^2)\dot{\omega}_3 \qquad \text{(rotational motion)} \tag{5-16}$$

where

$$\beta = \begin{cases} 2/5 & (spherical-particle) \\ 1/2 & (disk-shaped-particle) \end{cases}$$

The equations of motion, given by Eqs.(5-13) and (5-16), are integrated using a centered finite-difference procedure involving a timestep of Δt.

5.4.3 Timestep determination

The calculation cycle in PFC^{2D} is a timestepping algorithm that requires the repeated application of the law of motion to each particle and a force-displacement law to each contact as well as a constant updating of wall positions. Contacts, which may exist between two balls or between a ball and a wall, are formed and broken automatically during the course of a simulation. At the start of each timestep, the set of contacts is updated from the known particle and wall positions. The force-displacement law is then applied to each contact to update the contact forces based on the relative motion between the two entities at the contact and the contact constitutive model. Next, the law of motion is applied to each particle to update its velocity and position based on the resultant force and moment arising from the contact forces and any body forces acting on the particle. Also, the wall positions are updated based on the specified wall velocities.

The computed solution produced by the centered finite-difference procedure will remain stable only if the timestep does not exceed a critical timestep that is related to the minimum eigen period of the total system. However, global eigenvalue analyses are impractical to apply to the large and constantly changing system typically encountered in a PFC^{2D} simulation. Therefore, a simplified procedure is implemented here to estimate the critical timestep at the start of each cycle. The actual timestep used in any cycle is taken as a fraction of this estimated critical value.

First, consider a one-dimensional mass-spring system described by a point mass, m, and spring stiffness, k, with the coordinate system shown in Fig.5.4. The motion of the point mass is governed by the differential equation: $-kx = m\ddot{x}$. The critical timestep corresponding to a second-order finite-difference scheme for this equation is given by

$$t_{crit} = \frac{T}{\pi}; \qquad T = 2\pi\sqrt{m/k} \tag{5-17}$$

where T is the period of the system.

Next, consider the infinite series of point masses and springs in Fig.5.5. The smallest period of this system will occur when the masses are moving in synchronized opposing motion such that there is no motion at the center of each spring. The motion of a single point mass can be described by the two equivalent systems shown in Fig.5.5(b) and (c). The critical timestep for this system is found, using Eq.(5-17), to be

$$t_{crit} = 2\sqrt{m/(4k)} = \sqrt{m/k} \tag{5-18}$$

where k is the stiffness of each of the springs in Fig.5.5.

The above two systems characterize translational motion. Rotational motion is characterized by the same two systems in which mass m is replaced by moment of inertia I of a finite-sized particle, and the stiffness is replaced by the rotational stiffness. Thus, the critical timestep for the generalized multiple mass-spring system can be expressed as

$$t_{crit} = \begin{cases} \sqrt{m/k^{tran}} & (translational\ \ motion) \\ \sqrt{I/k^{rot}} & (rotational\ \ motion) \end{cases} \tag{5-19}$$

where k^{tran} and k^{rot} are the translational and rotational stiffnesses, respectively; and I is the moment of inertia of the particle.

The system modeled in PFC^{2D} is a two-dimensional collection of particles and springs, each of which may have a different mass and stiffness. A critical timestep is found for each particle by applying Eq.(5-19) separately to each degree-of-freedom and assuming that the degrees-of-freedom are uncoupled. The stiffnesses are estimated by summing the contribution from all contacts. The final critical timestep is taken to be the minimum of all critical timesteps computed for all degrees-of-freedom of all particles.

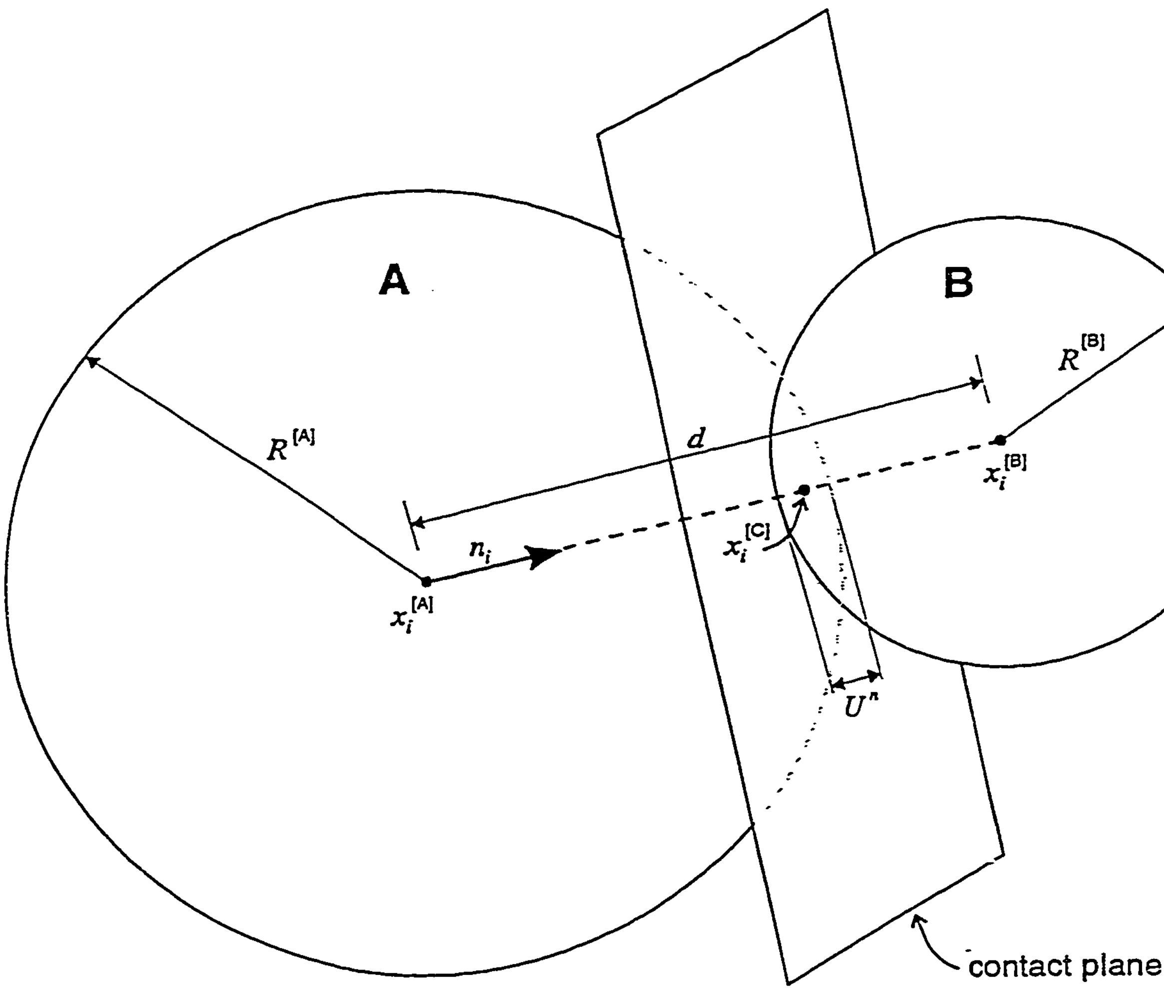

Fig.5.1 Notation used to describe ball-ball contact (after Itasca, 1994d)

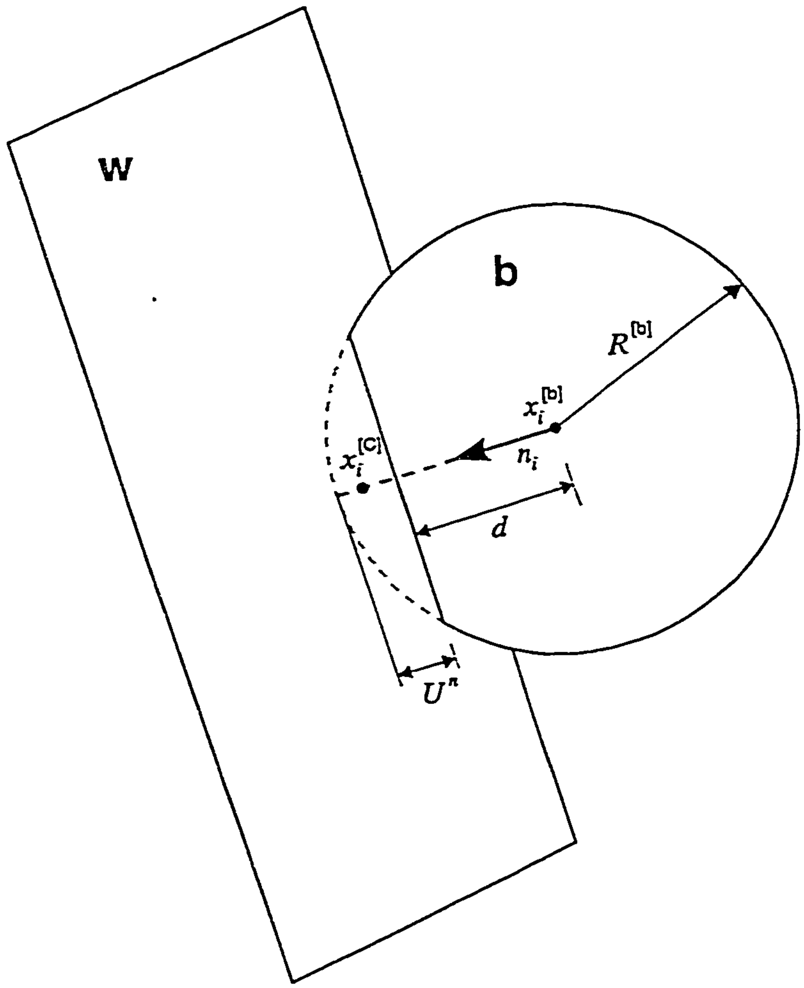

Fig.5.2 Notation used to describe ball-wall contact (after Itasca, 1994d)

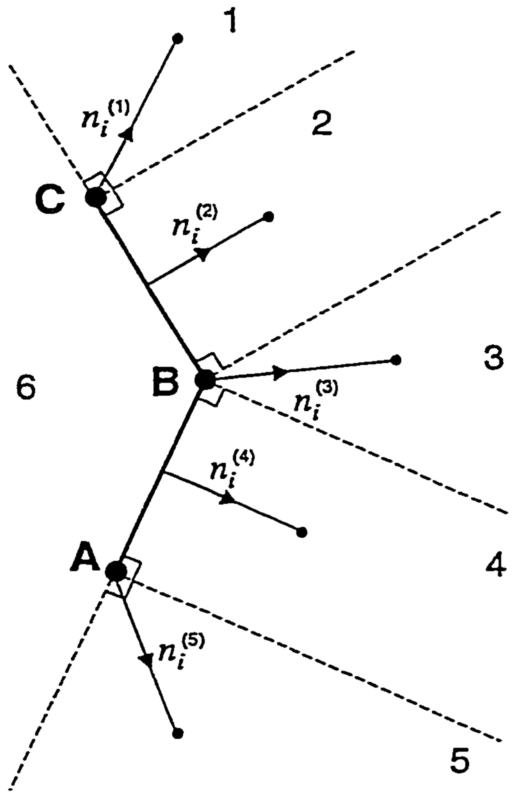

Fig.5.3 Determination of normal direction for ball-wall contact
(after Itasca, 1994d)

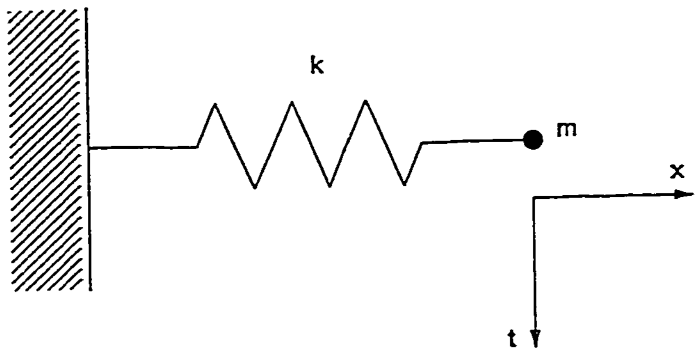

Fig.5.4 Single mass-spring system (after Itasca, 1994d)

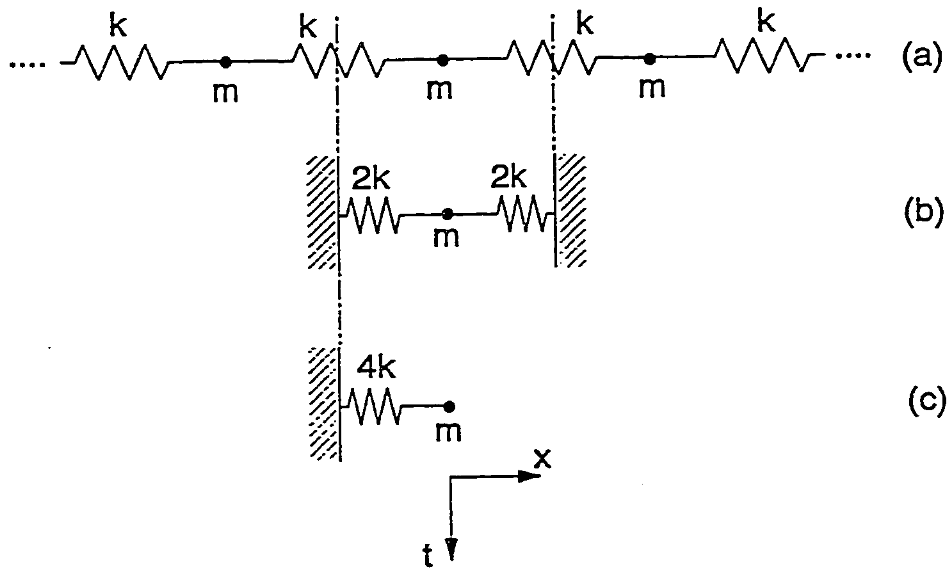

Fig.5.5 Multiple mass-spring system (after Itasca, 1994d)

CHAPTER 6
DEM SIMULATION OF SAND-STEEL INTERFACE BEHAVIOUR

6.1 Introduction

In this chapter, an attempt was made to explore the advantages and the limitations of using the discrete element method to simulate the behaviour of an interface between a granular soil and a steel plate. A two-dimensional discrete element program PFC^{2D} was used in the simulations. Circular particles, as well as units of two circular particles bonded together, i.e., peanuts, were used in various calculations to investigate the effect of particle shape. The strength-deformation behaviour of the dense sand - rough steel plate interface under constant normal stress and the loose sand - smooth steel plate interface with constant volume were simulated, and the results were compared with the test results.

6.2 Sand-Steel Interface Tests for Comparison

The interface tests were conducted using a multi-axial cyclic interface testing apparatus (Evgin and Fakharian, 1996) with the direct shear type soil container. An air-dry Silica sand was used in the tests, which has D_{50} of 0.6 mm, γ_{max} of 16.05 kN/m^3 and γ_{min} of 12.88 kN/m^3.

A two-dimensional monotonic test with a constant normal stress of 100 kPa was first conducted. The sand sample was in dense state and had a measured relative density of 81% after the application of constant normal stress, which was placed on a steel plate with a roughness of 25 μm.

The two-dimensional monotonic test under the condition of constant volume was conducted on a loose sand sample which was placed on a smooth steel plate with a roughness of 4 μm for a sampling length L = 0.8 mm. After applying a normal stress of 100 kPa, the sample had a relative density of 24%.

The results of these two tests are presented later with the DEM simulation results.

6.3 Simulation Model and Parameters

6.3.1 Simulation model

The constitutive model available in PFC^{2D} code for the behaviour of contact points between circular particles consists of three parts related to: (1) stiffness, (2) slip, and (3) bonding. The stiffness part of the model is an elastic relation between the contact force and relative displacement both in the normal and tangential directions. The slip part enforces a limit on the ratio between the shear force and the normal force. The two particles in contact may slip relative to one another if this ratio tends to exceed the coefficient of friction. The third part of the model provides bonds between particles, if desired, and also sets limits for the total tensile normal force and for the shear force that a contact can carry.

Previous experience confirms that circular particles have fewer number of contact points with neighbouring particles and they rotate with ease. On the other hand, elliptical particles have greater number of contacts and a larger resistance against rotation. Consequently, the strength of elliptical particle assemblies is higher (Rothenburg and Bathurst, 1992).

In some of the calculations of this study, bonds were generated at the contact point between two circular particles in order to investigate the effect of particle shape on the simulation results. A strong bond between two particles forced them to stay together without slip during shearing of the sample. As a result, two bonded particles behaved like one particle with the shape of number 8 which was referred to as "peanut" in this study.

The interface tests were simulated by a model with dimensions of 15 mm (height) × 40 mm (width) as shown in Fig.6.1. Two stationary vertical walls represented the sides of the direct shear box. The top horizontal boundary which was mobile in the vertical direction represented the platen used for the application of normal load. By using a numerical servo-control technique, the position of this boundary was adjusted in order to maintain the normal stress constant during shearing under constant normal stress or kept unchanged during shearing with constant volume. The bottom horizontal boundary was free to move only in the horizontal direction and it represented the steel plate. A velocity was specified, rather than specifying the force, to move the bottom boundary in the horizontal direction.

In the simulations of the sand-steel interface test under constant stress, the number of particles varied between 650 and 1300 in different runs. Calculations involved samples with same size particles and samples with different size of particles. At the beginning, all particles within the area of the shear box were generated with radii smaller than the actual values. Then, the radii were increased in stages in order to achieve a desired porosity in the model. The procedure of sample preparation influenced the initial fabric of the sample and consequently affected its strength and deformation behaviour. After this stage, gravity was applied. Once a stable state (i.e., unbalanced forces became small) was achieved under the gravity, the desired normal stress was applied at the top boundary of the sample. The shearing started subsequently by moving the bottom boundary horizontally at a certain velocity.

In the simulation of the sand-steel interface test with constant volume, only peanut shaped particle units were used. The units were formed by circular particles with the radius uniformly ranging from 0.2 mm to 0.5 mm. They had a maximum dimension varying from 0.4 mm to 1.0 mm with an orientation uniformly varying from 0° to 180°. In total, 600 peanuts were used. At the beginning, all particles within the area of 40 mm × 20 mm were generated with radii much smaller than the desired values. Then, the radii were increased in stages in order to avoid the crossing of peanuts and form a uniform loose state.

6.3.2 Parameters

In this study, the model parameters were determined from previous numerical studies and physical experiments. According to the suggestion made by Cundall and Strack (1979), the ratio of k_s/k_n was set to 2/3. In the calculations, both k_{np} and k_{nw} were equal to 1.5E7 N/m^2, and both k_{sp} and k_{sw} were equal to 1.0E7 N/m^2. The coefficient of friction, $\tan\phi_w$, was assigned the following values. For the side walls, it was 0.017 and for the top boundary, it was 1.0. For the bottom boundary, the value of $\tan\phi_w$ was chosen 0.75 for the simulation with constant normal stress because that was a measured value in the test. For the simulation with constant volume, it was assigned 0.35 which might be the most possible value according to the values measured in the constant normal stress tests and considering the effect of normal stress level. Very high values were assigned to the normal and shear bonding strengths, i.e., c_n and c_s =1.E60 N, and also the normal and shear parallel bonds had very high strength, i.e., 1.0E80 N/m^2. Therefore the bonds could not be broken during shearing. The normal and shear stiffnesses of the parallel bonds had the following values equivalent to the contact bond stiffnesses, 7.8E13 N/m^3 and 5.2E13 N/m^3, respectively, for the radius ratio of the contact disk of 0.5. The density of particles was equal to 2650 kg/ m^3. The horizontal velocity of the bottom boundary was related to the tangential displacement rate used in the laboratory test, i.e., 1 mm/min.

6.3.3 Calculated cases

The calculated cases with their specific characteristics are listed in Table 6.1, in which Cases D01 through D14 were designed for the simulation of dense sand - rough steel plate interface test under constant normal stress while Case D15 was designed for the simulation of loose sand -smooth steel plate interface test with constant volume. The computed results are discussed in the sections to follow.

Table 6.1 Description of all calculated cases

Case No.	Particle radius (mm)	Number of particles	Coefficient of friction between particles ($\tan\phi_p$)	Bonding at contact
D01	0.5	650	0.5	none
D02	0.5	675	0.5	none
D03	0.5	650	1.0	none
D04	0.5	675	1.0	none
D05	0.5	665	1.0	none
D06	0.5	670	1.0	none
D07	0.5	665	1.0	after applying gravitation
D08	0.2 → 0.5	1225	1.0	none
D09	0.2 → 0.5	1225	1.0	after applying gravitation
D10	0.2 → 0.5	1225 (5 layers)	1.0	after applying gravitation
D11	0.2 → 0.5	1225 (5 layers)	0.5	after applying gravitation
D12	0.2 → 0.5	1225 (5 layers)	1.0	before applying gravitation
D13	0.2 → 0.5	1250 (5 layers)	1.0	after applying gravitation
D14	0.2 → 0.5	1300 (5 layers)	1.0	after applying gravitation
D15	0.2 → 0.5	1200	0.5	before applying gravitation

6.4 Strength-Deformation Characteristics under Constant Normal Stress

All calculated cases were divided into two groups.

6.4.1 Group-I: Particles with same radius - round particles

In Group-I, all particles had 0.5 mm radius. The computed results for this group are shown in Fig.6.2. In this group, Case D05 gave the best simulation for the shear stress development. However, the calculated deformations almost in all cases of this group were different than the measured results represented by the heavy solid line in Fig.6.2.

In Case D04, the number of particles used was 675. The coefficient of friction between the particles was 1.0. These values made the sample fabric very strong so that only sliding took place at the contact surface after the maximum shear stress was reached at about 1.0 mm without any other change in the sample. However, in case D02 with the same number of particles, the reduction of $\tan\phi_p$ from 1.0 to 0.5 totally changed the strength characteristic of the sample. Sliding failure took place again but along some curved surface in the sample rather than at the contact surface. This indicated that the value of about 0.5 measured for the coefficient of friction in sand material by other investigators (Misra, 1995) could not be directly used for $\tan\phi_p$ in the discrete element simulation. It means that in the discrete element method $\tan\phi_p$ represents not only the coefficient of friction between sand particles but also influences the particle movements. A small reduction in the particle number in Case D03 compared with case D04 made the shear strength reduced excessively. In addition, the change of $\tan\phi_p$ from 1.0 to 0.5 for Case D03 and D01 resulted in a further reduction in shear strength. However, the change in $\tan\phi_p$ almost had no effect on the deformation behaviour of the sample. The sample in both Case D01 and Case D03 experienced compression after the maximum dilation. This meant that the total number of particles in both cases was too small to keep the sample fabric strong enough that the deformation trend could be maintained similar to the one observed in experiments after the peak shear strength was reached. According to the above discussion, it was concluded that a total number of particles between 650 and 675 with a radius of 0.5 mm was appropriate for a reasonable simulation.

In Case D06, the sample compressed less than the sample in Case D05, and also experienced an early failure in some parts of the sample in the shear box before the shear stress could be further increased to its peak value. A small reduction in the particle number in Case D05 produced a better simulation of shear strength, although the deformation behaviour was not satisfactory. In Case D07, bonding was introduced between particles in contact which improved the deformation behaviour of the sample but reduced the shear strength. Bonding was only applied to two particles at contact. Bonding was formed after the application of gravitational forces to the particles. This bonding could not be broken during the whole simulation process because of very high values assigned to the bonding strengths. As a result, in the simulation, two bonded particles behaved like one particle with a non-circular shape which was called "peanut".

6.4.2 Group-II: Particles with various radii - peanut shape particle units

In the second group, the DEM models had particles with various radii uniformly distributed within a range between 0.2 mm to 0.5 mm. In addition, peanut shape particle units were used in the analysis except in Case D08. The bonding was formed either before or after the application of gravity.

The computed results are shown in Fig.6.3. In this group, Case D10 gave the best simulation in both shear stress development and deformation behaviour (i.e., there was an initial contraction and subsequently continuing dilation as the shearing progressed). In this case, peanut shape particle units were used and all particles were generated in five layers.

In Case D08, the use of particles with various radii improved the simulation of deformation, although the peak shear stress remained low. Application of bonding between particles did not increase the shear strength. Bonding made the shear strength reduce in Case D09. On the other hand, the shear strength increased in Case D10, which had a comparatively uniform sample where the particles were generated in five layers. In Case D12, where the particle bonding was formed before applying gravitational forces to particles, the shear strength was lower than that of Case D10. All these cases showed the effect of fabric on sample behaviour.

However, when the coefficient of friction between particles was reduced again to 0.5 in Case D11, the calculated value of the interface shear strength became very low in spite of the improved fabric which used variable size peanut shape particles. This further confirmed that the value of about 0.5 measured for the coefficient of friction in sand material by other investigators could not be directly used in the discrete element simulations.

These observations showed that, the sample in the simulations was softer than measured in experiments before the peak shear strength was reached. An increase in the number of particles made the sample stiffer as in Case D13 and Case D14, but the failure took place before the expected peak shear strength could be developed. In these two cases, the sample dilated excessively. These cases indicated that increasing particle number was not always a good approach to make the sample stiffer.

6.5 Simulation of Interface Test under Constant Volume Condition

For the loose sand - smooth steel plate interface test with constant volume, the computed results for shear and normal stresses are presented in Fig.6.4. The general trend was simulated properly, i.e., the shear stress increased first to the peak value and then reduced as the normal stress decreased from the initial value. However, comparing with the test results, the difference is still obvious, i.e., the shear stress increased slowly, and both the shear and normal stresses decreased slowly. This shows the difficulties in the simulation of loose sand.

The difference between the simulation result and the experimental data observed in Fig.6.4 are most likely due to the effect of particle fabric. Therefore, there is a need for further investigation on the effect of sample fabric on the behaviour of interfaces with loose sand.

6.6 Summary

The discrete element method was used to simulate the mechanical behaviour of an interface between sand and a steel plate. It was found that the method provides reasonable simulations for sand-steel interface behaviour. Based on the calculations, the following general observations were made:

(1) The shear strength of the interface is related to the number of particles, sample fabric, the coefficient of friction between particles and the coefficient of friction between sand and the steel plate. However, the deformation characteristic almost has nothing to do with the coefficient of friction between particles in simulations.

(2) The value of the coefficient of friction in sand measured by other investigators cannot be directly used in the DEM simulations. What value can be used is strongly related to the fabric of sample. Also the fabric of the sample had a strong influence on the calculated strength and deformation behaviour.

(3) The particle shape plays an important role in the simulations. The simulations using the peanut shape particle units produced satisfactory results for both strength and deformation behaviour of an interface under constant normal stress.

(4) Although the maximum shear strength can be simulated reasonably well, the sample behaviour is softer than the experimentally observed behaviour before the peak shear strength is reached. Furthermore, the compressive deformations during shearing was not fully simulated. It was shown that increasing the number of particles is not a good approach to make the sample stiffer.

(5) DEM can simulate properly the general trend of normal and shear stress variations at the interface of loose sand - smooth steel plate in the monotonic constant volume loading condition. However, the results also showed the difficulties in the simulation of loose sand. There is still more space to explore the influence of sample fabric in the DEM simulation of the behaviour of loose sands.

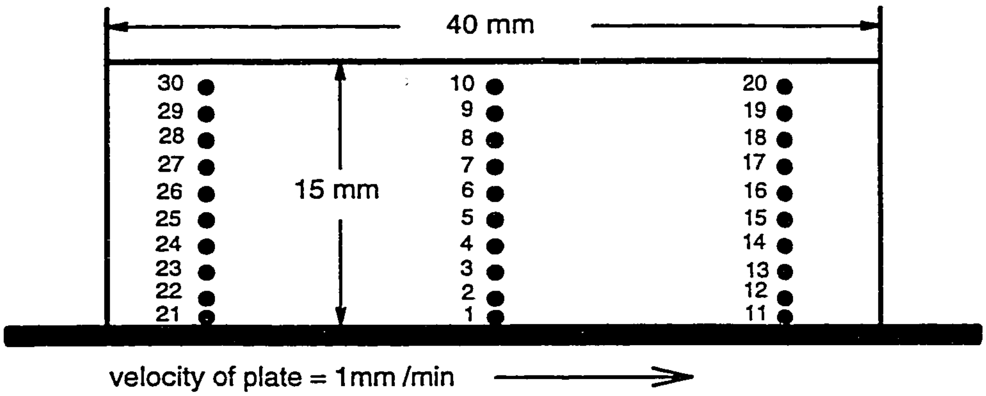

Fig.6.1 DEM simulation model

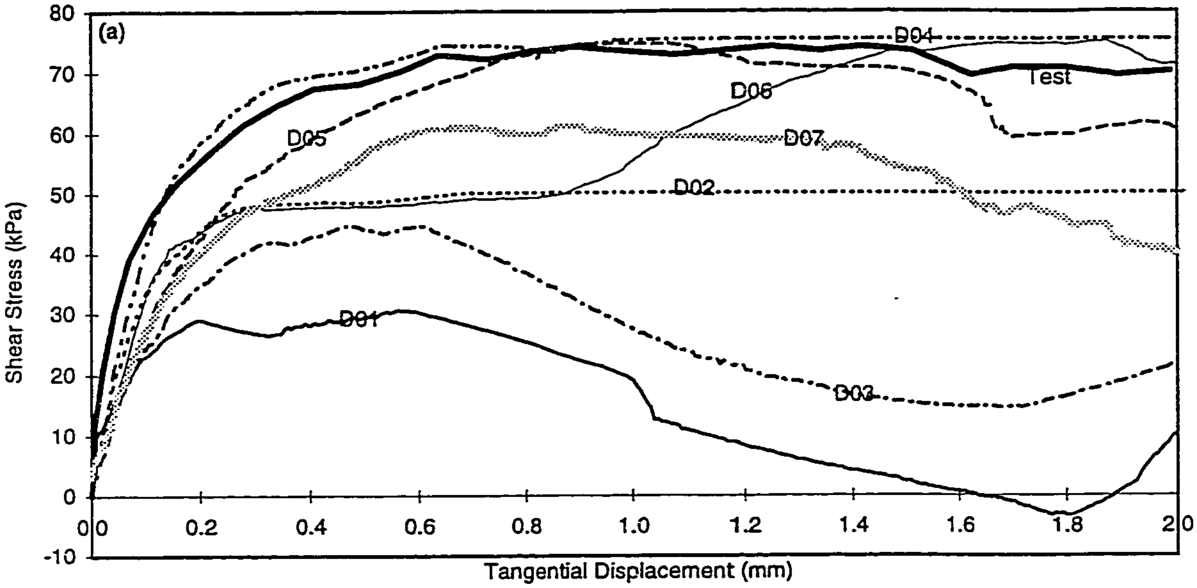

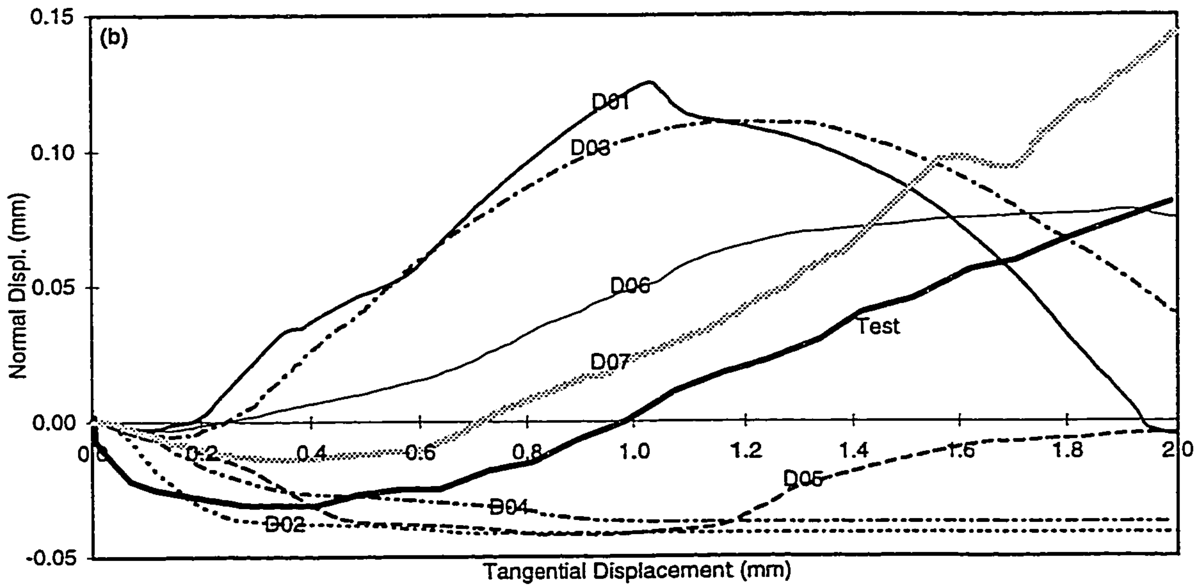

Fig.6.2 Computed results of DEM model (particle radius = 0.5 mm)

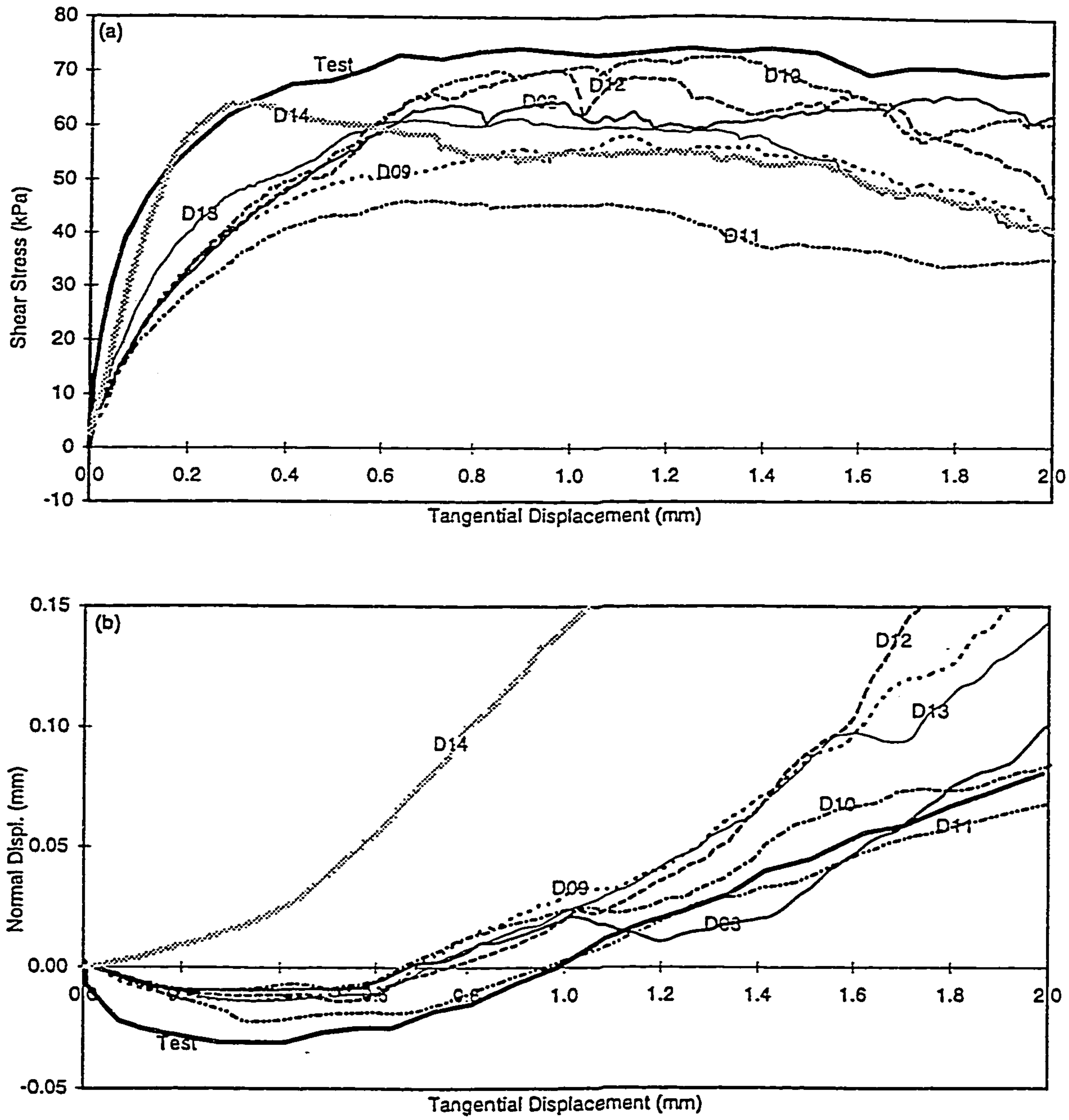

Fig.6.3 Computed results of DEM model (particle radius = 0.2 - 0.5 mm)

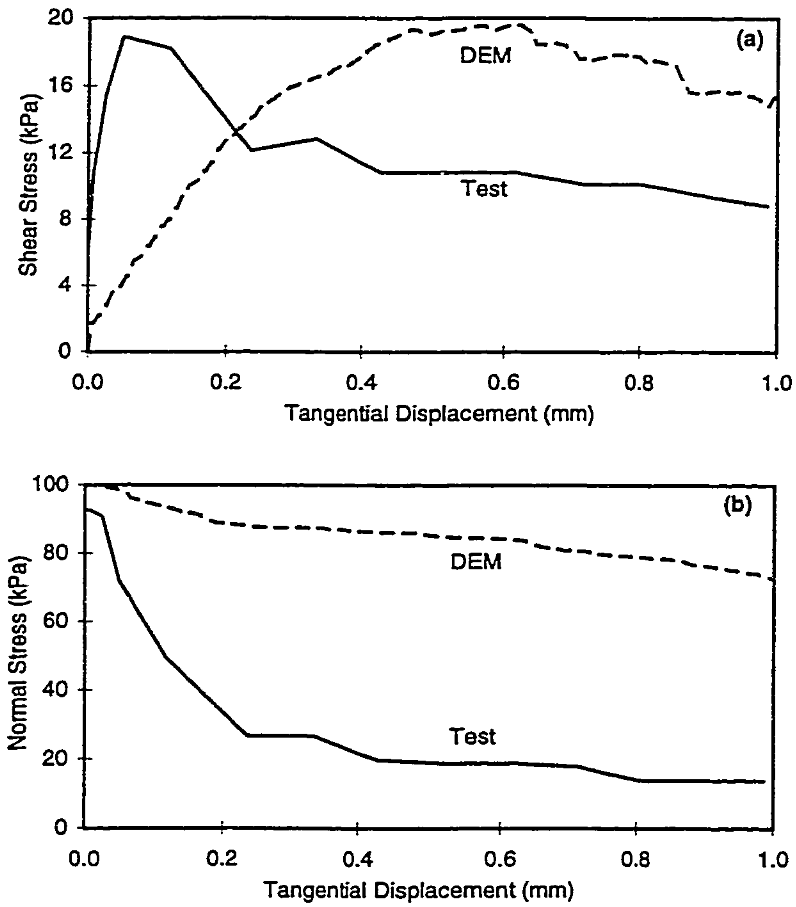

Fig.6.4 Computed results of DEM simulation of loose sand - rough steel plate interface test under constant volume condition

CHAPTER 7
PARTICLE MOVEMENTS AT SAND-STEEL INTERFACE

7.1 Introduction

In the previous chapter, it is shown that the discrete element method can be used to simulate the sand-steel interface behaviour properly. DEM also provides a useful method to "observe" particle movements at soil-structure interfaces. It can trace not only horizontal and vertical movements but also rotations of particles. The rolling of particles is an important part of the interface mechanism and the formation of a shear zone. In contrast, it is difficult to measure these rotational movements of particles in tests. In this section, first, the existing experimental investigations of sand particle movements at interfaces will be summarized. Then, the discrete element method will be used to investigate the interface mechanism, side wall effects of direct shear box and velocity field at a sand-steel interface test.

7.2 Existing Experimental Investigations

Yoshimi and Kishida (1981a, b) presented the observation results in ring simple shear type tests by tracing the positions of the embedded lead balls. Typical results of X-ray observations using steel and medium dense Tonegawa sand is shown in Fig.7.1. Each symbol with an arrow indicates a circumferential displacement of the metal ring from the initial position, and those without arrows show the displacement of lead markers (0.8 mm in diameter). Thus, the horizontal distance between the top symbol and the symbol with an arrow show the amount of slip at the sand-metal interface. When the metal is very smooth (Fig.7.1a,b), the sand is sheared uniformly without developing a shear zone; therefore the circumferential displacement of the metal consists mostly of slip. The phenomenon resembles that of solid-to-solid friction in that dynamic friction is smaller than static friction. This is reflected in Fig.7.1b′ in which the shear strain in the sand decreases as the slip distance increases. When the metal is slightly rough (Fig.7.1c,d), a shear zone develops near the metal surface immediately after a slip occurs. The shear zone begins to form when the shear stress ratio exceeds about 75 % of the coefficient of friction. When the metal is very rough (Fig.7.1e,f), on the other hand, a shear zone develops in the sand without a slip. This condition corresponds to the upper limit of coefficient of friction. The thickness of the shear zone for the tests was 5 to 8 times the mean grain size. It should be noted that the embedded lead balls are larger than the maximum particle diameter of the sand. Placing the balls in the sand sample can cause disturbance of the sand fabric. It was impossible to observe the particle rolling with the use of virtually spherical lead balls.

Uesugi et al. (1988) installed a glass window to the shear box for observing the particle movement near the interface by taking photographs. The particle movement was read with a coordinate measuring machine. Fig.7.2 shows the load-displacement relationship in friction test with a rough interface ($R_n = 68\times10^{-3}$). Also shown is the volumetric strain during the test. Photographs were taken at those points shown in the figure. By comparing these photographs, it was noticed that particles did not only slip but also rolled along the interface, the tangential displacement of particles was much smaller than the total displacement, the sand particles moved not only in the tangential direction but also in the direction normal to the interface. The sand mass was partitioned into 8 layers on the photograph prints. Each layer contained five tracked particles. Fig.7.3 shows the averages and the standard deviations of the increase in tangential displacement of the particles. Fig.7.4, on the other hand, shows the increase in normal displacement. From the start (O) to the peak (A_4), the sand deformed uniformly (Fig.7.3a). There was not a large increase in the sand volume (Fig.7.4a). Between A_4 and B_4, there was large shear deformation of sand near the sand-steel interface (Fig.7.3b). A clear increase was observed in the sand volume near the interface (Fig.7.4b). Between B_4 and C_4, there was large shear deformation of sand near the sand-steel interface (Fig.7.3c). The volume increase of sand was smaller than the previous stage (A_4 to B_4). During A_4 to C_4, the standard deviations were large in the tangential displacement of particles near the interface. It is typical of the particles to move randomly in a shear zone of sand mass. A shear zone formed within the sand mass along the sand-steel interface during the interface sliding. The shear zone thickness was visually determined by particle displacement. The particle displacement in a shear zone exceeds the value expected by extrapolating the displacement due to the shear deformation of sand mass. A shear zone is also characterized by the large deviation of particle displacement. A shear zone thickness of 3 - 4 times the diameter of sand particles was observed. Fig.7.5 shows the increase in tangential displacement of aluminum frames in test with a rough interface ($R_n = 68\times10^{-3}$). Between A_4 and B_4, the dilatant sand in the shear zone pushed up the aluminum frames about 1.5 mm. Also plotted are the average increase in particle displacement. The distance from the sand-steel interface was corrected according to the average normal displacement of the particles (Fig.7.4). As shown in Fig.7.5, the displacement of the aluminum frames is somewhat smaller than the displacement of the sand particles. In the test with a smooth interface ($R_n = 15\times10^{-3}$), both the volume increase and the shear deformation of the sand were much smaller than that with a rough interface. In contrast to rough interface, there was no rolling of sand particles. The major factor of interface sliding was slipping of particles on the steel surface. The displacement of particles was much smaller than the total displacement. It was also smaller than that in a test with a rough interface. The behaviour of sand particles in a sand-steel friction test with $R_n = 68\times10^{-3}$ under two-way repeated loading was also observed by Uesugi et al. (1989).

In 1990, Uesugi et al. presented their observations on particle movements in friction tests on sand-concrete interfaces. Before the peak of load-displacement curve, the sand deformed uniformly. There was not a large increase in the sand volume. After the peak, there was large shear deformation of sand along the sand-concrete interface. The sand volume increased along the interface. A shear zone formed along the rough interface between sand and concrete. The relative density of sand in shear zone was lower than that of the sand before the interface failure. The lower density of sand in the shear zone resulted in the lower maximum shear stress ratio. The upper limit to the coefficient of friction decreased because of the shear zone formation. In the test with a smooth interface ($R_n = 18\times10^{-3}$), the shear deformation of sand mass was smaller than that with a rough interface. The volume increase in the sand mass was negligibly small. The sand mass slipped along the smooth interface without a clear formation of shear zone. In the test with a rough interface under two-way repeated loading, the sand mass deformed uniformly before the peak of shear stress ratio. After the peak, interface displacement became large and the volume increased near the interface. A shear zone formed along the interface. In the 15th cycle, the sand mass deformed just after the reversing of loading direction. The shear deformation was largest along the interface. After reaching a constant value of the shear stress ratio, the tangential displacement consisted of interface sliding and shear zone deformation. In the first cycle of the test with a smooth interface under two-way repeated loading, there was small shear deformation of sand mass before the interface yielding. After reaching a constant value of shear stress, a large portion of the tangential displacement became interface sliding. In the 15th cycle, the sand mass deformed during the load increase just after the reversal. After reaching the constant shear stress ratio, the shear deformation became negligibly small along the sand-concrete interface. The interface sliding became the major factor of the tangential displacement. The formation of shear zone along smooth interface was caused by the particle crushing along sand-concrete interface under two-way repeated loading. The crushed particles have the diameter much smaller than that in the original state. With the increase of normalized roughness, the coefficient of friction increased causing the formation of a shear zone along the sand-concrete interface.

During the test in the plane strain apparatus the localized shear zone was observed by Tejchman and Wu (1995) with the help of X- rays. The radiographs are shown in Fig.7.6. The dilated zone along the steel plate in dense specimen can be clearly observed. The thicknesses of the dilated zone for fine sand were approximately 1 mm (i.e., $2{\times}D_{50}$) for a rough plate and 3 mm (i.e., $6{\times}D_{50}$) for a very rough plate. No dilated zone, however, could be observed in loose sand or in dense sand in contact with a smooth steel plate. An empirical relation was used to roughly estimate the thickness of the dilated zone in dense sand from direct shear tests:

$$D\gamma_d = \gamma_{cr}(D + v_{hmax}) \tag{7-1}$$

where D is the shear zone thickness, γ_d and γ_{cr} stand for the initial and the critical density respectively and v_{hmax} is the maximum vertical displacement of sand. This relation was established under the assumption that the sand in the shear zone changes its density from the initial value to the critical value and the same number of grains was involved in the shearing, i.e., filtration and mixing are excluded. According to the above relation $D \cong 2.5$ mm (i.e., $5 \times D_{50}$) for a very rough plate and $D \cong 1.1$ mm (i.e., $2 \times D_{50}$) for a rough plate (dense fine sand). For a dense, coarse sand in contact with a very rough and a rough plate the thickness of the dilated zone is $D \cong 5.5$ mm (i.e., $4 \times D_{50}$) and $D \cong 0$ mm, respectively.

7.3 DEM Simulation of Particle Movements

In the simulations presented in the previous chapter, it was concluded that under constant normal stress condition, considering the shear stress - tangential displacement and normal displacement - tangential displacement curves, Case D05 and Case D10 gave the best simulation in each group (see Fig.7.7). The initial particle arrangement for these two cases are shown in Fig.7.8. In this section, particle movements in these two cases will be presented in order to provide information about what happens inside the sample and to discuss the effect of particle shape on DEM simulations of sand-steel interfaces.

7.3.1 Interface mechanism

The movements of particles at the locations labeled from 1 to 10 (see Fig.6.1) were traced. Horizontal displacements, vertical displacements and angular movements of particles in Case D05 are shown in Figs.7.9 through 7.11, respectively. Fig. 7.12 shows the particle positions traced for the specific moments indicated in Fig.7.7. It can be seen that the top two particles had little horizontal displacements but relatively larger downward displacements which produced an unrecovered compression of the sample. In this sample, particle 3 developed relatively large downward movements and angular displacements. Particle 6 experienced negative angular displacements. In Fig.7.12, there was no apparent pattern of particle movements in the shear box.

For Case D10, horizontal displacements, vertical displacements, angular movements, and particle position traces are shown in Figs.7.13 through 7.16, respectively. In contrary to the results of case D05, these plots showed an obvious pattern for particle movements. Fig.7.13 clearly shows that the particles closer to the contact surface had larger horizontal displacements. These horizontal displacements remained almost unchanged especially for those top particles after the peak shear stress was reached at about 1.3 mm. There is also a little jump for horizontal displacements below the top four particles. The horizontal displacements of the top four particles were small. The difference between the heavy solid line (indicating the horizontal displacement of the plate) and the medium solid line (indicating the horizontal displacement of particle 1) approximately represented the relative displacement, i.e. sliding, between the steel plate and the particles at the bottom of the sample. The relative displacement started to increase at about 0.2 mm horizontal displacement of the plate and gradually increased during shearing. These horizontal displacements remained almost unchanged after the peak shear stress was reached at about 1.3 mm.

Figure 7.14 shows the vertical displacements of the particles. The figure does not show a clear pattern of vertical displacements for all particles, especially at the initial part of shearing due to the effect of local fabric. However, it is apparent that the top four particles moved the same amount vertically after the peak shear stress was reached. The same observation can be made in Fig.7.17. This observation suggested that the dilation of the sample resulted from the accumulation of the relative upward displacements of those particles within an approximately 10 mm thick layer of particles next to the contact surface. This height coincided with the height where the horizontal displacements of particles became significant (Fig.7.17a).

Fig. 7.15 presents a trend such that the particles closer to the contact surface had larger angular movements developed during shearing. For other particles, angular movement plots moved around the above mentioned curves. It should be noted that the movements of an individual particle were also effected by the local fabric around that particle. Generally, all particles had positive angular movements (representing counter-clockwise rotation) within the range of 1 degree (for particles away from the interface) to 7 degree (for particles near the interface).

7.3.2 Effects of side walls of direct shear box

The pattern of particle movements described above was not the same for the particles near the side walls of the soil container due to the boundary effects. This problem was examined by tracing the positions of those particles near the side walls shown in Fig.6.1. For those particles 5 mm away from the right wall, the particle movements are plotted in Figs 7.18 and 7.19; and for those particles 5 mm away from the left wall, the particle movements are plotted in Figs7.20 and 7.21. It was clear that the side walls of direct shear type soil container had a definite influence on the movement pattern of particles.

7.3.3 Velocity field analysis

An overall picture of the particle kinematics in the shear box is presented by the velocity plot at different times during the test as shown in Fig.7.22. The velocities of particles shown in this figure were normalized with respect to the largest velocity of particles. At moment "a", the particles moving with a relatively large horizontal velocity were concentrated in an approximately 8 mm thick layer next to the contact surface. The thickness of this layer was a little smaller than the one obtained from the observations of displacements (Fig.7.17). The particles close to the right wall climbed up, and the particles close to the left wall moved downwards. In addition, some whirlpool type movements were observed. At moment "b", the velocities of particles were reduced due to sliding at the contact surface. However, the movements of the particles were still following a pattern in the central portion of the sample. At moment "c", upward movements started to develop. Only a small number of particles near the contact surface were still moving horizontally. At moment "d", almost all particles moved upward. Generally, non-uniformities of particle movements depended on the loading stage and they could be found even in the middle part of the sample.

From these velocity plots of particles at sand-steel interface shown in Fig.7.22, the side wall effect of direct shear box on particle movements can also be clearly observed.

7.4 Summary

The behaviour of sand particles has an important role on the friction at sand-steel interfaces. Measuring the displacement of sand particles is a useful method for understanding the interface mechanism. It is important to observe shear zone formation in order to explain the reduction of shear stress ratio after the interface yielding. In terms of existing experimental investigations, some major observations can be summarized as follows:

(1) The interface is a thin zone along the contact surface between the soil mass and the construction material. The interface soil undergoes very large structural changes and grain crushing during the localized shear. The thickness of the interface is essentially independent of the problem considered after large enough deformations take place. The interface thickness can be visually determined by particle displacement. The particle displacement in an interface zone exceeds the value expected by extrapolating the displacement due to the shear deformation of sand mass. The interface thickness is usually within the range of 2 to 8 times the mean grain size.

(2) The particles move not only in the tangential direction but also in the direction normal to the interface. Before the peak of frictional resistance, there was little sliding at the interface. The sand mass deformed uniformly. There was not a large increase in the sand volume. At the peak, the interface started sliding. Along a rough interface, the particles slipped, rolled and moved up and down. Along a smooth interface, on the other hand, sand mass slipped without large deformation. A shear zone formed in the sand along a rough interface during sliding accompanying a volume increase. It is typical of the particles to move randomly in a shear zone. A shear zone formation explains the reduction in frictional resistance during the interface sliding. When the interface was smooth, there was no formation of shear zone.

(3) The relative density of sand in shear zone is lower than that of the sand before the interface failure. The lower density of sand in the shear zone results in the lower maximum shear stress ratio. Therefore the upper limit to the coefficient of friction decreases because of the shear zone formation.

(4) The front wall of the shear box prevents horizontal movements and therefore creates a complex load transfer mechanism in the region between the horizontal plane (along the interface) and the vertical wall. This may influence the accuracy of measurements. Therefore, it is strongly suggested that interface behaviour should be evaluated based on the measurements taken in the middle area of the shear box or using a larger shear box in order to reduce the side wall effects.

Based on the DEM simulations of particle movements in a sand-steel interface test, the following conclusions are drawn:

(1) The simulations using the peanut shape particle units of various size produced reasonable movement patterns for the particles near the sand-steel interface.

(2) The movements of an individual particle may be effected by the local fabric around that particle, but a general trend of particle movement pattern can be observed.

(3) The particles closer to the contact surface had larger horizontal displacements. The relative displacement, i.e., sliding, started to increase at about 0.2 mm horizontal displacement of the plate and gradually increased during shearing. The horizontal displacements of particles remained almost unchanged after the peak shear stress was reached at about 1.3 mm.

(4) The numerical experiments show that the total dilation of the sample results from the accumulation of the relative upward displacements of those particles within a layer of particles 10 mm above the contact surface.

(5) The particles closer to the contact surface had larger angular movements developed during shearing. Generally, all particles had positive angular movements (representing counter-clockwise rotation) within the range of 1 degree (for particles away from the interface) to 7 degree (for particles near the interface).

(6) A shear band was formed within a thickness of 10 mm above the contact surface. This shear band thickness was decided on the basis of the observations in the horizontal, vertical and angular movements of particles. This thickness is a little more than that is calculated from the particle velocity plots. Considering the particle bonding effect, the thickness of the interface is about 7 times the average diameter of units of particles.

(7) The movements of particles located along different vertical sections of the shear box were not identical. The side walls of direct shear type soil container have an influence on the movement pattern of particles at least 5 mm away from the vertical boundaries.

(8) Generally speaking, the DEM simulation of particle movements at sand-steel interface presented here agrees well with the existing experimental observations.

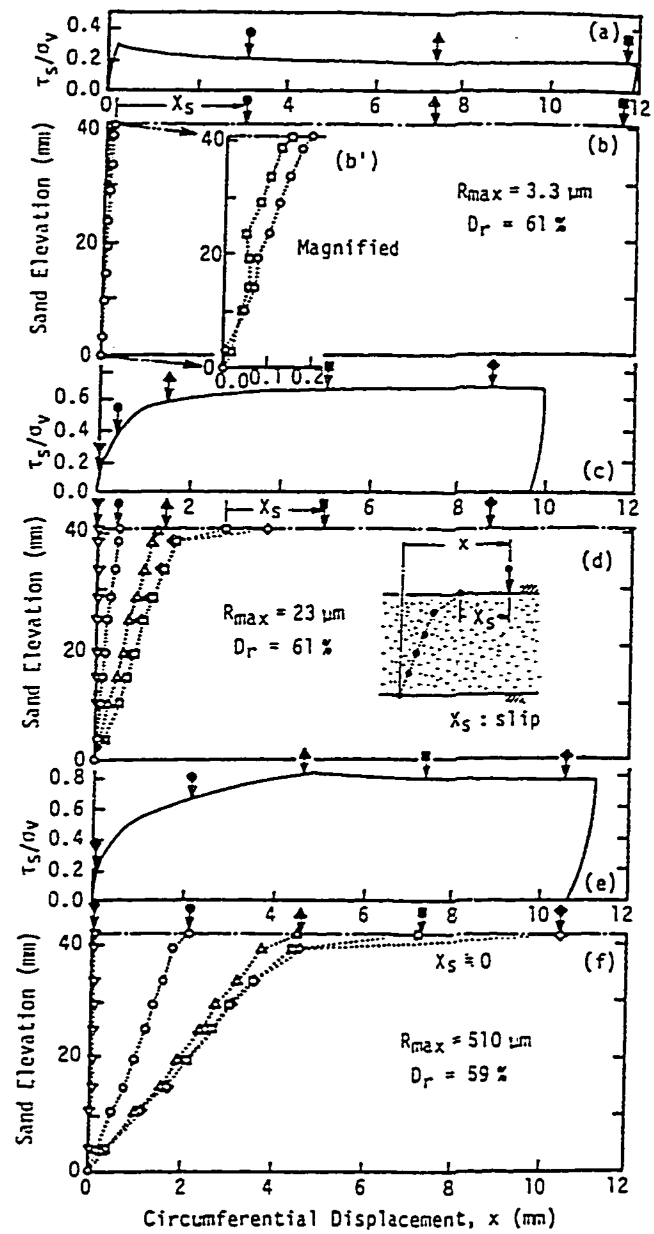

Fig.7.1 Deformation of sand observed by radiography (steel and Tonegawa sand) (after Yoshimi and Kishida, 1981b)

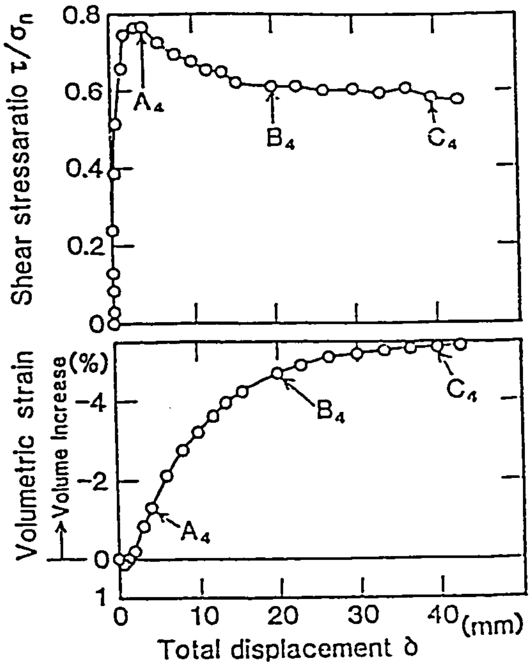

Fig.7.2 Load-displacement relationship with a rough interface (after Uesugi et al., 1988)

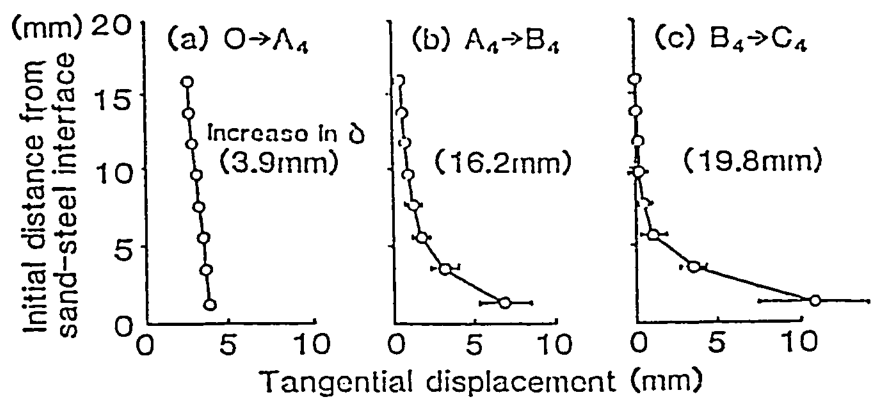

Fig.7.3 Tangential displacement of particles with a rough interface (after Uesugi et al., 1988)

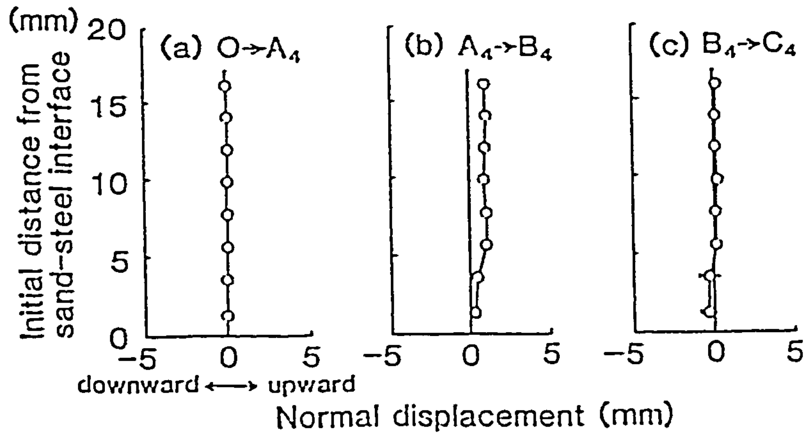

Fig.7.4 Normal displacement of particles with a rough interface (after Uesugi et al., 1988)

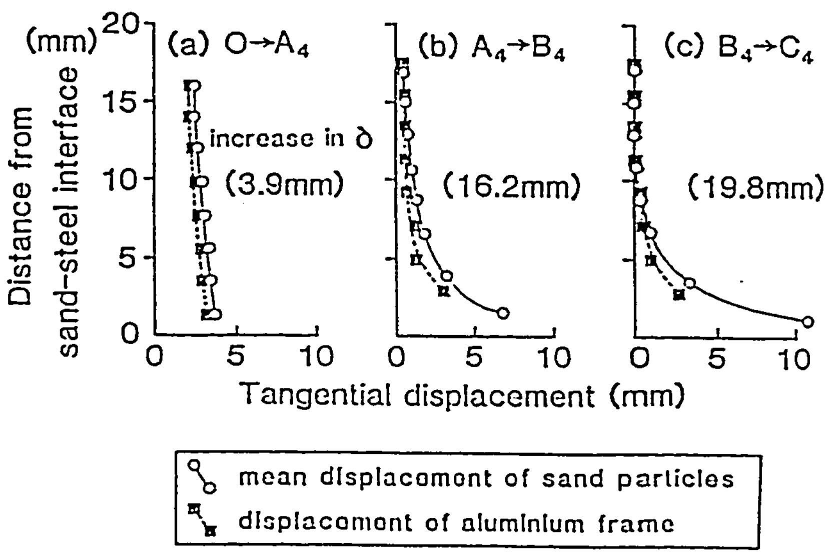

Fig.7.5 Tangential displacement of sand particles and aluminium frames with a rough interface (after Uesugi et al., 1988)

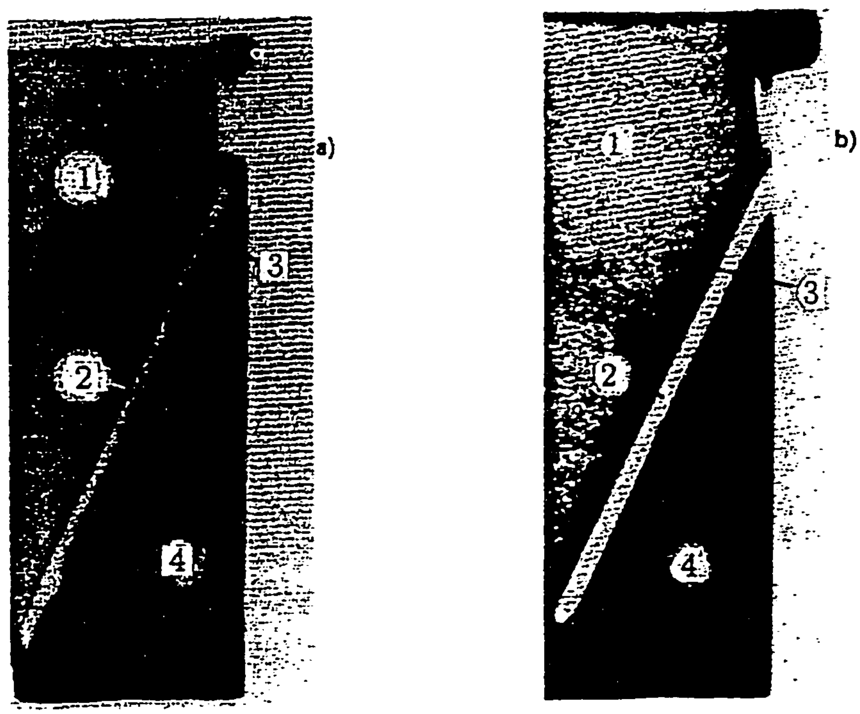

Fig.7.6 Radiographs from the plane strain tests with (a) rough plate and (b) very rough plate: (1) sand specimen, (2) steel plate, (3) dilated zone, (4) wooden wedge (after Tejchman and Wu, 1995)

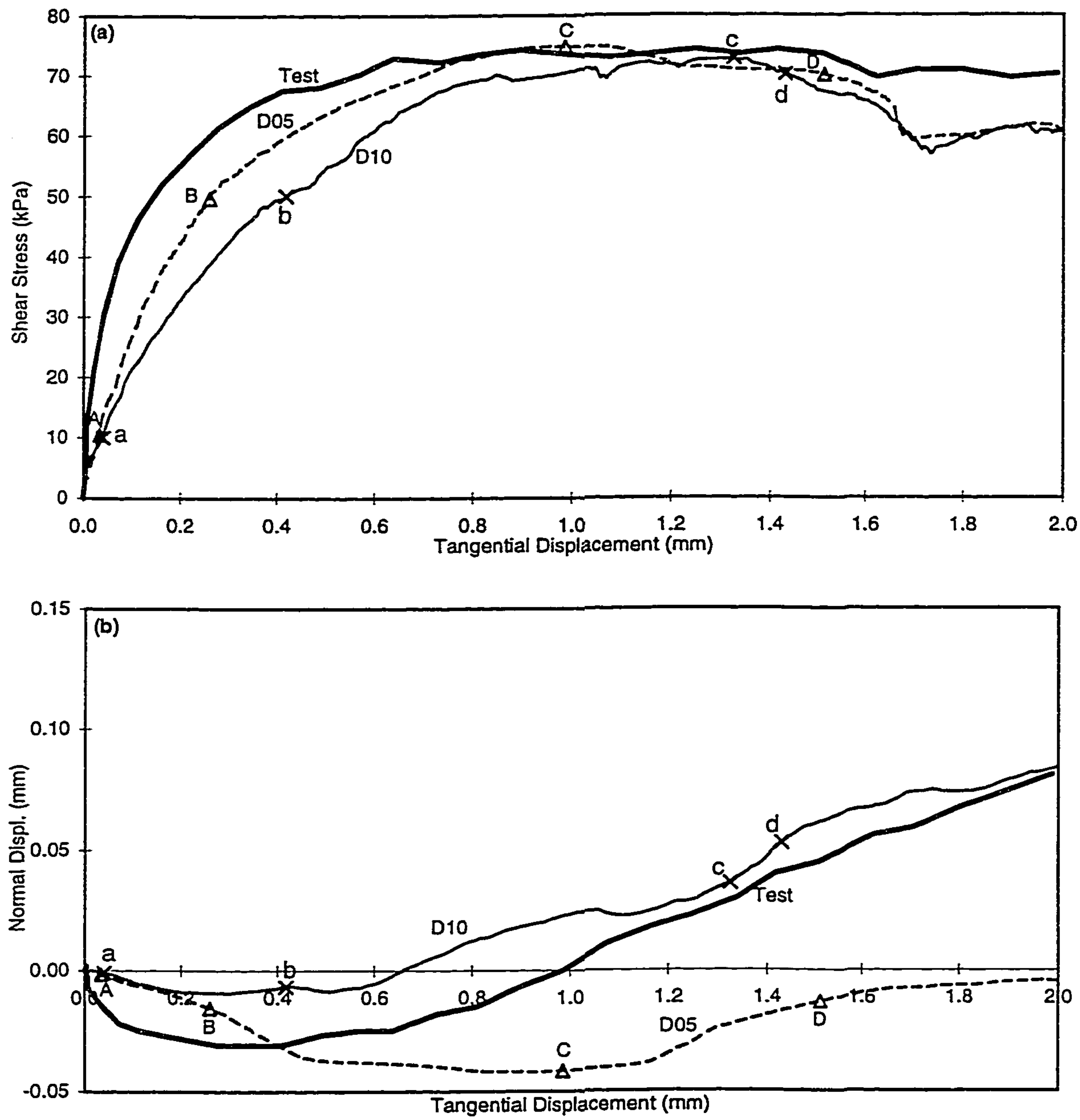

Fig.7.7 DEM simulations of interface test under constant normal stress condition and moment points for plotting particle positions

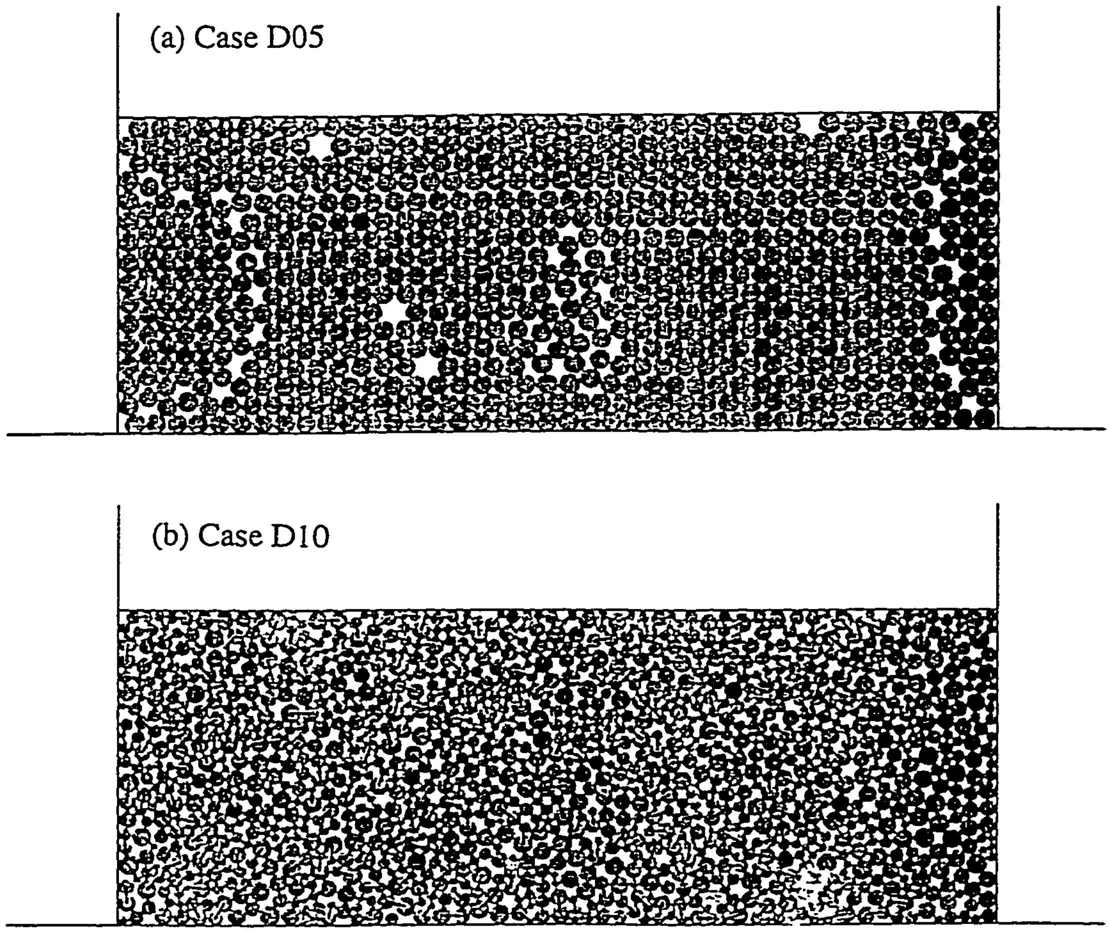

Fig.7.8 Initial particle arrangements in DEM simulations

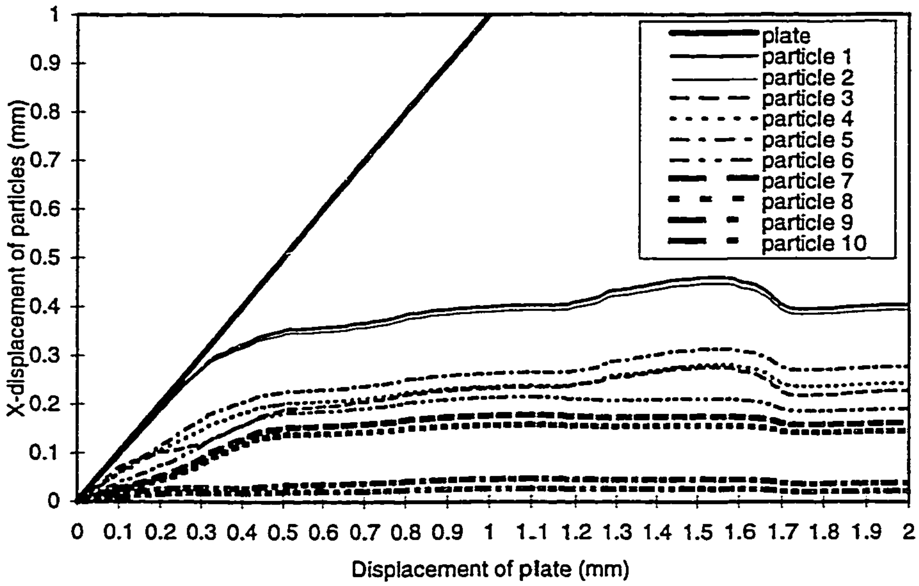

Fig.7.9 Horizontal displacements of particles at the middle of shear box for Case D05

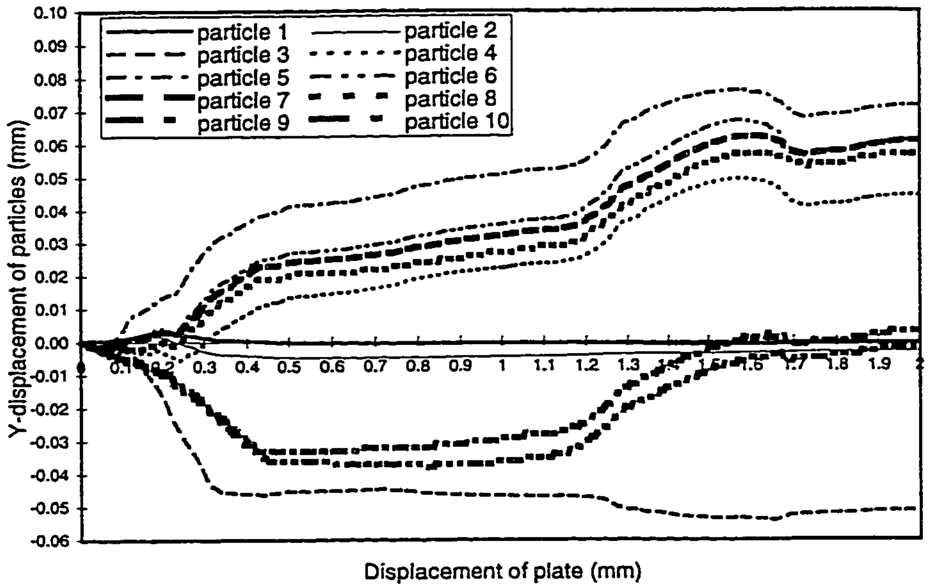

Fig.7.10 Vertical displacements of particles at the middle of shear box for Case D05

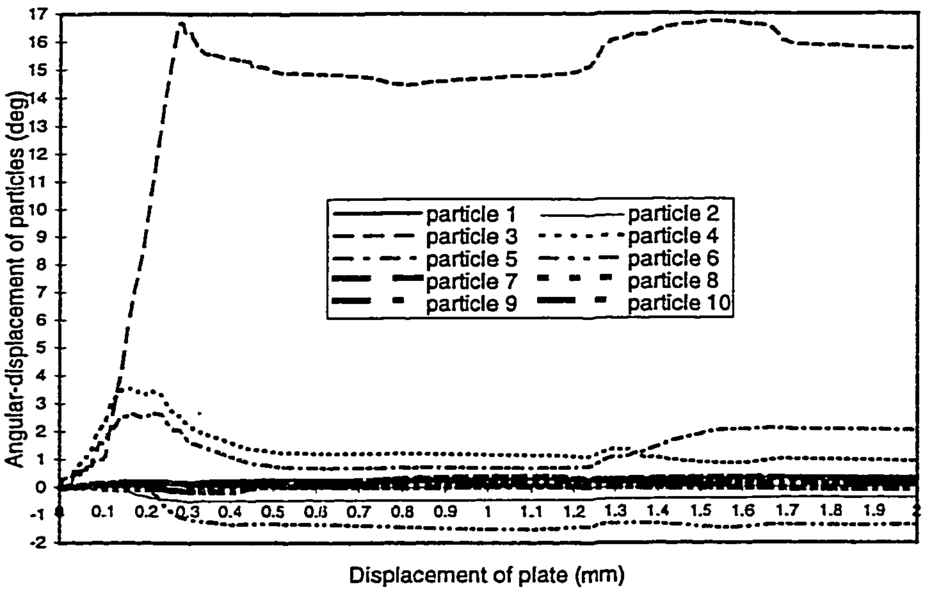

Fig.7.11 Angular displacements of particles at the middle of shear box for Case D05

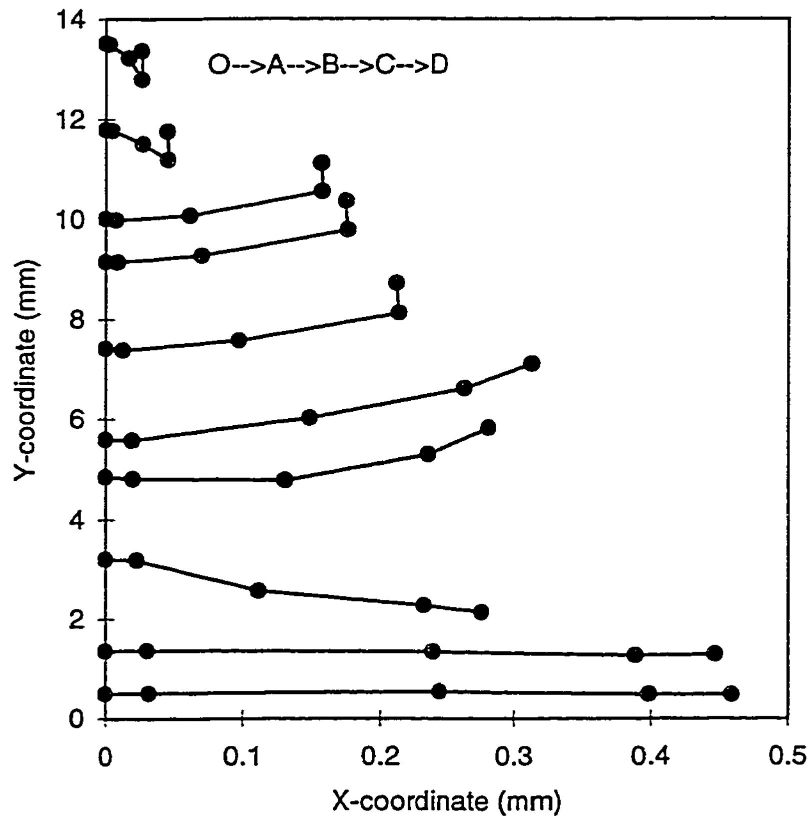

Fig.7.12 Movement traces of particles at the middle of shear box for Case D05 (vertical displacements are magnified 20 times)

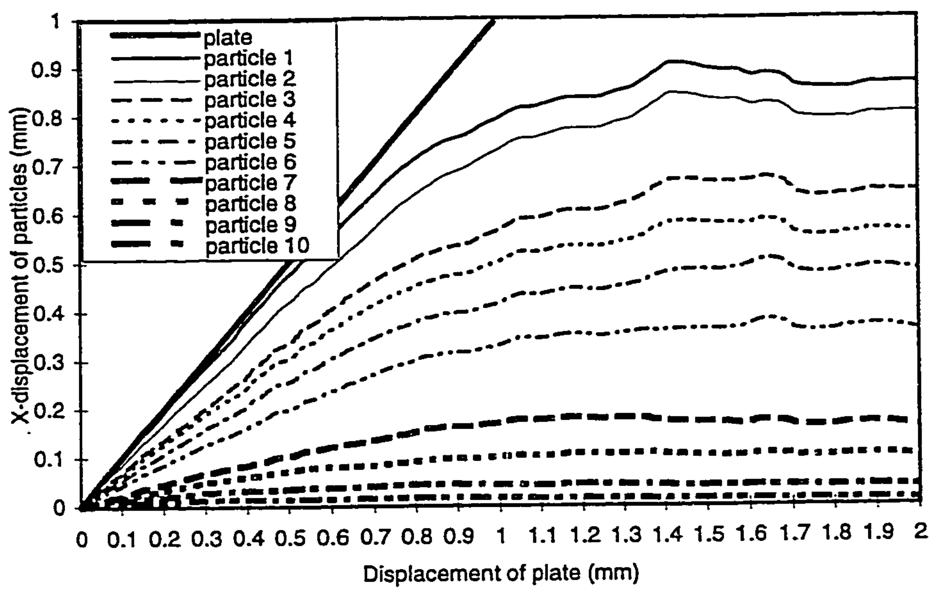

Fig.7.13 Horizontal displacements of particles at the middle of shear box for Case D10

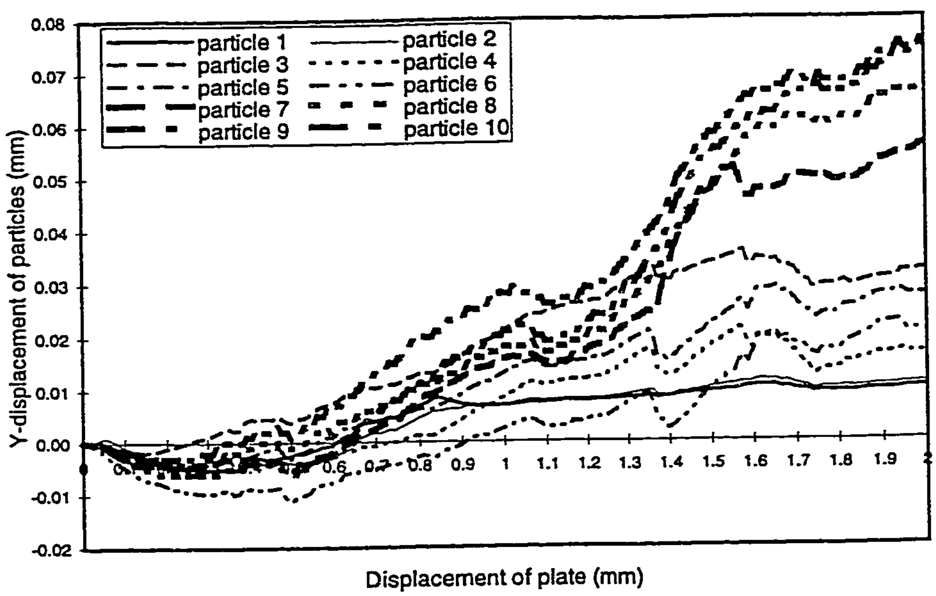

Fig.7.14 Vertical displacements of particles at the middle of shear box for Case D10

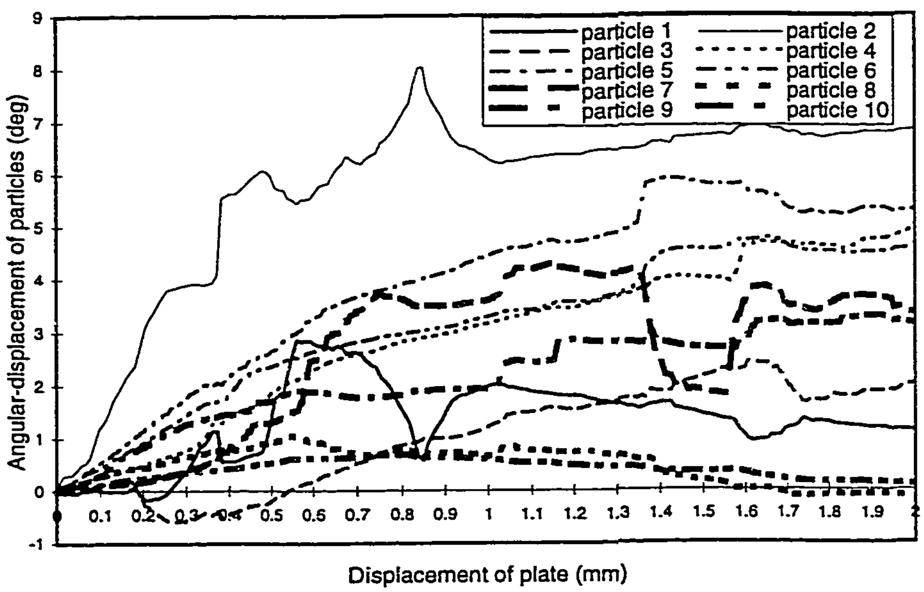

Fig.7.15 Angular displacements of particles at the middle of shear box for Case D10

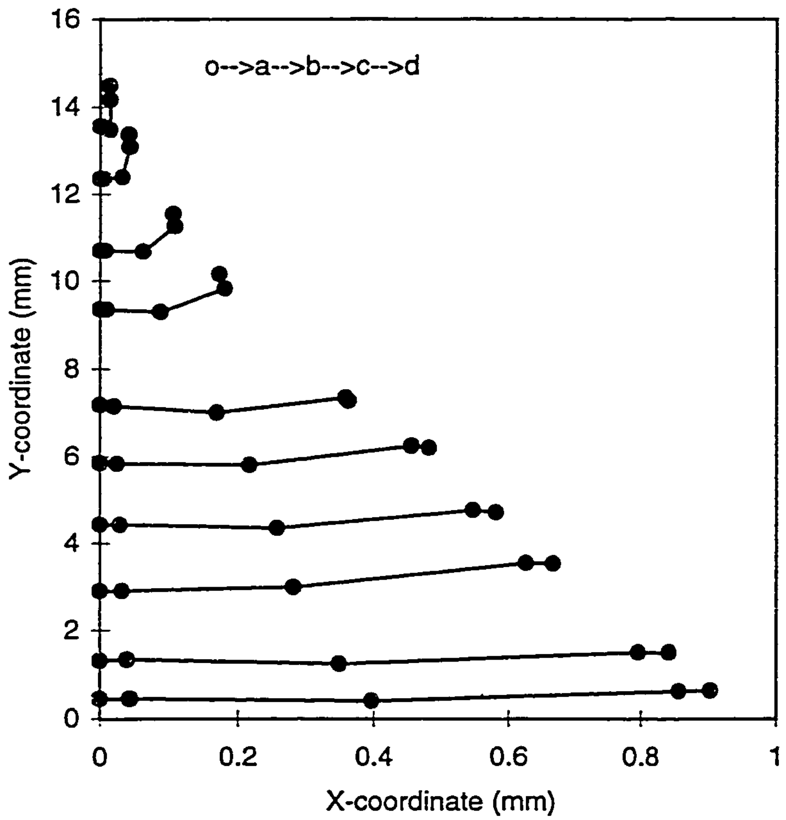

Fig.7.16 Movement traces of particles at the middle of shear box for Case D10
(vertical displacements are magnified 20 times)

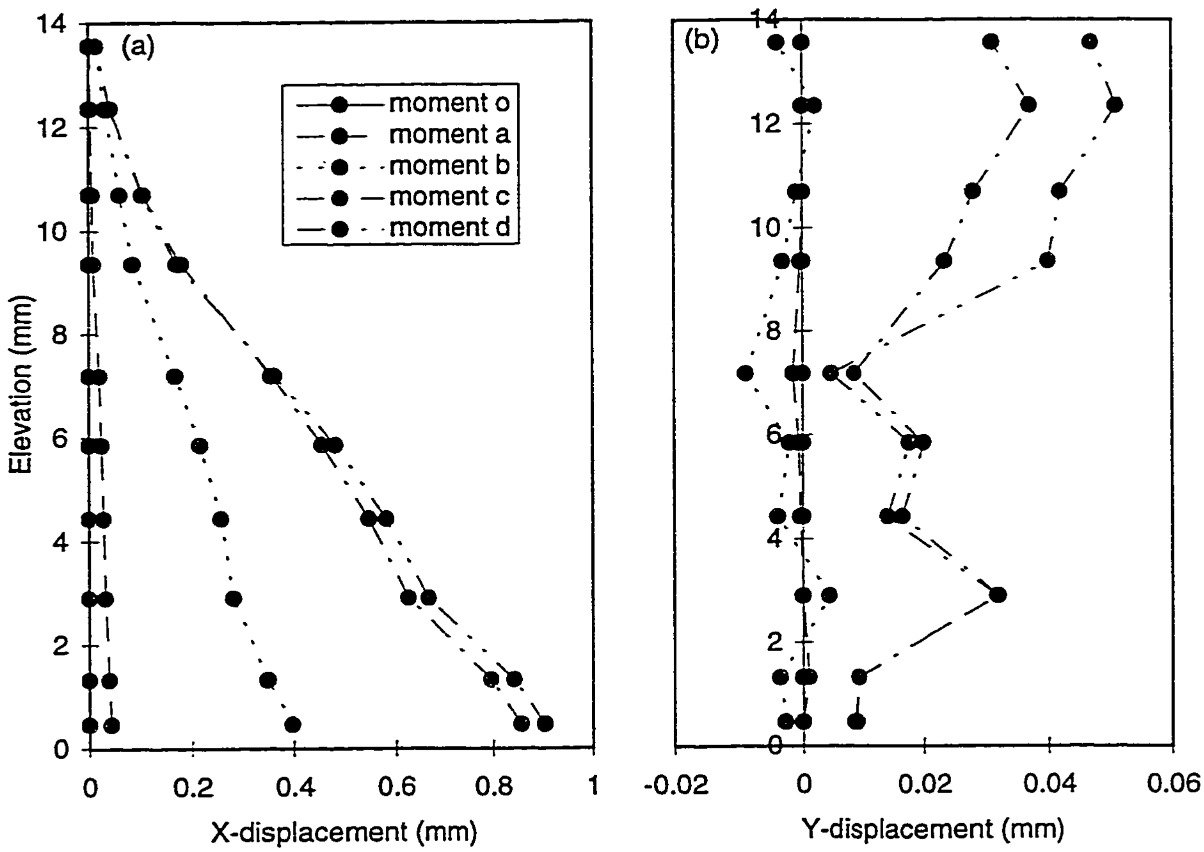

Fig.7.17 Horizontal and vertical displacements of particles at the middle of shear box for specific moments for Case D10

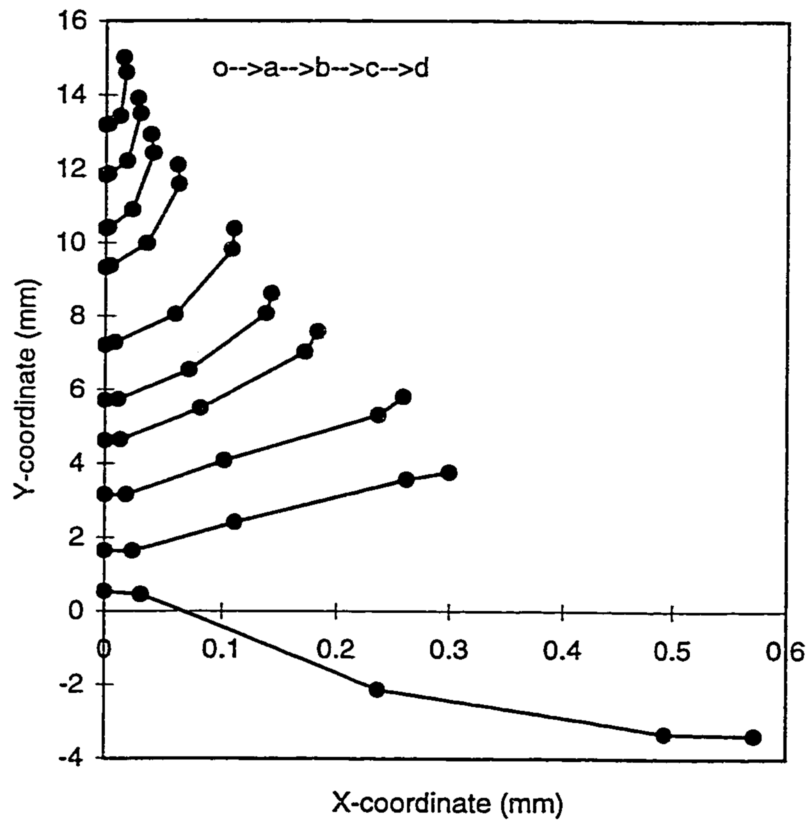

Fig.7.18 Movement traces of particles on the right side in shear box for Case D10 (vertical displacements are magnified 20 times)

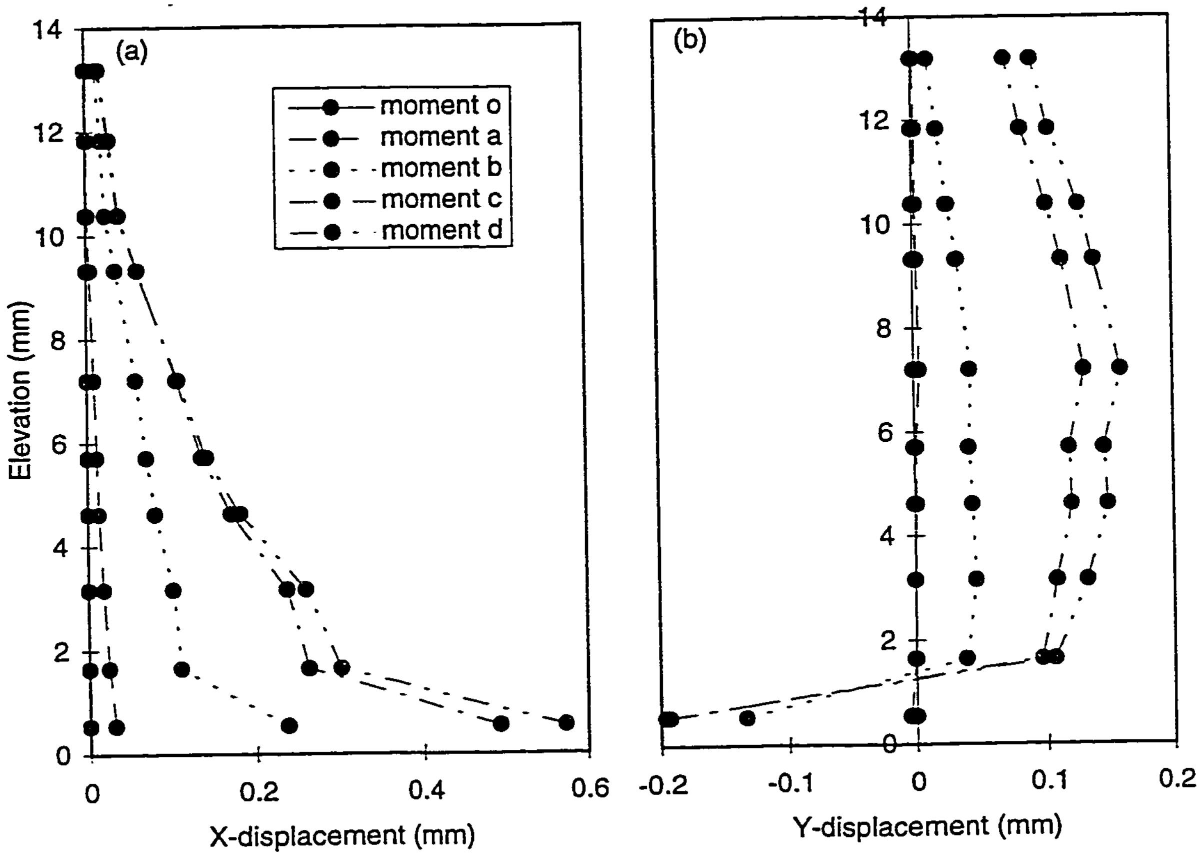

Fig.7.19 Horizontal and vertical displacements of particles on the right side in shear box for specific moments for Case D10

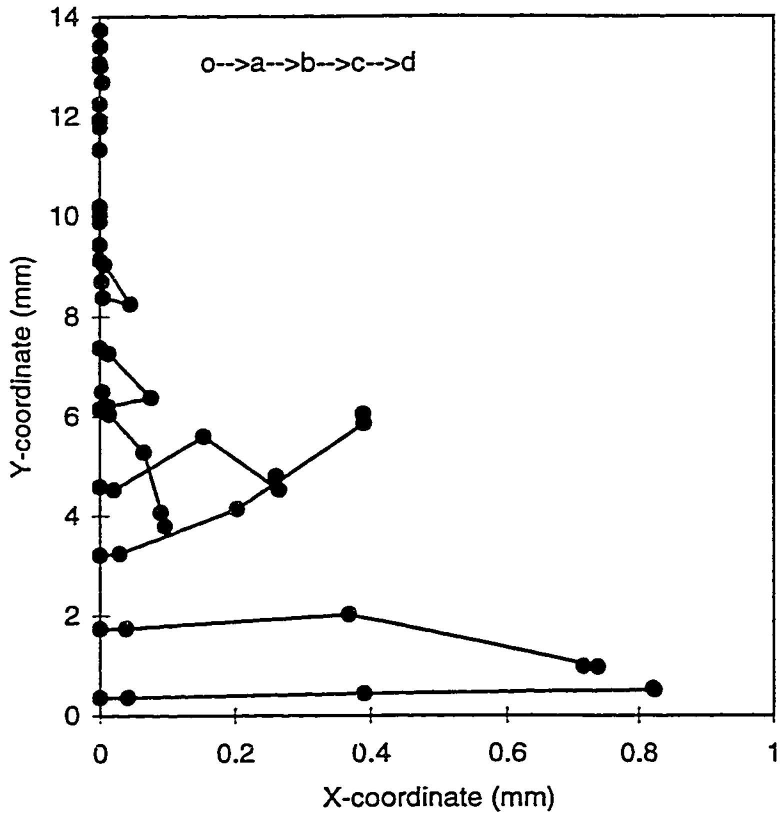

Fig.7.20 Movement traces of particles on the left side in shear box
for Case D10 (vertical displacements are magnified 20 times)

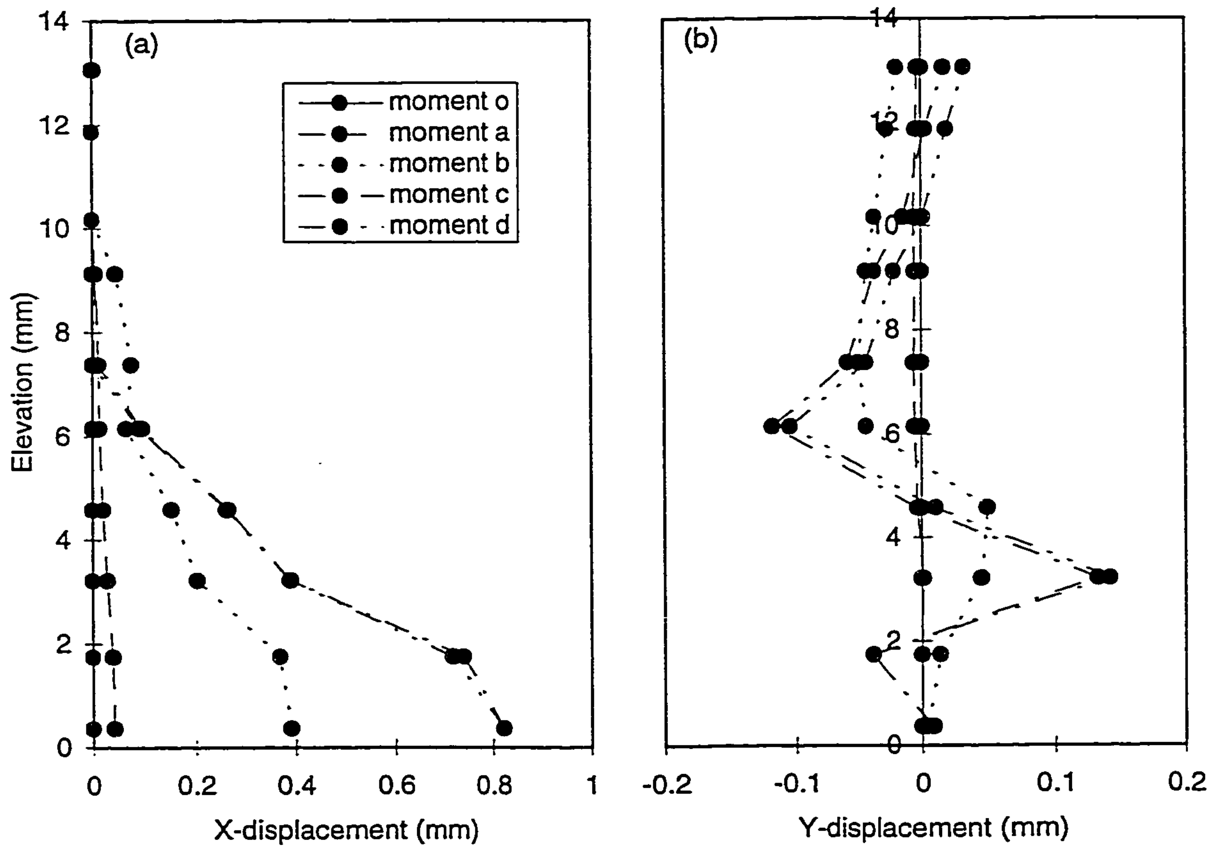

Fig.7.21 Horizontal and vertical displacements of particles on the left side in shear box for specific moments for Case D10

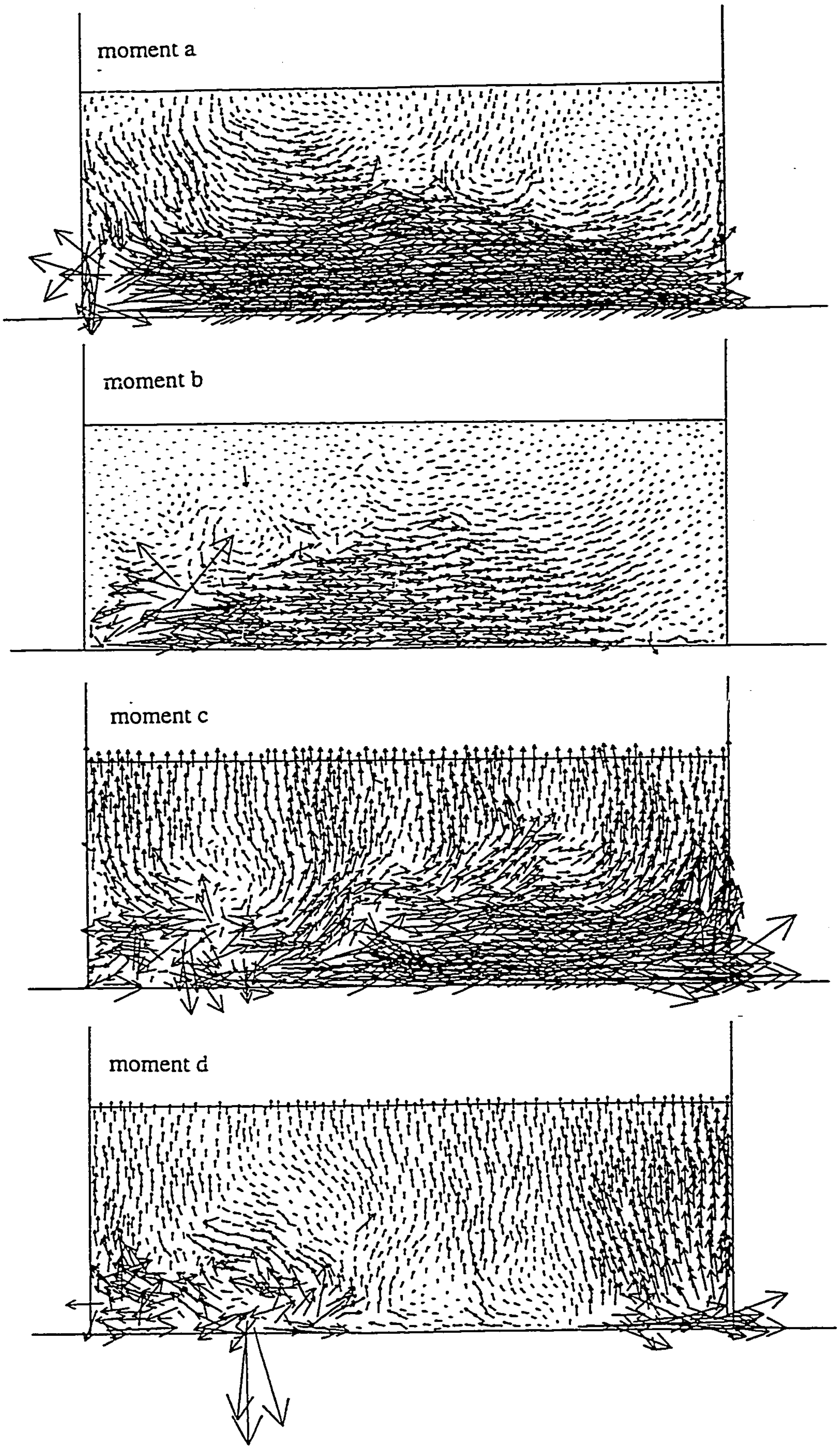

Fig.7.22 Velocity plot of Case D10 at four moments

CHAPTER 8

CONCLUSIONS AND RECOMMENDATIONS FOR FUTURE RESEARCH

8.1 Conclusions

Based upon the results of experimental investigation and the discrete element method simulation of sand-steel interface behaviour, the following conclusions are drawn:

(1) The initial state of sand-steel interface specimen (i.e., relative density of sand and normal stress) makes difference in interface behaviour. It influences the pattern of stress-displacement development and the deformation characteristics. The coefficient of friction developed at the interface is also influenced to some extent.

(2) Liquefaction indicated by "zero" normal stress may takes place in the interface tests using loose sand under the monotonic constant volume loading condition. It is also true for a relatively dense sand sample under the cyclic constant volume loading condition even at a small amplitude of displacement cycles such as one quarter of the tangential displacement at failure under the constant normal stress condition.

(3) The discrete element method has the potential to simulate all aspects of soil-structure interface behaviour. In the discrete element method, both rotations and translations of individual grains are monitored. The method can effectively deal with very large relative displacements, complicated material constitutive behaviour and formation of shear bands at interfaces.

(4) The discrete element method model provides reasonable simulations for sand-steel interface behaviour, in which particle shape and sample fabric play important roles. The simulations using the peanut shape particle units produced better results than using round particles for both strength and deformation behaviour of an interface under constant normal stress, although the results showed some difficulties in the simulation of loose sand in monotonic constant volume loading condition.

(5) The numerical simulations show that the particles closer to the contact surface had larger tangential displacements, the total dilation of the sample resulted from the accumulation of the relative upward displacements of those particles within a layer of particles 10 mm above the contact surface, and the particles closer to the contact surface had larger angular displacements developed during shearing. Generally, all particles had positive angular displacements (representing counter-clockwise rotation) within the range of 1 degree (for particles away from the interface) to 7 degree (for particles near the interface).

(6) By taking into consideration the horizontal, vertical and angular displacements of particles, it was concluded that a shear band was formed within a thickness of 10 mm above the contact surface. Considering the particle bonding effect, the thickness of the interface is about 7 times the average diameter of units of particles. This agrees well with experimental results.

(7) The movements of particles located along different vertical sections of the shear box were not identical. The side walls of direct shear type soil container have an influence on the movement pattern of particles within a distance of 5 mm from the vertical boundaries.

8.2 Recommendations for Future Research

Based upon literature review and this research, some future studies are suggested as follows:

(1) The sand may have certain moisture content, or may be fully saturated. Two kinds of drainage conditions, i.e., consolidated - drained condition and consolidated - undrained condition, may exist at the interface. The consolidated - undrained condition at the interface makes more sense in experimental investigation of liquefaction at soil-structure interfaces, which requires a specially designed testing device.

(2) The interface behaviour under earthquakes may be evaluated with tests under cyclic loading conditions. However, other dynamic loading conditions such as an impact load may change the interface behaviour significantly from that in static and cyclic loading.

(3) Although constant or variable normal stiffness conditions are more likely to exist across the interface in situ rather than constant normal stress or displacement, the interface response under constant or variable normal stiffness has not received much attention in the literature.

(4) Based on the principle of graphical procedures representing the shear behaviour of geological discontinuities (Goodman, 1980; Saeb and Amadei, 1989) and sands and clays (Ladanyi et al., 1965; Ladanyi, 1969), Fortin et al. (1988) developed an algorithm which allows the prediction of normal and shear stresses and dilatancy as functions of the shear displacement along a discontinuity under any normal stiffness boundary condition. The test data under standard constant normal stress condition is used to produce two unique three-dimensional surfaces defining the relationships among shear stress, normal stress, shear displacement and normal displacement. Relying on a polynomial interpolation principle, the algorithm leads to a complete shear stress - shear displacement relationship of a discontinuity under any normal stiffness conditions and any initial normal stress within the domain bounded by the experimental data considered as input, which corresponds to a specific path along these well defined surfaces. Fortin et al. (1990) further verified this approach using experimental results under variable normal stiffness condition. Up to now, no similar work has been done using this approach for simulating the effect of normal boundary conditions on soil-structure interface behaviour. Actually this provides a physical basis for understanding the existence of a constitutive model for different normal boundary conditions.

(5) The discrete element method is a kind of numerical method based on the micro-structure of sample. So, the quality of the discrete element method simulation depends on how to organize the micro-structure of sample. Comparing with the real life, the simulation sample has idealized parameters and idealized particle shapes. All these limit the use of DEM in some areas. Considering its inherent characteristics, attention should be paid to three points in simulation: parameters, particle shapes, and fabric. Among

these, fabric plays an important role in interface behaviour for both loose and dense sand samples. Therefore, how to arrange a reasonable fabric structure to represent a realistic sample with certain particle size distribution and relative density, is a fundamental study in the discrete element method. In the simulation of sand-steel interface behaviour, it is necessary to understand clearly how these factors influence the behaviour of interfaces. The sample preparation should be done correctly so that the interface sample will behave in an expected way.

REFERENCES

Acar, Y.B., Durgunoglu, H.T. and Turnay, M.T. (1982), Interface properties of sand. *J. of Geotech. Eng.*, ASCE, **108**(GT4), 648-654.

Bazant, Z.P. and Lin, F.B. (1988), Nonlocal yield limit degradation. *Int. J. Num. Meth. Eng.*, **26**, 1805-1823.

Beer, G. (1985), An isoparametric joint/interface element for finite element analysis. *Int. J. Num. Meth. Eng.*, **21**, 585-600.

Belytschko, T., Plesha, M. and Dowding, C. (1984), A computer method for stability analysis of caverns in jointed rock. *Int. J. Num. & Anal. Meth. in Geomech.*, **8**, 437-492.

Benalla, A., Billardon, R. and Geymonat, G. (1991), Localization phenomena at the boundaries and interfaces of solids. In *Proc. 3rd In. Conf. Constitutive Laws for Engineering Materials: Theory and Applications*, Tucson, Arizona, pp.387-390.

Boulon, M. and Plytas, C. (1986), Soil structure directionally dependent interface constitutive equation - application to the prediction of shaft friction along piles. In *Proc. of 2nd Int. Symp. on Num. Models in Geomech.*, Ghent, pp.43-54.

Boulon, M. (1988), A soil-structure incremental interface constitutive equation application to the prediction of piles behaviour. In *Proc.2nd Int.Conf. on Constitutive Laws for Engineering Materials*, C.S.Desai et al. (eds.), pp.1011-1018.

Boulon, M. and Nova, R. (1990), Modelling of soil-structure interface behaviour: A comparison between elastoplastic and rate type laws. *Computers and Geotechnics*, **9**, 21-46.

Brumund, W.F. and Leonards, G.A. (1973), Experimental study of static and dynamic friction between sand and typical construction materials. *J. of Testing and Evaluation*, **1**(2), 162-165.

Burman, B.C. (1971), *A Numerical Approach to the Mechanics of Discontinua*, Ph.D. Thesis, James Cook University of North Queensland, Townsville, Australia.

Chen, Z. and Schreyer, H.L. (1986), *A constitutive model for simulating soil-concrete interfaces*. Report AFWL-TR-86-06, Air Force Weapons Laboratory, New Mexico.

Clough, G.W. and Duncan, J.M. (1971), Finite element analyses of retaining wall behavior. *J. of the Soil Mech. & Found. Div.,* ASCE, **97**(SM12), 1657-1673.

Cosserat, E.F. (1909), Théorie des corps déformables. A.Hermann et Fils, Paris.

Cundall, P.A. (1971), A computer model for simulating progressive, large-scale movements in block rock systems. In *Int. Symp. on Rock Fracture*, Nancy, France, II-8.

Cundall, P.A. and Strack, O.D.L. (1979), A discrete numerical model for granular assemblies. *Geotechnique*, **29**(1), 47-65.

Desai, C.S. and Holloway, D.M. (1972), Load-deformation analysis of deep pile foundations. In *Proc. Symp. on Appl. of Finite Elem. Meth. in Geotech. Eng.*, Vicksburg, Miss..

Desai, C.S. (1974), Numerical design analysis of piles in sands. *J. of Geotech. Eng. Div.*, ASCE, **100**, 613-635.

Desai, C.S. and Appel, G.C. (1976), 3-D analysis of laterally loaded structures. In *Proc. of the 2nd Int. Conf. on Num. Meth. in Geomech.*, Blacksburg, VA, Vol.**1**, pp.405-418.

Desai, C.S. (1981), Behavior of interfaces between structural and geologic media. In *Proc. of Int. Conf. on Recent Advances in Geotech. Earthq. Eng. and Soil Dyn.*, St. Louis, MO, Vol.**II**, pp.619-638.

Desai, C.S., Phan, H.V. and Perumpral, J.V. (1982), Mechanics of three-dimensional soil-structure interaction. *J. of Eng. Mech. Div.*, ASCE, **108**(EM5), 731-747.

Desai, C.S., Zaman, M.M., Lightner, J.G. and Siriwardane, H.J. (1984), Thin-layer element for interfaces and joints. *Int.J. for Num. and Anal. Meth. in Geomech.*, **8**, 19-43.

Desai, C.S., Drumm, E.L. and Zaman, M.M. (1985), Cyclic testing and modeling of interfaces. *J. Geotech. Eng.*, ASCE, **111**(6), 793-815.

Desai, C.S. and Fishman, K.L. (1991), Plasticity-based constitutive model with associated testing for joints. *Int.J.Rock Mech. and Min.Sci.*, **28**(1), 15-26.

Drumm, E.C. and Desai, C.S. (1983), Testing and constitutive modeling for interface behavior in dynamic soil-structure interaction. Report to National Science Foundation, Washington, DC.

Evgin, E., Boulon, M., and Armand, G. (1996). Effect of oil contamination on the behaviour of an interface. In *49th Canadian Geotechnical Conference*, St.John's, Sept. 23-25, pp.377-384.

Evgin, E. and Fakharian, K. (1996). Effect of stress path on interface behaviour of sand-steel interfaces. *Canadian Geotechnical Journal*, **33**(6), 853-865.

Fakharian, K. and Evgin, E. (1993), A three dimensional apparatus for cyclic testing of interfaces. In *Proc. of 46th Annual Canadian Geotech. Conf.*, Saskatoon, pp.485-493.

Fakharian, K. and Evgin, E. (1996), An automated apparatus for three-dimensional monotonic and cyclic testing of interfaces. *Geotech. Testing J.*, **19**(1), 22-31.

Fakharian, K. (1996), Three-dimensional monotonic and cyclic behaviour of sand-steel interfaces: testing and modelling. Ph.D. thesis, Dept. of Civil Eng., Univ. of Ottawa.

Fishman, K.L. and Desai, C.S. (1987), A constitutive model for hardening behaviour of rock joints. In *Constitutive Laws for Engineering Materials: Theory and Application*, C.S. Desai *et al.* (eds.), pp.1043-1050.

Ghaboussi, J., Wilson, E.L. and Isenberg, J. (1973), Finite element for rock joints and interfaces. *J. of the Soil Mech. & Found. Div.*, ASCE, **99**(SM10), 833-848.

Goodman, R.E., Taylor, R.L. and Brekke, T.R. (1968), A model for the mechanics of jointed rock. *J. of the Soil Mech. & Found. Div.*, ASCE, **94**(SM3), 637-659.

Goodman, R.E. and DuBois, J. (1972), Duplication of dilatancy in analysis of jointed rocks. *J. of the Soil Mech. & Found. Div.*, ASCE, **98**(SM4), 399-422.

Griffiths, D.V. (1985), Numerical modelling of interfaces using conventional finite elements. In *Proc. of the 5th Int. Conf. on Num. Meth. in Geomech.*, Nagoya, Vol.**2**, pp.837-844.

Hocking, G., Williams, J.R. and Mustoe, G.G.W. (1985), Dynamic global forces on an offshore structure from large ice floe impacts. In *ARCTIC'85 Conf.*, ASCE, San Francisco, March.

Hocking, G., Mustoe, G.G.W. and Williams, J.R. (1985), Influence of artificial island side-shapes and ice ride up and pile up. In *ARCTIC'85 Conf.*, ASCE, San Francisco, March.

Hocking, G., Mustoe, G.G.W. and Williams, J.R. (1987), Dynamic analysis for generalized three-dimensional contact and fracturing of multiple bodies. In *NUMETA'87, Numerical Methods in Engineering, Theory and Application,* Swansea, UK, July 6-10, A.A.Balkema Publishers, Rotterdam.

Huck, P.J., Liber, T., Chiapetta, R.L., Thomopoulos, N. T. and Singh, N.M. (1973), Dynamic response of soil / concrete interfaces at high pressure. Report AFWL-TR-73-264, Air Force Weapons Laboratory, New Mexico.

Huck, P.J. and Saxena, S.K. (1981), Response of soil-concrete interface at high pressure. In *Proc. of 10th ICSMFE*, Stockholm, Sweden.

Isenberg, J. and Vaughan, D.K. (1981), Nonlinear effects in soil-structure interaction. In *Proc. of the Symp. on Implementation of Computer Procedures and Stress-Strain Laws in Geotech. Eng.*, Chicago, pp.29-44.

Itasca Consulting Group, Inc. (1994a), *UDEC (Universal Distinct Element Code),* Version 2.0. Minneapolis: ICG.

Itasca Consulting Group, Inc. (1994b), *3DEC (3-Dimensional Distinct Element Code),* Version 1.5. Minneapolis: ICG.

Itasca Consulting Group, Inc. (1994c), *FLAC (Fast Lagrangian Analysis of Continua),* Version 3.2. Minneapolis: ICG.

Itasca Consulting Group, Inc. (1994d), PFC^{2D} *(Particle Flow Code in 2 Dimensions),* Version 1.0. Minneapolis: ICG.

Kawai, T. (1977), New discrete structural models and generalization of the method of limit analysis. In *Int. Conf. on Finite Elements in Nonlinear Solid and Structural Mechanics*, Norway, **2**. G04.1-G04.20.

Kawai, T., Kawabata, K.Y., Kondou, I. and Kumagai, K. (1978), A new discrete model for analysis of solid mechanics problems. In *Proc. 1st Conf. on Num. Meth. in Fracture Mech.*, Swansea, UK, pp.26-37.

Kawai, T. (1979), Collapse load analysis of engineering structures by using new discrete element models. In *IABSE Colloquium*, Copenhagen.

Kishida, H. and Uesugi, M. (1987), Tests of the interface between sand and steel in the simple shear apparatus. *Geotechnique*, **37**(1), 45-52.

Leichnitz, W. (1985), Mechanical properties of rock joints. *Int. J. Rock Mech. Min. Sci. and Geomech.*, **22**(5), 313-321.

Lemos, J., Hart, R.D. and Cundall, P.A. (1985), A generalized distinct element program for modelling jointed rock mass. In *Fundamentals of Rock Joints*, O.Stephansson (ed.), Centek Publishers, Lulca, pp.335-343.

Mahtab, M.A. and Goodman, R.E. (1970), Three-dimensional finite element analysis of jointed rock slopes. In *Proc. of 2nd Congress of the Int. Soc. for Rock Mech.*, Belgrade, Yugoslavia, Vol.**3**, pp.353-360.

Maini, T., Cundall, P.A., Marti, J., Beresford, N.L. and Asgian, M. (1978), *Computer Modeling of Jointed Rock Masses*, Tech. Report N-78-8, Us Army Waterways Experiment Station, Vicksburg, MS., August.

Misra, A. (1995), Interfaces in particulate materials. In *Mechanics of Geomaterial Interfaces*, Selvadurai, A.P.S. and Boulon, M. (eds.), Elsevier Science B.V., Amsterdam, pp. 513-536..

Miura, S. and Toki, S. (1982), A sample preparation method and its effect on static and cyclic deformation-strength properties of sand. *Soils and Foundations*, **22**(2), 61-77.

Mühlhaus, H.B. and Vardoulakis, I. (1987), The thickness of shear bands in granular materials. *Geotechnique*, **37**, 271-283.

Mühlhaus, H.B. (1989), Stress and couple stress in a layered half plane with surface loading. *Int. J. Num. Anal. Meth. Geomech.*, **13**, 545-563.

Mustoe, G.G.W. (1989), Special elements in discrete element analysis. In *1st U.S. Conf. on Discrete Element Methods*, G.G.W.Mustoe, M.Henriksen and H.-P.Huttelmaier (eds.), Golden, Colorado, CSM Press.

Mustoe, G.G.W., Henriksen, M. and Huttelmaier, H.-P. (1989), In *1st U.S. Conf. on Discrete Element Methods*, , Golden, Colorado, CSM Press.

Navayogarajah, N. (1990), Constitutive modeling of static and cyclic behaviour of interfaces and implementation in boundary value problems. Ph.D. thesis, Dept. of Civil and Engineering Mechanics, University of Arizona, USA.

Navayogarajah, N., Desai, C.S. and Kiousis, P.D. (1992), Hierarchical single-surface model for static and cyclic behaviour of interfaces. *J. of Eng. Mech.*, ASCE, **118**(5), 990-1011.

Negussey, D., Wijewickreme, W.K.D. and Vaid, Y.P. (1988), Constant-volume friction angle of granular materials. *Can. Geotech.J.*, **25**, 50-55.

Ooi, L.H. and Carter, J.P. (1987), A constant normal stiffness direct shear device for static and cyclic loading. *Geotech. testing J.*, **10**(1), 3-12.

Paikowsky, S.G., Player, G.M. and Connors, P.J. (1995), A dual interface apparatus for testing unrestricted friction of soil along solid surfaces. *Geotech. Testing J.*, **18**(2), 168-193.

Pande, G.N. and Sharma, K.G. (1979), On joint/interface elements and associated problems of numerical ill-conditioning. *Int. J. Num. Anal. Meth. Geomech.*, **3**, 293-300.

Potyondy, J.G. (1961), Skin friction between various soils and construction materials. *Geotechnique*, **11**(4), 339-353.

Rothenburg, L. and Bathurst, R.J. (1992), Micromechanical features of granular assemblies with planar elliptical particles. *Geotechnique*, **42**(1), 79-95.

Schaeffer, D.G. (1990), Instability and ill-posedness in the deformation of granular materials. *Int. J. Num. Anal. Meth. Geomech.*, **14**, 253-278.

Shi, G.H. and Goodman, R.E. (1988), Discontinuous deformation analysis - a new method for computing stress, strain and sliding of block systems. In *Key Questions in Mechanics*, P.A.Cundall et al. (eds.), Balkema, Rotterdam, pp.381-393.

Tejchman, J. and Wu, W. (1994), Numerical study on sand and steel interfaces. *Mechanics Research Communications*, **21**(2), 109-119.

Tejchman, J. and Wu, W. (1995), Experimental and numerical study of sand-steel interfaces. *Int. J. for Num. and Anal. Meth. in Geomech.*, **19**, 513-536.

Toki, K., Sata, T. and Miura, F. (1981), Separation and sliding between soil and structure during strong ground motion. *Earthq. Eng. and Struct. Dyn.*, **9**, 263-277.

Uesugi, M. and Kishida, H. (1986a), Influential factors between steel and dry sand. *Soils and Foundations*, **26**(2), 33-46.

Uesugi, M. and Kishida, H. (1986b), Frictional resistance at yield between dry sand and mild steel. *Soils and Foundations*, **26**(4), 139-149.

Uesugi, M., Kishida, H. and Tsubakihara, Y. (1988), Behavior of sand particles in sand-steel friction. *Soils and Foundations*, **28**(1), 107-118.

Uesugi, M., Kishida, H. and Tsubakihara, Y. (1989), Friction between sand and steel under repeated loading. *Soils and Foundations*, **29**(3), 127-137.

Uesugi, M., Kishida, H. and Uchikawa, Y. (1990), Friction between dry sand and concrete under monotonic and repeated loading. *Soils and Foundations*, **30**(1), 115-128.

Vermeer, P.A. (1983), Frictional slip and nonassociated plasticity. *Scand. J. Metall.* **12**, 268-276.

Vaughan, D.K. and Isenberg, J. (1983), Nonlinear rocking response of model containment structures. *Earthq. Eng. and Struct. Dyn.*, **11**, 275-296.

Walton, O.R.(1982), Explicit particle dynamics model of granular materials. In *4th Int. Conf. on Num. Meth. in Geomech.*, Edmonton, Canada, pp.1261-1268.

Watanabe, M. and Kawai, T. (1980), Simulation of the bending collapse of ice plates using a new discrete model. *J. Soc. Naval Arch.*, Japan, **147**, 306-315 (in Japanese).

Williams, J.R., Hocking, G. and Mustoe, G.G.W. (1985), The theoretical basis of the discrete element method. In *NUMETA'85, Numerical Methods in Engineering, Theory and Application,* Swansea, UK, January 7-11, A.A.Balkema Publishers, Rotterdam.

Williams, J.R., Mustoe, G.G.W. and Worgan, K. (1986), Force transfer and behavior of rubble piles. In *IAHR Ice Symposium*, Iowa City.

Williams, J.R. and Mustoe, G.G.W. (1987), Model methods for the analysis of discrete systems. *Int. J. of Computers and Geotechnics*, **4**, 1-19.

Williams, J.R. and Mustoe, G.G.W. (1993), *Proceedings of the 2nd International Conference on Discrete Element Methods (DEM)*, MIT, MA., IESL Publications.

Wilson, E.L. (1977), Finite elements for foundations, joint and fluids. In *Finite Elements in Geomechanics*, G. Gudehus (ed), Chapt.**10**, Wiley, Chichester.

Yoshimi, Y. and Kishida, T. (1981a), A ring torsion apparatus for evaluating friction between soil and metal surfaces. *Geotech. Testing J.*, **4**(4), 145-152.

Yoshimi, Y. and Kishida, T. (1981b), Friction between sand and metal surface. In *Proc. of 10th ICSMFE*, Vol.1, pp.831-834.

Zienkiewicz, O.C., Best, B., Dullage, C. and Stagg, K.G. (1970), Analysis of nonlinear problems in rock mechanics with particular reference to jointed rock systems. In *Proc. of 2nd Congress of the Int. Soc. for Rock Mech.*, Belgrade, Yugoslavia, Vol.**3**, pp.501-509.

APPENDIX A

PROCEDURES FOR CONDUCTING INTERFACE TESTS WITH C3DSSI UNDER VARIOUS BOUNDARY CONDITIONS

The interface tests are conducted in a three-dimensional interface testing apparatus (Fakharian and Evgin, 1996). The apparatus is displacement- or load-controlled in three directions, its operation and data acquisition are automated by a computer controlled system installed with a software BENCHMATE (Sciemetric Instruments Inc.). BENCHMATE is a menu-driven software platform that can be customised. Within this application, it is specified with some controllers and sensors.

A.1 Introduction to the Apparatus

The interface tests are conducted by using a new apparatus, 3-D Cyclic Interface Testing Apparatus. It has several advantages, such as: (1) either displacement-controlled or load-controlled test can be conducted simultaneously in all three directions; (2) both monotonic and cyclic loading manners can be adopted; (3) loading rate can be adjusted; (4) interface shearing path can be easily adjusted; (5) various boundary conditions normal to the interface plane can be applied; and (6) both the direct shear type soil container and the simple shear type soil container can be used.

The apparatus is schematically illustrated in Fig.3.1. Three independent forces need to be applied to induce the three stress components at the interface plane, σ_n, τ_x and τ_y, shown in Fig.A.1. The tangential shear stresses are applied to the interface plane through an X-Y loading table. Two identical ball screw stepper motors are used to directly apply the tangential forces to the contact surface. A motorised air regulator, which is operated by a built-in stepper motor, adjusts the pressure for the E/P actuator to apply load in normal direction. Three load cells are respectively attached to the stepper motors and the pneumatic actuator with an accuracy of 5 N. Five LVDTs are employed to measure the displacements in the three directions with an accuracy of 0.002 mm.

The direct shear type soil container is a 25 mm thick, hollow aluminium box with an inside area of 100×100 mm. A thin layer of foam which is covered by a Teflon sheet is pasted to the bottom of the hollow aluminium box to prevent the leakage of the sand particles and to minimise the friction between the box and steel plate. Two LVDTs are used to measure the tangential displacements in the x and y directions as shown in Fig.A.2. LVDT a_x measures the relative tangential displacement, u_x, between the direct shear box and steel plate in the x direction (Fig.A.2a). LVDT a_y measures, u_y, in the y direction, which is perpendicular to the direction of u_x (Fig.A.2b).

The simple shear type soil container is a stack of 2 mm thick anodised, Teflon coated, square aluminium plates with an inside area of 100×100 mm (Fig.A.3). Two sets of tangential displacements are measured to distinguish between the sliding displacement (slip) along the contact surface and the shear deformation of the soil mass in both x and y directions. In the x direction, the total tangential displacement, u_{xa}, is measured between the top aluminium plate and the steel specimen by LVDT a_x. The shear deformation of the soil mass, u_{xb}, is measured by LVDT b_x, which reads the relative tangential displacement between the top and bottom aluminium plates. The sliding displacement at the soil-steel interface, u_x, is obtained from $u_x = u_{xa} - u_{xb}$ (Fig.A.3a). It is also true in the y direction (Fig.A.3b).

The plane view of the arrangement of LVDTs is shown in Fig.A.4. In the software, LVDT a_x, LVDT b_x, LVDT a_y and LVDT b_y are labelled by LVDT-X1, LVDT-X2, LVDT-Y1 and LVDT-Y2, respectively.

A.2 Introduction to the Software

The software used consists of various modules represented by customised menus that permit users to adjust parameters involved in testing. The main menu includes the following options:

<START TESTING>

<LOAD SETUP>

<CONFIGURE SEQUENCE>

<CONFIGURE INPUTS>

<CONFIGURE CONTROLS>

<CONFIGURE GRAPHICS>

<QUIT>

By entering these options and changing the values of various attributes, a specific test can be defined and conducted.

A.2.1 Modules

(1) **SENSOR** module is used to configure sensors for the testing operation.

(2) **CONTROL** module is used to configure controllers for the testing operation.

(3) **GRAPHICS** module is used to configure X-Y and TIME-Y graphs required for an application.

(4) **SEQUENCER** module is used to configure test sequence that incorporate the sensors and controllers. This sequence will be specific to the application at hand with the ability to change certain parameters dictated by the test design.

A.2.2 Sensors

(1) **LABEL** is the name of some sensor in which the sensor will be referred to in other parts of the program.

(2) **LVDT-X1** and **LVDT-X2** are used to measure the displacements in X direction.

(3) **LVDT-Y1** and **LVDT-Y2** are used to measure the displacements in Y direction.

(4) **LVDT-Z** is used to measure the displacement in Z direction.

(5) **LOADC-X**, **LOADC-Y** and **LOADC-Z** are used to measure the loads in X, Y and Z directions, respectively.

(6) **K** is a math sensor used to calculate the stiffness in Z direction.

A.2.3 Controllers

(1) **CONTROL TYPE** specifies the type of control to be used. In this specific application, **Stepper Motor Closed** is used to control a stepper motor in a closed loop fashion. The stepper motor will be adjusted to maintain the feedback sensor at the setpoint level.

(2) **LABEL** is the name by which the control will be referred to in other menus.

(3) **STEPM-XD** and **STEPM-XL** are used to control the displacement and load in X direction, respectively.

(4) **STEPM-YD** and **STEPM-YL** are used to control the displacement and load in Y direction, respectively.

(5) **MOT.REG-D**, **MOT.REG-L** and **MOT.REG-K** are used to control the displacement, load and stiffness in Z direction, respectively.

A.2.4 Sequencer

(1) The **Test Sequence** can be built through the **CONFIGURE SEQUENCE**. It consists of several steps belonging to different types.

(2) **Operation Steps**

DO starts a DO/LOOP which is used to control program flow, and can be nested to run smaller sequences within larger ones.

LOOP ends a DO/LOOP.

EXIT LOOP creates an exit condition for a DO/LOOP. If the condition becomes true, the closest loop will end.

SCAN GROUP scans a sensor group.

SAVE GROUP saves a group of sensors to a disk file.

ZERO SENSOR adjusts a sensor's offset value so the current reading is zero.

(3) **Controller Steps**

SET CONTROLLER sets a controller to specified setpoint.

ANCHOR SINE sets the initial phase of **SINE WAVE**.

SINE WAVE sets a controller's setpoint to follow a sine wave of a specified amplitude and frequency.

(4) **Displaying Steps**

RESET GRAPH resets a graph and assigns it to a specified display.

RESET CURVE clears a curve's buffer.

GRAPH POINT graphs a sensor vs. time or versus another sensor.

SHOW SENSOR initiates a panel meter for a specified sensor on a specified display.

A.3 Classification of Interface Tests

In terms of various combinations of controllers, many types of interface tests can be realised by SEQUENCER. Some of displacement-controlled tests are listed in the following.

A.3.1 Two-dimensional cases

(1) Two-dimensional monotonic loading test with constant normal stress

(2) Two-dimensional monotonic loading test with constant volume

(3) Two-dimensional monotonic loading test with constant normal stiffness

(4) Two-dimensional displacement-controlled cyclic test with constant normal stress

(5) Two-dimensional displacement-controlled cyclic test with constant volume

(6) Two-dimensional displacement-controlled cyclic test with constant normal stiffness

A.3.2 Three-dimensional cases

(1) Three-dimensional monotonic stepwise loading test with constant normal stress

First the interface is sheared up to a tangential displacement of 5 mm in X direction under a constant normal stress, then the shear stress in X direction is lowered to zero and maintained at zero while the interface is thereafter sheared in Y direction under the same normal stress.

(2) Three-dimensional monotonic simultaneous loading test with constant normal stress

Under a constant normal stress the interface is subjected to a shear stress, first in Y direction, less than the peak shear strength in a 2-D test. Thereafter, the interface is sheared in X direction while the shear stress in Y direction and the constant normal stress are maintained at constant value.

(3) Three-dimensional displacement-controlled cyclic test with a constant shear stress in the orthogonal direction and a constant normal stress

Under a constant normal stress the interface is subjected to a shear stress, first in Y direction, less than the peak shear strength in a 2-D test. Thereafter, the interface is displacement-controlled cyclically sheared in X direction while the shear stress in Y direction and the constant normal stress are maintained at constant value.

(4) Three-dimensional rotational loading test with a constant normal stress

First, the interface is sheared in X direction to the position with the maximum displacement. Then it is sheared in a displacement-controlled manner on an elliptical or circular path on X-Y plane.

In addition to the condition of constant normal stress, constant volume and constant normal stiffness can also be applied to three-dimensional cases.

A.4 Technical Approaches for Conducting Tests

For conducting tests with various paths and conditions, certain technical approaches need to be adopted in order to properly combine the apparatus with the software.

(1) In **CONTROLLER MENU**, the **default setpoint** of controller defines its initial value. By using "**DIAGNOSTIC**", the controller is initiated and the value change process can be observed. Therefore, the position of the loading table can be adjusted and the initial normal condition can be applied by using this function.

(2) **Setpoint** is designated to determine the direction and limit of the loading table movement and to maintain the expected value of normal condition during testing.

(3) 2-D monotonic tests can be performed by calling **SET CONTROLLER** in **SEQUENCER MENU** for **STEPM-XD** with certain value of **setpoint**, while for conducting 2-D cyclic tests **SINE WAVE** need to be called within **DO/LOOP** of **SEQUENCER MENU** for **STEPM-XD** in order to drive X stepper motor by displacement-controlled sine wave fashion.

(4) By calling certain controller with certain value of **setpoint** within **SEQUENCER MENU**, the test sequence can be created for conducting some type of test with certain normal condition. For example, for conducting the test with constant normal stress, the initial normal stress is applied by setting **default setpoint** of **MOT.REG-L** at some value, then call it again in **SEQUENCER MENU** with a **setpoint** value same as the **default setpoint** value; for conducting the test with constant volume, the initial normal stress is applied by setting **default setpoint** of **MOT.REG-L** at some value, constant volume is maintained during testing by setting **default setpoint** of **MOT.REG-D** at 0 and calling **MOT.REG-D** with sp=0 in **SEQUENCER MENU;** for conducting the test with constant normal stiffness, the desired normal stiffness is given by setting **default setpoint** of **MOT.REG-K**, then this constant normal stiffness is maintained during testing by calling **MOT.REG-K** in **SEQUENCER MENU** with a **setpoint** value same as the desired value.

(5) The initial normal stress condition can be applied in two manner within **CONTROLLER MENU.** If use **AUTO**, the stress can be set by changing the value of default setpoint; if use **MAN**, the stress can be adjusted by pressing **RAISE** or **LOWER** on the control panel of the apparatus. The result can be observed by "**Enter**" "**DIAGNOSTIC**".

(6) For driving stepper motor, SUPERIOR ELECTRIC Motor Drive (Model SS2000DS) is used, which has various setting levels of step resolution. In our application, the eighth setting (i.e., 20000 pulses per revolution) is used. The stepper motor control algorithm estimates the required steps and direction to put the feedback sensor at the setpoint and then outputs the appropriate steps. It gets the estimation from a learned response from the previous estimation. In this manner the algorithm continuously recalibrates itself. In **CONTROLLER MENU**, the **RATE** (one of control parameters) is

used to set the rate of the pulses in pulses/second. It should be set according to the motor used. In running displacement-controlled monotonic tests, **RATE=-400** for **STEPM-XD** is enough. In running displacement-controlled cyclic tests, **RATE=-2000** for **STEPM-XD** is necessary at least. And higher the **RATE** is, more accurate the controlling is. For running load-controlled tests, the **RATE** for **STEPM-XL** needs to be adjusted. The same thing also happens to other controllers. So, it can be seen that this control parameter is very important for accurately driving stepper motor to realise designed tests.

(7) Since the loading platen causes a normal stress of 5 kPa on a 100×100 mm area, a targeted normal stress should be set minus 5. For example, a targeted normal stress of 100 kPa can be realised by setting **MOT.REG-L** at 95.

(8) When conducting 2-D tests, either X stepper motor or Y stepper motor is used. Usually, another unused stepper motor is switched off so that it doesn't need to be specified within menus. The measurements of corresponding sensors are displayed with almost constant values. Switching off the unused stepper motor is also helpful to prevent the apparatus from being damaged due to improper specification of some attribute of this stepper motor. When conducting 3-D tests, both X and Y stepper motors are used. The corresponding attributes in menus need to be harmoniously specified in order to realise the desired test path.

(9) During running the test, the measurements are displayed on the screen. At the bottom of the screen, there is a runtime menu for switching **DISPLAY 1** and **DISPLAY 2**, and **ABORT** the test.

(10) All sensors are grouped in Group 1 so that they are scanned and saved together in group. The 8-channel bridge conditioner is used so that up to eight sensors can be scanned. The scanning process is conducted with a rate of 100 Hz. By calling **SAVE GROUP**, the measurements of all sensors are saved to a disk file which can be used for post-processing. The disk file is opened, a record written, and closed every time this step is called according to the save rate (e.g., 0.2 Hz). For each test, the disk file (i.e., original output data file) should be distinguished from others, otherwise the data coming from the preceding test will exist in the same file. Therefore, the data files must be established in certain order for continuous tests.

A.5 Operation Procedures

For conducting tests with various paths and conditions, it is more important to build a specific testing sequence regarding to certain test path and condition. For this purpose, some testing sequences have be built up and installed in different sub-directories, respectively.

A.5.1 2-D monotonic loading test under constant normal stress condition

Step 1. Sample preparation and placement

(1) Put the steel plate on the loading table, and fasten the four bolts at the corners. Place the shear box at the centre of the steel plate. Lower the loading platen into the shear box for further adjustment. Then fix the shear box with four clamps at the corners, and loosen the four bolts.

(2) Move the steel plate with the shear box from the loading table for raining the sand into the box with certain method. the top part of the sand specimen is levelled by a suction device.

(3) The steel plate is fixed on the loading table with the four bolts again, the four clamps are then removed.

(4) The loading platen is slowly moved downward to touch the sand surface,. LVDTs are mounted before starting a test.

Step 2. Accessing the software (c:\interfac\soil01\)

At the command prompt type the following to access the software:

(1) Put the runtime key on the rear of the computer.

(2) **cd interfac** (Enter)

(3) **cd soil01** (Enter)

(4) **soil** (Enter)

Step 3. Application of the normal load

(1) On the main menu, select **CONFIGURE CONTROLS**.

(2) From **CONFIGURE CONTROLS** select **MOT.REG-L** to set the initial normal stress by changing the value of default setpoint. The value change can be observed by "Enter" the last column (**DIAGNOSTIC**), and then return by pressing **Esc**.

Step 4. Adjusting horizontal load to zero

(1) Select **STEPM-XL** to set default setpoint at zero. To initiate the process, "Enter" **DIAGNOSTIC** .

(2) Return to the main menu by pressing **Esc**.

Step 5. Adjustment of LVDTs

From the main menu select **CONFIGURE INPUTS**, and then select **CONFIGURE SENSORS**.

(1) Select **LVDT-X1**, "Enter" the last column (**DIAGNOSTIC**), zero the value by pressing "z".

(2) Adjust **LVDT-X1** to about 6.5 mm if the steel plate would move to the left (since a high limit of 7 mm is already set), or 0.5 mm if the steel plate is to move to the right.

(3) Zero the value of **LVDT-X1** By pressing "z".

(4) Do the same thing to **LVDT-Z**, i.e., zero its value and adjust it to about 1.5 mm, then zero it again.

(5) Press **Esc**, select "**DONE**", and "**Enter**" into the main menu.

Step 6. Modifying the parameters of the test sequence

(1) Select **CONFIGURE SEQUENCE** to display the test sequence.

(2) Go to line 16, set the targeted normal stress of **MOT.REG-L**(minus 5) at column 5.

(3) Go to line 17, give a value to setpoint for **STEPM-XD**. If the steel plate would move to the left during the test, enter "-6"; otherwise enter "+6".

(4) Go to line 19, and give a name to the output data file, e.g., c:\excel\tests\m2cnl.csv, at column 5.

(5) Press **Esc**, "Enter" at "**<CURRENT>**" for returning to the main menu.

Step 7. Running the test

(1) Select **START TESTING**.

(2) Enter the file name of test sequence, e.g., "test1".

Step 8. Exiting the software and ending the test

(1) By pressing "**Esc**" or "Enter" "**ABORT**" in the runtime menu at the bottom of the screen, the test can be interrupted, the main menu is then prompted.

(2) At the end of test, the main menu is also prompted. From there, select **QUIT**.

(3) At the end of the test, remove the normal load on the sample and relax the LVDTs. Loosen the four bolts and move the steel plate, then clean the loading platen and loading table for next test.

Step 9. Presentation of the test results

(1) Through **Window**, go to the original data file c:\excel\tests\m2cnl.csv. Open it, highlight the first column of data sheet; press "**Test to Columns**" from "**Data**" button; press "**next**" then "**finish**" in order to convert data sheet into columns.

(2) Copy the first 7 columns of the original data file, and paste them to the template file (e.g., m100sst.xlt) in the first 7 columns. In the template file, all data are further calculated for final presentation.

(3) Copy the transformed data columns of the template file, then paste them to the final data file. This final data file can be created by using "**save as**" the existing file, e.g., save "test35.xls" as "test36.xls". Because the data in the template file are stored with formulas, it is necessary to select "**paste special**" and then "**value**" for copying.

(4) The graphs of the test results are presented in chart.

(5) When exit **Excel**, it is recommended to save changes for the final file and not to save changes for the original data file and template file.

A.5.2 2-D monotonic loading test under constant volume condition

The basic procedures are the same as in 2-D monotonic loading test under constant normal stress condition. Some differences are listed in the following:

Step 2. (c:\interfac\soil02\)

(3) **cd soil02** (Enter)

.

Step 6.

(2) sp=0 for MOT.REG.-D is same for all tests of this type, so no need to do this substep.

Step 9.

(1) Through **Window**, go to the original data file c:\excel\tests\m2cv.csv. Open it, highlight the first column of data sheet; press "**Test to Columns**" from "**Data**" button; press "**next**" then "**finish**" in order to convert data sheet into columns.

A.5.3 2-D monotonic loading test under constant normal stiffness condition

The basic procedures are the same as in 2-D monotonic loading test under constant normal stress condition. Some differences are listed in the following:

Step 2. (c:\interfac\soil03\)

(3) **cd soil03** (Enter)

Step 3.

(2) From **CONFIGURE CONTROLS** select **MOT.REG.-K** to set the default setpoint at a desired value. The value change can be observed by "Enter" the last column (**DIAGNOSTIC**), and then return by pressing **Esc**.

Step 6.

(2) Go to line 16, give a desired value to the setpoint of **MOT.REG.-K** (at the fifth column) same as the value of its default setpoint in **CONTROLLER MENU**.

Step 9.

(1) Through **Window**, go to the original data file c:\excel\tests\m2cv.csv. Open it, highlight the first column of data sheet; press "**Test to Columns**" from "**Data**" button; press "**next**" then "**finish**" in order to convert data sheet into columns.

A.5.4 2-D displacement-controlled cyclic test under constant normal stress condition

The basic procedures are the same as in 2-D monotonic loading test under constant normal stress condition. Some differences are listed in the following:

Step 2. (c:\interfac\soil04\)

(3) **cd soil04** (Enter)

Step 5.

(2) Adjust **LVDT-X1** to about 3.5 mm.

Step 6.

(2) Go to line 16, set the maximum time of testing by changing **Max DT**.

(3) Go to line 17, set the targeted normal stress of **MOT.REG-L**(minus 5) at column 5.

(4) Go to line 18, specify the amplitude and frequency of **SINE WAVE** at column 5 and 6, respectively.

(5) Go to line 20, and give a name to the output data file, e.g., c:\excel\tests\c2cnl.csv, at column 5.

(6) Press **Esc**, "Enter" at "**<CURRENT>**" for returning to the main menu.

Step 9.

(1) Through **Window**, go to the original data file c:\excel\tests\c2cnl.csv. Open it, highlight the first column of data sheet; press "**Test to Columns**" from "**Data**" button; press "**next**" then "**finish**" in order to convert data sheet into columns.

A.5.5 2-D displacement-controlled cyclic test under constant volume condition

The basic procedures are the same as in 2-D monotonic loading test under constant normal stress condition. Some differences are listed in the following:

Step 2. (c:\interfac\soil05\)

(3) **cd soil05** (Enter)

Step 5.

(2) Adjust **LVDT-X1** to about 3.5 mm.

Step 6.

(2) Go to line 16, set the maximum time of testing by changing **Max DT**.

(3) Go to line 18, specify the amplitude and frequency of **SINE WAVE** at column 5 and 6, respectively.

(4) Go to line 20, and give a name to the output data file, e.g., c:\excel\tests\c2cv.csv, at column 5.

Step 9.

(1) Through **Window**, go to the original data file c:\excel\tests\c2cv.csv. Open it, highlight the first column of data sheet; press "**Test to Columns**" from "**Data**" button; press "**next**" then "**finish**" in order to convert data sheet into columns.

A.5.6 2-D displacement-controlled cyclic test under constant normal stiffness condition

The basic procedures are the same as in 2-D monotonic loading test under constant normal stress condition. Some differences are listed in the following:

Step 2. (c:\interfac\soil06\)

(3) **cd soil06** (Enter)

Step 3.

(2) From **CONFIGURE CONTROLS** select **MOT.REG.-K** to set the default setpoint at a desired value. The value change can be observed by "Enter" the last column (**DIAGNOSTIC**), and then return by pressing **Esc.**

Step 5.

(2) Adjust **LVDT-X1** to about 3.5 mm.

Step 6.

(2) Go to line 16, set the maximum time of testing by changing **Max DT**.

(3) Go to line 17, give a desired value to the setpoint of **MOT.REG.-K** (at the fifth column) same as the value of its default setpoint in **CONTROLLER MENU**.

(4) Go to line 18, specify the amplitude and frequency of **SINE WAVE** at column 5 and 6, respectively.

(5) Go to line 20, and give a name to the output data file, e.g., c:\excel\tests\c2cns.csv, at column 5.

(6) Press **Esc**, "Enter" at "**<CURRENT>**" for returning to the main menu.

Step 9.

(1) Through **Window**, go to the original data file c:\excel\tests\c2cns.csv. Open it, highlight the first column of data sheet; press "**Test to Columns**" from "**Data**" button; press "**next**" then "**finish**" in order to convert data sheet into columns.

A.5.7 3-D monotonic stepwise loading test under constant normal stress condition

The basic procedures are the same as in 2-D monotonic loading test under constant normal stress condition. Some differences are listed in the following:

Step 2. (c:\interfac\soil07\)

(3) **cd soil07** (Enter)

Step 4.

(1) Select **STEPM-XL** to set default setpoint at zero. To initiate the process, "**Enter**" **DIAGNOSTIC** . The same thing should be done for **STEPM-YL**.

Step 5.

(5) Do the same thing for **LVDT-Y1** as did for **LVDT-X1**.

(6) Press **Esc**, select "**DONE**", and "**Enter**" into the main menu.

Step 6.

(2) Go to line 16, line 31 and line 44, set the targeted normal stress of **MOT.REG-L**(minus 5) at column 5.

(3) Go to line 17, give a value to setpoint for **STEPM-XD**. If the steel plate would move to the left during the test, enter "-5"; otherwise enter "+5".

(4) Go to line 46, give a value to setpoint for **STEPM-YD**. If the steel plate would move backwards during the test, enter "-5"; otherwise enter "+5".

(5) Go to line 19 and line 48, and give a name to the output data file, e.g., c:\excel\tests\m3step.csv, at column 5.

(6) Press **Esc**, "Enter" at "**<CURRENT>**" for returning to the main menu.

Step 9.

(1) Through **Window**, go to the original data file c:\excel\tests\m3step.csv. Open it, highlight the first column of data sheet; press "**Test to Columns**" from "**Data**" button; press "**next**" then "**finish**" in order to convert data sheet into columns.

(2) Copy the original data file, and paste them to the template file (e.g., m100sst.xlt). In the template file, all data are further calculated for final presentation.

A.5.8 3-D monotonic simultaneous loading test under constant normal stress condition

The basic procedures are the same as in 2-D monotonic loading test under constant normal stress condition. Some differences are listed in the following:

Step 2. (c:\interfac\soil08\)

(3) **cd soil08** (Enter)

Step 4.

(1) Select **STEPM-XL** to set default setpoint at zero. To initiate the process, "**Enter**" **DIAGNOSTIC** . The same thing should be done for **STEPM-YL**.

Step 5.

(5) Do the same thing for **LVDT-Y1** as did for **LVDT-X1**.

(6) Press **Esc**, select "**DONE**", and "**Enter**" into the main menu.

Step 6.

(2) Go to line 16 and line 31, set the targeted normal stress of **MOT.REG-L**(minus 5) at column 5.

(3) Go to line 17, give a value to setpoint for **STEPM-YL**. If the steel plate would move forwards, the setpoint should have a sign of "+"; otherwise "-".

(4) Go to line 32, give a value to setpoint for **STEPM-YL** same as in (2).

(5) Go to line 33, give a value to setpoint for **STEPM-XD**. If the steel plate would move to the left during the test, enter "-5"; otherwise enter "+5".

(6) Go to line 19 and line 35, and give a name to the output data file, e.g., c:\excel\tests\m3simu.csv, at column 5.

(7) Press **Esc**, "Enter" at "**<CURRENT>**" for returning to the main menu.

Step 9.

(1) Through **Window**, go to the original data file c:\excel\tests\m3simu.csv. Open it, highlight the first column of data sheet; press "**Test to Columns**" from "**Data**" button; press "**next**" then "**finish**" in order to convert data sheet into columns.

(2) Copy the original data file, and paste them to the template file (e.g., m100sst.xlt). In the template file, all data are further calculated for final presentation.

A.5.9 3-D displacement-controlled cyclic test under the condition of a constant shear stress in the orthogonal direction and a constant normal stress

The basic procedures are the same as in 2-D monotonic loading test under constant normal stress condition. Some differences are listed in the following:

Step 2. (c:\interfac\soil09\)

(3) **cd soil09** (Enter)

Step 4.

(1) Select **STEPM-XL** to set default setpoint at zero. To initiate the process, "**Enter**" **DIAGNOSTIC** . The same thing should be done for **STEPM-YL**.

Step 5.

(2) Adjust **LVDT-X1** to about 3.5 mm.

(5) Select **LVDT-Y1**, "Enter" the last column (**DIAGNOSTIC**), zero the value by pressing "z".

(6) Adjust **LVDT-Y1** to about 6.5 mm if the steel plate would move backwards, or 0.5 mm if the steel plate is to move forwards.

(7) Zero the value of **LVDT-X1** By pressing "z".

(8) Press **Esc**, select "**DONE**", and "**Enter**" into the main menu.

Step 6.

(2) Go to line 16 and line 32, set the targeted normal stress of **MOT.REG-L**(minus 5) at column 5.

(3) Go to line 17, give a value to setpoint for **STEPM-YL**. If the steel plate would move forwards, the setpoint should have a sign of "+"; otherwise "-".

(4) Go to line 33, give a value to setpoint for **STEPM-YL** same as in (3).

(5) Go to line 34, specify the amplitude and frequency of **SINE WAVE** for **STEPM-XD** at column 5 and 6, respectively.

(6) Go to line 19 and line 36, and give a name to the output data file, e.g., c:\excel\tests\c3simu.csv, at column 5.

(7) Press **Esc**, "Enter" at "**<CURRENT>**" for returning to the main menu.

Step 9.

(1) Through **Window**, go to the original data file c:\excel\tests\c3simu.csv. Open it, highlight the first column of data sheet; press "**Test to Columns**" from "**Data**" button; press "**next**" then "**finish**" in order to convert data sheet into columns.

(2) Copy the original data file, and paste them to the template file (e.g., m100sst.xlt). In the template file, all data are further calculated for final presentation.

A.5.10 3-D rotational loading test under constant normal stress condition

The basic procedures are the same as in 2-D monotonic loading test under constant normal stress condition. Some differences are listed in the following:

Step 2. (c:\interfac\soil10\)

(3) **cd soil10** (Enter)

Step 4.

(1) Select **STEPM-XL** to set default setpoint at zero. To initiate the process, "**Enter**" **DIAGNOSTIC** . The same thing should be done for **STEPM-YL**.

Step 5.

(2) Adjust **LVDT-X1** to about 3.5 mm.

(5) Do the same thing for **LVDT-Y1** as for **LVDT-X1**.

(6) Press **Esc**, select "**DONE**", and "**Enter**" into the main menu.

Step 6.

(2) Go to line 16 and line 34, set the targeted normal stress of **MOT.REG-L**(minus 5) at column 5.

(3) Go to line 17, give a value to setpoint for **STEPM-XD**, e.g., if the steel plate would move to the left during the test, enter "-0.5"; otherwise enter "+0.5".

(4) Go to line 35, specify the amplitude and frequency of **SINE WAVE** for **STEPM-XD** at column 5 and 6, respectively.

(5) Go to line 36, specify the amplitude and frequency of **SINE WAVE** for **STEPM-YD** at column 5 and 6, respectively.

(6) Go to line 20 and line 38, and give a name to the output data file, e.g., c:\excel\tests\rota.csv, at column 5.

(7) Press **Esc**, "Enter" at "**<CURRENT>**" for returning to the main menu.

Step 9.

(1) Through **Window**, go to the original data file c:\excel\tests\rota.csv. Open it, highlight the first column of data sheet; press "**Test to Columns**" from "**Data**" button; press "**next**" then "**finish**" in order to convert data sheet into columns.

(2) Copy the original data file, and paste them to the template file (e.g., m100sst.xlt). In the template file, all data are further calculated for final presentation.

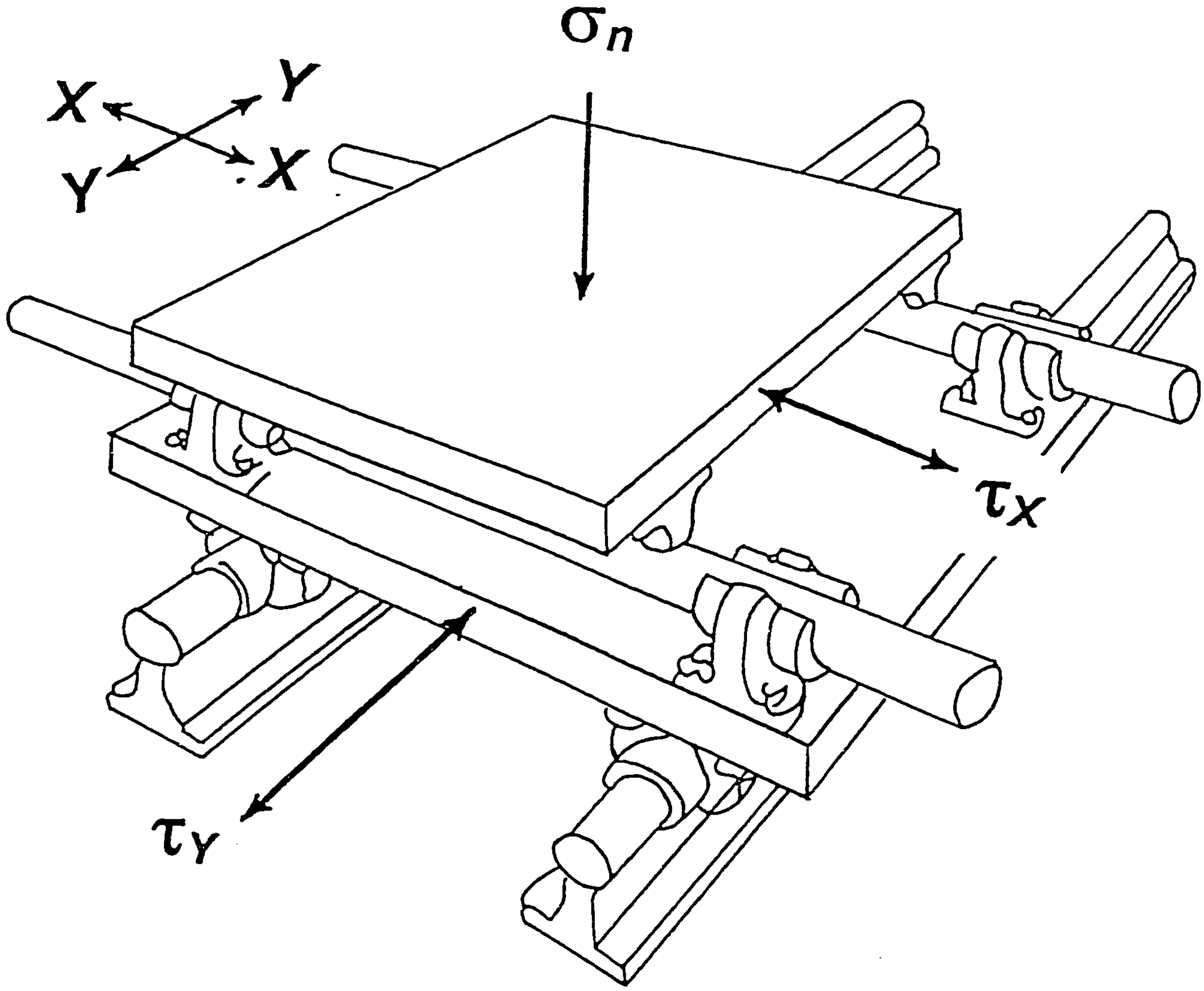

Fig.A.1 Perspective of the X-Y loading table (after Fakharian, 1996)

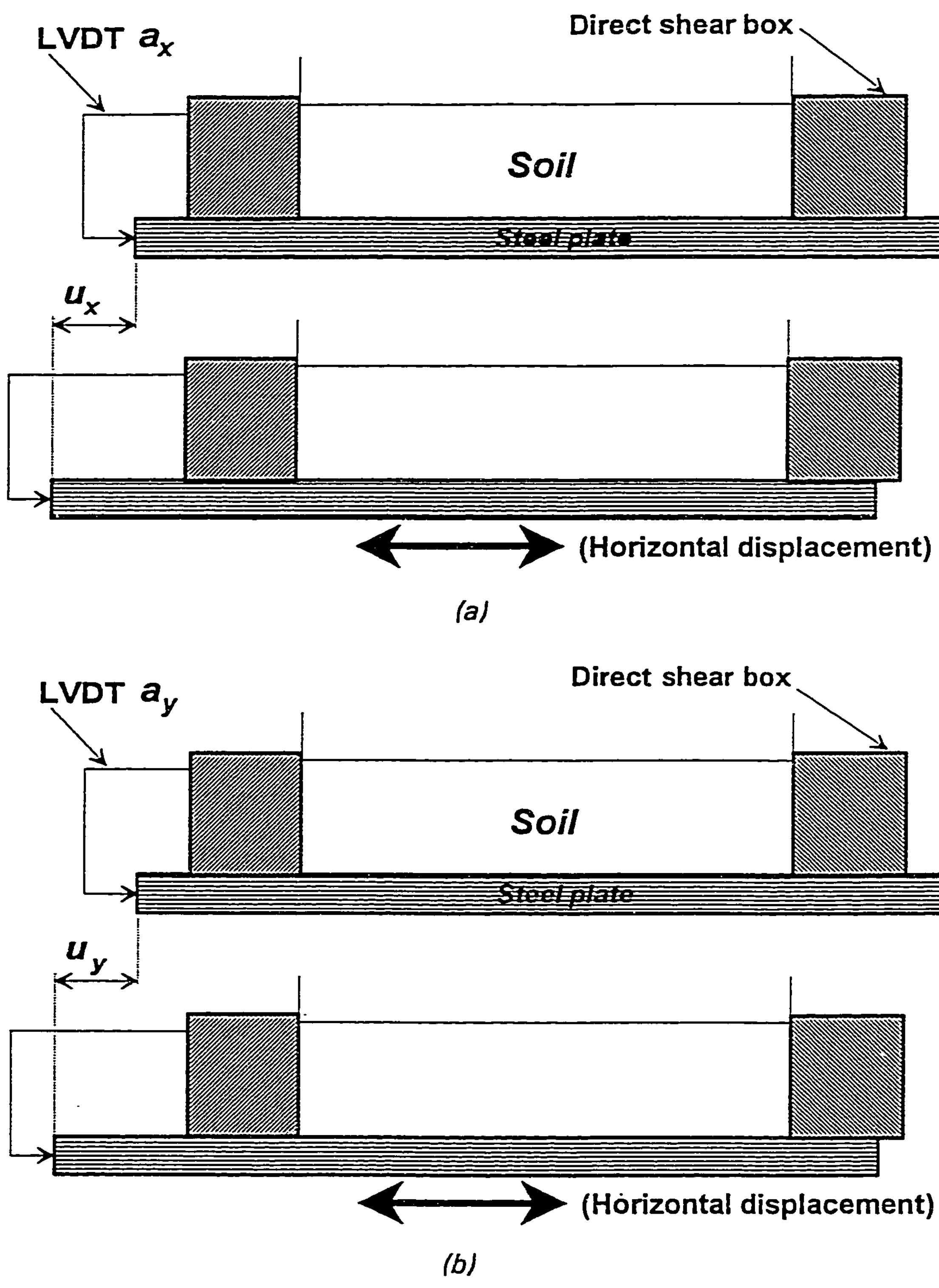

Fig.A.2 Schematic diagrams of tangential displacements for direct shear box: (a) x-direction; (b) y-direction (after Fakharian, 1996)

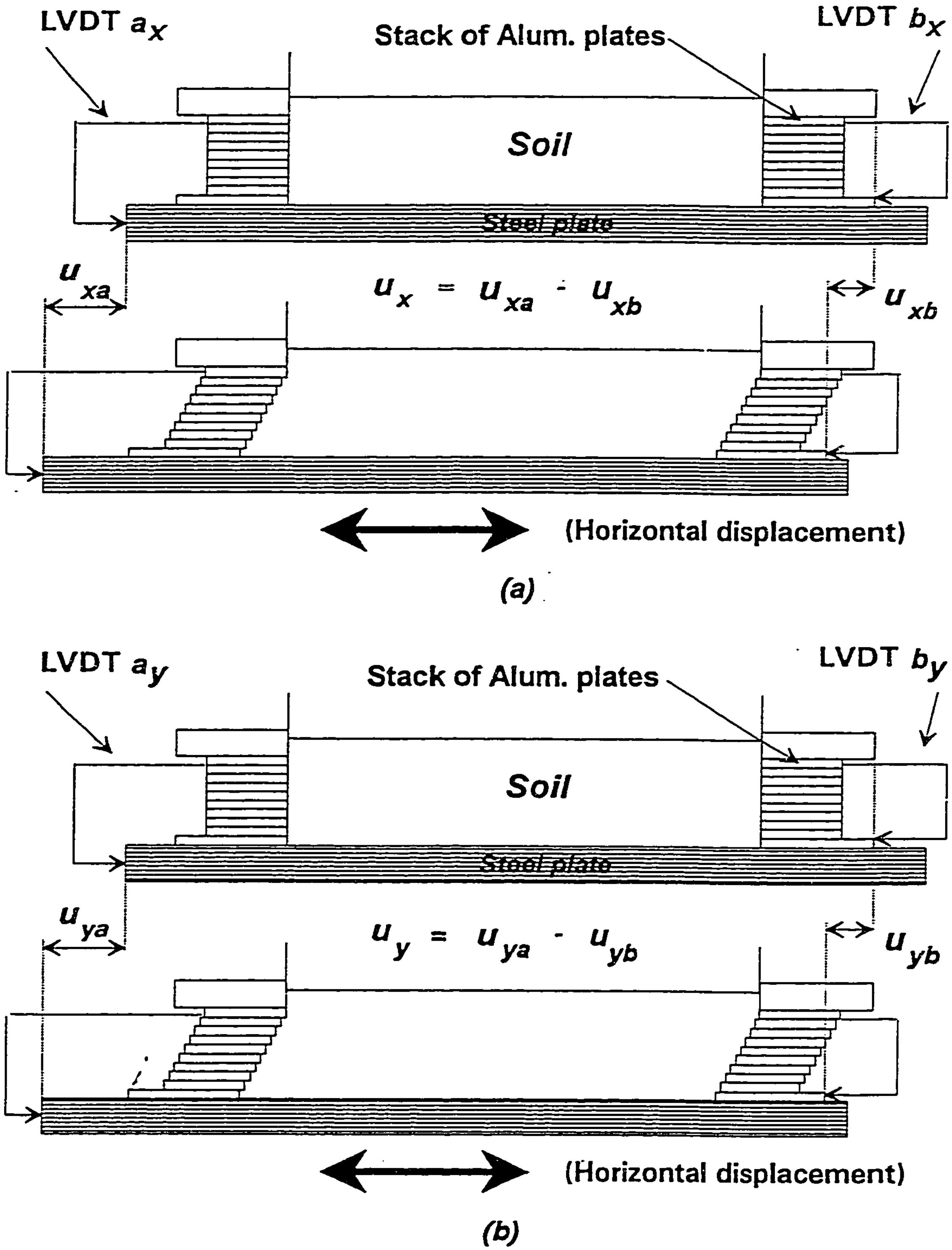

Fig.A.3 Schematic diagrams of tangential displacements for simple shear box: (a) x-direction; (b) y-direction (after Fakharian, 1996)

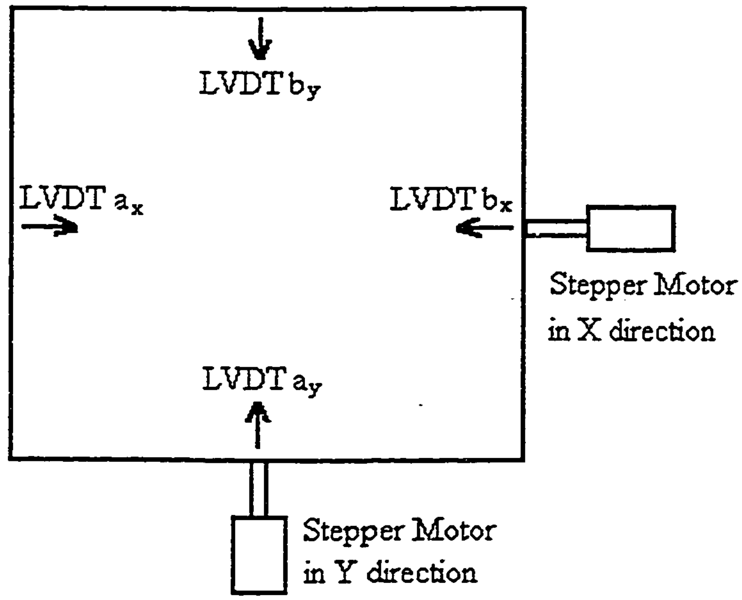

Fig.A.4 Plan view of the arrangement of LVDTs

IMAGE EVALUATION
TEST TARGET (QA-3)

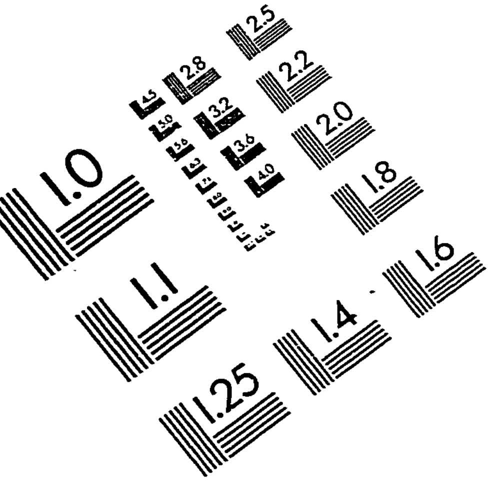

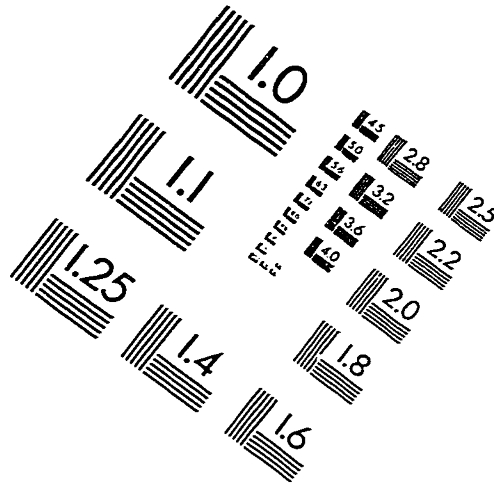

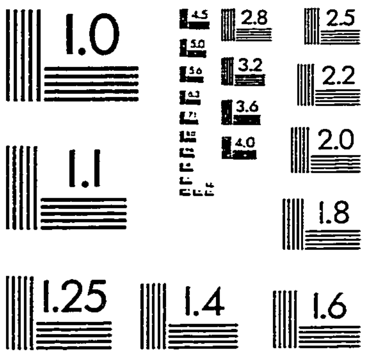

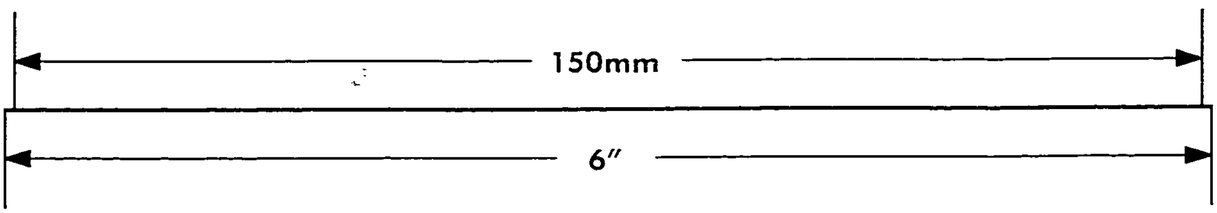

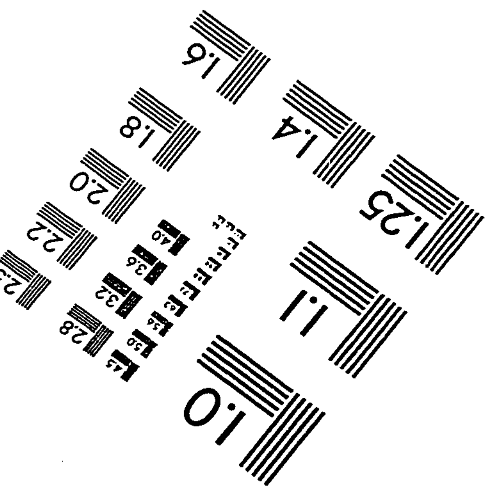

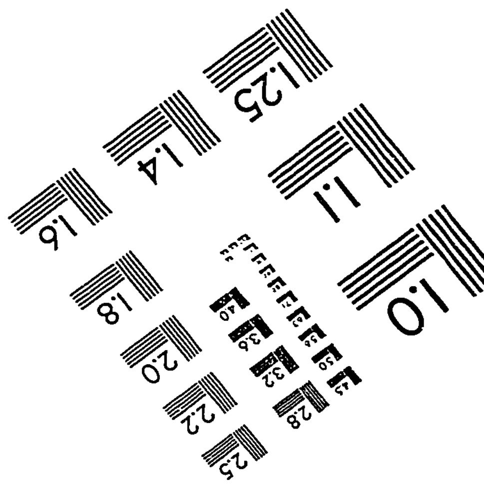

APPLIED IMAGE . Inc
1653 East Main Street
Rochester, NY 14609 USA
Phone: 716/482-0300
Fax: 716/288-5989